DEVELOPMENT OF A COMBINED ANGIOGRAPHY AND LATE GADOLINIUM ENHANCEMENT MR SEQUENCE

A Thesis
Presented to
The Academic Faculty

By

Adrian Lam

In Partial Fulfillment
of the Requirements for the Degree
Doctor of Philosophy in the
Bioengineering Program and Department of Biomedical Engineering

Georgia Institute of Technology

December 2015

Copyright © 2015 by Adrian Lam

DEVELOPMENT OF A COMBINED ANGIOGRAPHY AND LATE GADOLINIUM ENHANCEMENT MR SEQUENCE

Approved by:

John N. Oshinski, Advisor
Department of Radiology and Imaging Sciences
Emory University School of Medicine

Michael Lloyd
Department of Cardiac Electrophysiology
Emory University School of Medicine

Xiaoping Hu
Department of Biomedical Engineering
Georgia Institute of Technology

Orlando Simonetti
Department of Biomedical Engineering
Ohio State University

David Ku
Department of Mechanical Engineering
Georgia Institute of Technology

Date Approved: November 10th, 2015

Dedicated to Tiffany for her love and support across 2500 miles

ACKNOWLEDGEMENTS

Part of what makes science and engineering so enjoyable to work in is that this world has always been a collaboration with so many hands on deck. And I have been fortunate enough to have a group of wonderful people, both at Georgia Tech and Emory to support my work and myself.

I believe that one's experience in graduate school can almost entirely be determined by your adviser, and I have been extremely fortunate to be able to call Dr. John Oshinski my adviser. He has always let me forge my path to solve problems, but will provide a nudge when needed to help stay me on track. And regardless of what the data looks like, he is willing to work with me and support me with resources to unravel whatever I may need to. His scientific writing is exemplary – a combination of concision and simplicity to convey scientific ideas toward others, and I have found that by going through his edits that I can improve my own writing leaps and bounds. And lastly, I have found that it is in fact possible to have both a very successful professional career and social life, even if you are a professor.

Of course, a lab never complete without its members, and the Oshinski lab has treated me well during my time here. As Luke has previously mentioned, without them I probably be a hermit in my cubicle. The lab dynamic has always been quite special, filled with an assortment of small adventures, including (but not limited to): hooking up an N64 to play 007, holding "afternoon lab meetings", and even introducing new music to me. And beyond that, their help and input has been instrumental in my own work. Ian, Jonathan, Luke were an immense help when I first started out, especially in working out CFD and MATLAB. And everyone who has stepped through the Oshinski lab doors

afterwards – Lizz, Jason, Greg, Ankit, Erica, and John have always pitched in their ideas and support to help improve my work. But most importantly, that I can at any moment in the day ask a question to any labmate for a fresh pair of eyes is something that has always been appreciated.

I would like to acknowledge my committee members for helping me throughout this journey. Without their comments and insight, this work would never have gone as far as it did. Specifically, I would like to thank Dr. Xiaoping Hu has for his vital knowledge of MRI and Dr. David Ku for his critical analysis of the methods used in this work. For being a flexible long-distance committee member and for offering his years of MR expertise, I would like to thank Dr. Orlando Simonetti. I would like to thank Dr. Michael Lloyd has been an excellent clinical collaborator, in supporting our research with his help and clinical insight. And while not officially on my committee, Dr. Xiaodong Zhong has helped me out immensely me with pulse programming, especially in the starting stages when I was just trying to get a grasp of C++.

I would like to acknowledge my funding sources to allow me to travel to a variety of conferences. I received a T32 training grant from the NIBIB which allowed me to attend an imaging conference in Bethesda, and have also received predoctoral fellowship from AHA which helped fund an exciting trip to Milan for the International Society for Magnetic Resonance for Medicine. The opportunity to be able to present my work in front of experts of my field and meet other like-minded people has helped broaden my knowledge of the field and improve my research skills.

I have been lucky enough to meet others who help me keep my sanity outside of work. I would like to recognize my ALTA tennis team, for giving me something to look

forward to every Saturday morning. I would like to acknowledge Le Chiem for being an extremely generous tennis captain and of course all my teammates – Doug Kenny, Kayree Lee, Kien Lam, Mike Dushner, Jorge Altamirano, Dusty Davis, Balaji Lakshimapathy, Josh Brisbane, Andrew Hemings, Kyle Simmons, Shun Hsu and Greg Llewellyn. To have a group of people so diverse and talented who all hold passion for the game has allowed me to experience and play some of the best tennis in my life. I have also been a part of a group of friends that started the tradition known as "cooking night", a Saturday evening which we would cook and eat dinner together that was filled with fun and occasionally chaos. These friends – Samson Lai, Jeff Wong, Wenny Liu, Elaine Tang, Ken Pradel, Samantha Lo, Brian Gestner, Yizheng Chen, Grace Lee, and Irene Lai – have become some of my closest bonds during my time in Atlanta.

Lastly, I would like to acknowledge my family for their love and support. Their selflessness and hard work has provided me with opportunities that have brought me to where I am now. I would most certainly not be here if not for everything that they have done for me.

TABLE OF CONTENTS

LIST OF TABLES

LIST OF FIGURES

LIST OF SYMBOLS OR ABBREVIATIONS

3D	Three-dimensional
AF	Atrial fibrillation
AHA	American Heart Association
AIV	Anterior interventricular vein
CMR	Cardiac magnetic resonance
CNR	Contrast-to-noise ratio
CRT	Cardiac Resynchronization Therapy
CS	Coronary sinus
ECG	Electrocardiogram
FLASH	Fast Low Angle SHot
FoV	Field of View
GCV	Great cardiac vein
Gd	Gadolinium
GRE	Gradient Echo
HF	Heart failure
HIPAA	Health Information Privacy and Accountability Act
HR	High resolution
ICE	Image Calculation Environment
IR	Inversion Recovery
IRB	Institutional Review Board
LBBB	Left Bundle Branch Block

LGE	Late gadolinium enhanced/enhancement
LIPV	Left inferior pulmonary vein
LMV	Left marginal vein
LSPV	Left superior pulmonary vein
LV	Left ventricle/ventricular
MI	Myocardial infarction
MRI	Magnetic Resonance Imaging
NYHA	New York Heart Association
PDS	Parc Data Store
PSIR	Phase sensitive inversion recovery
PV	Pulmonary Vein
PIV	Posterior interventricular vein
PVI	Pulmonary Vein Isolation
PVLV	Posterior vein of the left ventrile
RIPV	Right inferior pulmonary vein
RG	Respiratory gated
RSPV	Right superior pulmonary vein
RV	Right ventricle
SharK	Shared K-space
SNR	Signal-to-noise ratio
SSFP	Steady-State Free Precession
STEMI	ST segment Elevated Myocardial Infarction

TE	echo time
TI	Inversion time
TR	repetition time
TRICKS	Time-Resolved Imaging of Contrast-Kinetics

SUMMARY

With the rapid growth of catheter-based interventional cardiology procedures, knowledge of the vasculature surrounding the heart relative to the distribution of scar tissue can provide important information for procedural planning and appropriate patient selection. Two examples of this are: (1) selecting patients for Cardiac Resynchronization Therapy (CRT), or (2) evaluating the outcome for atrial fibrillation (AF) patients who have undergone Pulmonary Vein Isolation (PVI).

CRT uses a biventricular pacemaker to restore synchronous myocardial contraction in heart failure patients with evidence of ventricular dyssynchrony. Optimal improvement from therapy necessitates that the left ventricular pacing lead, which is transvenously implanted through the coronary veins, is situated at the latest contracting site that is not predominantly myocardial scar. In order to achieve this, co-registered images of the coronary veins and myocardial scar are necessary. However, current MR imaging protocols use separate sequences to image these features, complicating co-registration.

PVI aims to circumferentially ablate around the pulmonary veins to electrically isolate triggers from reaching the left atrium. In order to evaluate ablation effectiveness, segmentation of the atrial wall is necessary. Yet, the thin nature of the atrial wall and low contrast at the blood-atrial wall interface make segmentation a challenge. While angiography images clearly delineate the inner atrial wall, co-registration is still necessary to the scar images.

These examples benefit from co-registration between MR angiography and scar images yet use different MR sequences making image registration cumbersome, preventing a unified display. The overall goal of this project was to develop a sequence that would produce inherently co-registered angiography and scar images using a single acquisition sequence and create image processing methods for a combined display. This sequence uses a slow infusion of gadolinium with a centric-ordered k-space acquisition scheme for angiographic imaging. Central k-space will be re-acquired at the end of the sequence (~10 mins after injection) and share outer k-space from the initial angiographic k-space to create inherently co-registered scar images. This sequence will be validated by imaging porcine hearts and then tested on two patient groups: (1) patients with known previous myocardial infarct (MI), and (2) patients with AF who have undergone PVI, to use LGE to evaluate ablation effectiveness. Algorithms will be developed to combine coronary vein and myocardial scar displays to allow LV lead planning. In addition, the concept of a pulmonary vein bullseye will be created to allow quantification of the extent of circumferential ablation in post-PVI patients.

Chapter I

INTRODUCTION AND BACKGROUND

1.1 Scope

While the purpose of this dissertation is to use MRI as a tool toward improving interventional cardiac electrophysiology procedures, the scope of this background section is designed to describe the disease conditions, the current research that has been performed, and the current limitations in the field to provide a stage for the motivation toward developing these tools. As such, the reader will be assumed to have knowledge of MR physics and basics of imaging work will not be discussed in this section.

The research in this dissertation is aimed at improving two interventional therapies: Cardiac Resynchronization Therapy (CRT) and Pulmonary Vein Isolation (PVI). This section will review heart failure, its relationship with dyssynchrony, and how CRT has been used to improve cardiac function in patients with dyssynchronous heart failure. It will continue into discussing how MRI has been used to study CRT as well as the current limitations. We will also review atrial fibrillation (AF), and how PVI has been used to treat AF. Then we will discuss the role of MRI in assessing PVI and the current limitations that MR faces.

1.2 Heart Failure

Heart failure is a syndrome in which the heart cannot meet the body's metabolic requirements under normal pressure conditions due to the impairment of the heart to fill or eject blood. It is a major health problem in the United States, affecting approximately

Table 1.1 Functional classes for New York Heart Association, categorized by the limitations in physical activity.

Class I	No limitation of physical activity. Ordinary physical activity does not cause undue fatigue, palpitation, dyspnea (shortness of breath)
Class II	Slight limitation of physical activity. Comfortable at rest. Ordinary physical activity results in fatigue, palpitation, dyspnea (shortness of breath).
Class III	Marked limitation of physical activity. Comfortable at rest. Less than ordinary activity causes fatigue, palpitation, or dyspnea.
Class IV	Unable to carry on any physical activity without discomfort. Symptoms of heart failure at rest. If any physical activity is undertaken, discomfort increases.

2-3% of the population costing at least 5% of the entire healthcare budget (1). Once diagnosed, heart failure has a 50% mortality rate after 4 years. Currently, heart failure is classified by the New York Heart Association (NYHA) into four classes based on functional limitations from HF (Table 1.1) as determined by the severity of symptoms from physical activity (2).

1.2.2 Heart Failure Development

HF most commonly starts as a result of myocardial infarction (MI), resulting in ~70% of patients with HF, but can also arise due to increased vascular resistance from hypertension, valvular diseases, or other infiltrative processes (3). Early remodeling (within 72 hours) from MI involves degradation of myocardial ECM by serine proteases and activated matrix metalloproteinases (MMPs) around the injured region along with removal of dead myocytes as a result of inflammation (4,5). This simultaneously causes wall thinning and increased wall stresses, resulting in ventricular dilation. After inflammation, cardiac fibroblasts proliferate and secrete ECM proteins to create a tightly cross-linked fibrotic scar that replaces dead myocytes (5). Late remodeling (beyond 72 hours) occurs as a response to distribute increased wall stresses more evenly, and

myocytes respond by eliciting a hypertrophic growth response, causing LV wall thickening and/or ventricular dilatation (6).

Hypertension, the most important risk factor for heart failure, can also cause ventricular remodeling due to increased myocardial load (5) . Myocytes respond to increased load by enlarging, leading to hypertrophy to reduce wall stresses. Chronic pressure overload stimulates fibroblast differentiation into myofibroblasts, which are capable of secreting collagen and fibronectin proteins (7,8). Increased fibrosis reduces compliance and oxygen diffusion capacity, furthering heart failure.

1.2.3 Dyssynchrony in Heart Failure

The extent of ventricular remodeling has the potential to affect conduction pathways as the once homogeneous myocardium has remodeled into heterogeneous myocardium and fibrous tissue (9). 30-50% of patients with HF exhibit a symptom where the LV walls do not contract synchronously, also known as dyssynchrony (10,11). One cause of LV dyssynchrony is due to a regional conduction defect, such as Left Bundle Branch Block (LBBB). In this case, electrical activation first occurs through the septum but slowly propagates via intra-myocardial conduction to the lateral wall. Another cause of conduction defects is the presence of non-conductive fibrotic tissue from myocardial infarction or other disease. Regardless of the reason for defect, this temporal delay in electrical activity results in decreased LV systolic function and myocardial efficiency as blood is “sloshed” from the early activated wall to the later activated wall instead of ejected out the ventricle. Currently, dyssynchrony is diagnosed as a QRS interval > 120 ms and is a major risk factor for HF patients. Although fewer than half of all HF patients

have dyssynchrony, those with dyssynchrony are eleven times more likely to be hospitalized or die than those without dyssynchrony (12,13).

1.3 Cardiac Resynchronization Therapy

Cardiac Resynchronization Therapy uses a biventricular pacemaker to restore synchronous contraction of the ventricles in heart failure patients with ventricular dyssynchrony. This pacemaker has 3 leads: an atrial sensing lead placed in right atrium, a pacing lead placed in the apex of the right ventricle (RV) and a pacing lead placed in the posterolateral wall of the left ventricle (LV). The atrial sensing lead detects electrical excitation and sends a signal to the two pacing leads for synchronous ventricular contraction. The right pacing lead is implanted stimulates the apex of the RV as well as the interventricular septum. The left pacing lead is implanted via a catheter through the coronary sinus into a coronary vein branch, typically on the posterolateral wall of the left ventricle.

An estimated 40,000 patients undergo CRT each year (14). Current class I indications for CRT are: QRS duration > 150 ms, patients with LBBB, or NYHA class ≥ II with LBBB and QRS duration> 150 ms. Class IIa indications for CRT include patients with LVEF ≤ 35%, LBBB, and QRS duration 120-150 ms (15). These recommendations are based on several multi-center trials that have demonstrated both short and long term benefits of CRT, including improvements in NYHA class, 6 minute walk distance, ejection fraction, quality of life, and increased survival rate (12,16,17). Statistics taken from the Nationwide Inpatient Sample estimate that Yet, approximately 30% of all CRT patients do not benefit from therapy (12). This non-response to CRT can be partially explained by the implantation location of the LV lead. The lead should be placed in the

latest contracting region of myocardium that is not predominantly myocardial scar for optimal response to therapy. As the LV lead is implanted in a coronary vein, the ideal site must have coronary venous access. However, current clinical care procedures do not consider these factors during CRT implantation.

1.3.1 LV Lead Placement and Dyssynchrony

Multiple clinical studies have shown that improvements to CRT are associated with LV lead placement in the myocardial segment with the greatest delay in electrical activation and mechanical contraction [REFs]. Pacing the latest contracting segment forces the segment to contract earlier, resulting in resynchronization of ventricular contraction. Retrospective studies have shown that pacing in the latest contracting segment or an adjacent segment led to significant decreases in mechanical dyssynchrony as assessed by the time delay in peak radial strain in anteroseptal-to-posterior delay or assessed by the difference in time delay from QRS onset to aortic/pulmonic valve opening (18). Significantly higher improvements in ejection fraction, peak oxygen consumption, and NYHA functional class post-CRT have also been shown in patients with LV lead implantation directly in or adjacent to the latest contracting segment when compared to those with LV lead implantation in segments further away from the latest contracting segment (19).

The Targeted Left Ventricular Lead Placement to Guide CRT (TARGET) further demonstrated the benefits of targeted LV lead implantation in the latest contracting segment by using echocardiography to determine the latest contracting segment to guide LV lead implantation in the latest contracting myocardial segment. The targeted group had a 70% response rate as defined by a $\geq$ 15% reduction in LVESV, as opposed to the

control group's 55% response rate(20). In addition, the targeted group showed 18% higher improvement in NYHA functional class ≥ 1, with a lower rates of heart-failure related hospitalization Most importantly, 3-year survival rates were significantly higher in patients with the LV lead placed at the latest site of contraction (80% vs 54%) (21).

1.3.2 LV Lead Placement and Myocardial Scar

Due to the electrical resistivity properties of myocardial scar which impede electrical propagation of pacing, the amount, scar location and transmurality have been shown to be predictors of response to CRT. Patients with < 33% scar in the LV and < 51% transmurality in any American Heart Association (AHA) segment were associated with 2.3 times greater response rates (22). In addition, patients with posterolateral scar experienced significantly lower response rates when compared to patients without posterolateral scar (81% vs 14%) (23) .

The location of the LV lead relative to myocardial scar has also been shown to affect response. Patients with the LV lead implanted outside of scar experienced higher 6-minute walk distances, quality of life scores and responder rates when compared to patients with the LV lead placed over scar. Placing the LV lead in a segment that had myocardial scar also resulted in lower 3-year survival rates (87% vs 58%) (21).

1.3.3 Coronary Vein Imaging for CRT

The coronary venous anatomy consists of the coronary sinus which drains into the left atrium, the great cardiac vein, the posterior and anterior interventricular veins, and lateral or posterolateral branches (Figure 1.1). However, the number of lateral/posterolateral venous branches as well as their angle of bifurcation from the great cardiac vein can vary

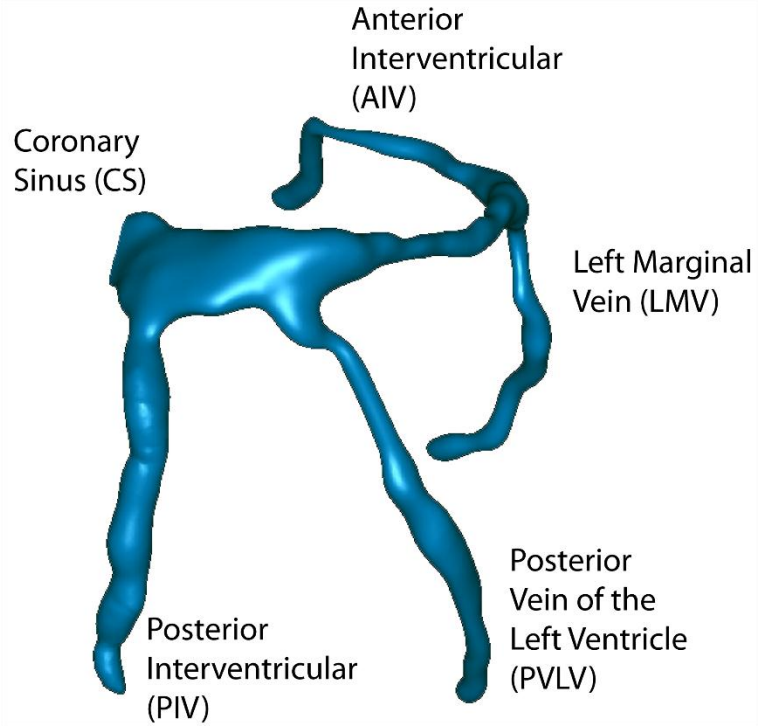

between patients. While the PIV and AIV are visible in more than 90% of patients, fewer

Figure 1.1 Sample coronary venous anatomy created in Geomagic (Raleigh, NC)

than half of all patients have both lateral and posterolateral branches. Additionally, the branch angle of the lateral/posterolateral veins can vary up to 30° between patients (24).

Current clinical procedures only image the coronary veins during the CRT procedure by catheter-based x-ray fluoroscopy to guide LV lead implantation. The coronary sinus (CS) is cannulated with an introducer sheath, and a balloon catheter is inflated to include the sinus. An iodinated contrast agent is injected retrograde through the coronary sinus to visualize the venouos system. Cine images at 30° left anterior oblique (LAO) and right anterior oblique (RAO) are acquired as references for LV lead positioning.

The current method for biventricular pacemaker implantation impedes pre-procedural planning for LV lead implantation as information about the location of the coronary

venous anatomy and the branches present are not known until the pacemaker implantation. As a result, even if an optimal LV lead implantation location exists, it is unknown whether that location has coronary venous access.

1.3.4 The Role of MRI in CRT

MRI is currently the only single imaging modality that can quantify dyssynchrony, determine the extent of myocardial scar, and visualize the coronary venous anatomy. Dyssynchrony has been assessed with high temporal resolution (~30 ms), breath-held steady state free precession (SSFP) cine images. Multiple slices are taken in a short-axis orientation for full LV coverage. Regional dyssynchrony can be quantified on these images by tracking the endocardial and/or epicardial borders and calculating the contraction curves based on distance from the LV centroid or finding the time-to-maximum LV wall thickness (25,26). Results can be projected onto an AHA 17-segment bullseye for simpler visualization (Figure 1.2).

Coronary vein imaging by MRI can be achieved using a variety of non-contrast and contrast-enhanced sequences. Non-contrast techniques have utilized magnetization transfer or T2-preparation pulses with SSFP sequences to null myocardium and maximize contrast-to-noise ratio (CNR) (27,28). Contrast-enhanced sequences have dominated coronary venous imaging due to drastically increased SNR and CNR in visualizing the coronary venous anatomy. These sequences are navigator- and ECG-gated, inversion-recovery SSFP or GRE sequences combined with a slow infusion (0.3 mL/sec at 0.2 mmol/kg) of gadolinium (29). The inversion time (TI) is set to 200 ms to null healthy myocardium.

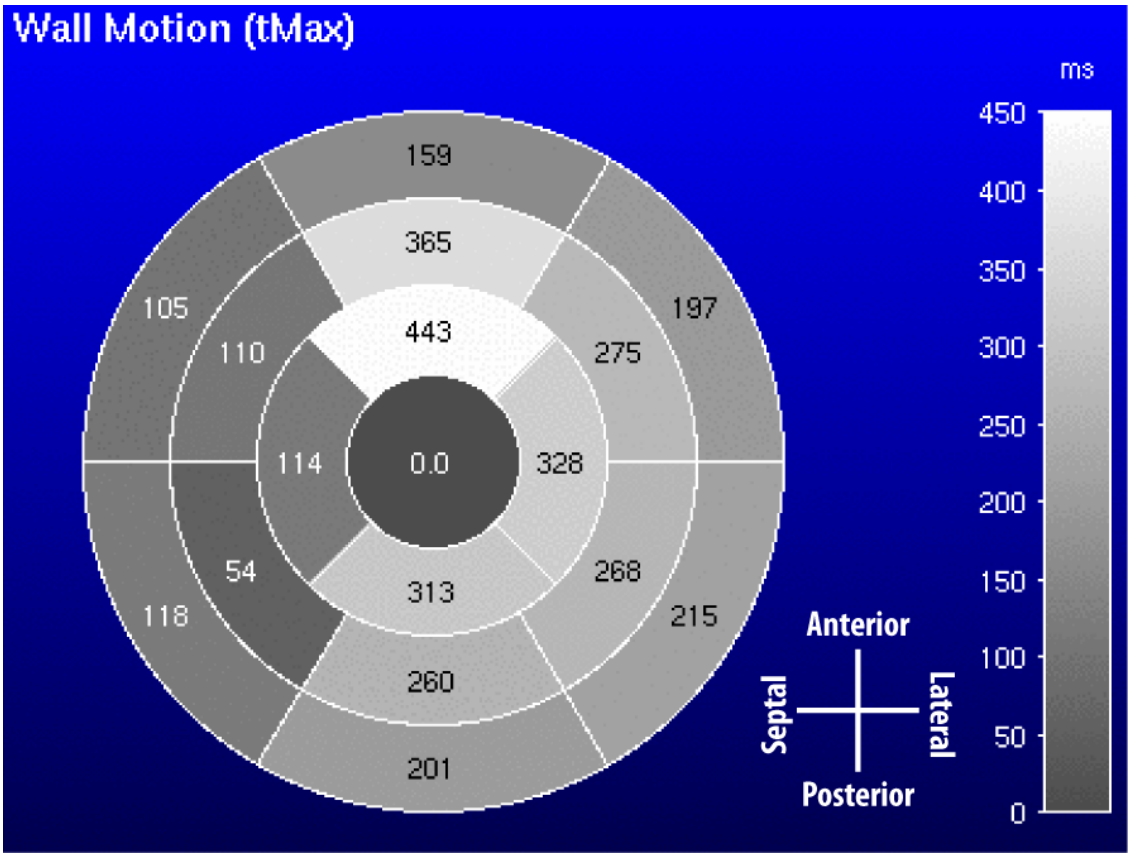

Figure 1.2 Sample bullseye grayscale color-coded to represent time to maximum radial wall motion. Anterior rings represent wall motion of basal slices while interior rings represent wall motion of apical slices. The axis represents the transformation between the x-y directions on the bullseye and the anatomical positions

Approximately 10-15 minutes post-contrast injection, gadolinium preferentially diffuses into regions of myocardial scar due to increased myocardial interstitial space from myocyte death and decreased washout kinetics from reduced vascularity (30–33). The increased concentration of contrast within scar results in hyperintense pixels on T1-weighted images. Late gadolinium enhancement (LGE) for scar imaging is performed during this period of time. A look-locker sequence that uses a range of TIs at a mid-short-axis LV segment is applied to determine the optimal TI to null healthy myocardium (34). Multiple 2D, breath-hold phase sensitive inversion recovery (PSIR) slices with the determined TI are acquired in the short-axis orientation for full LV coverage. Myocardial

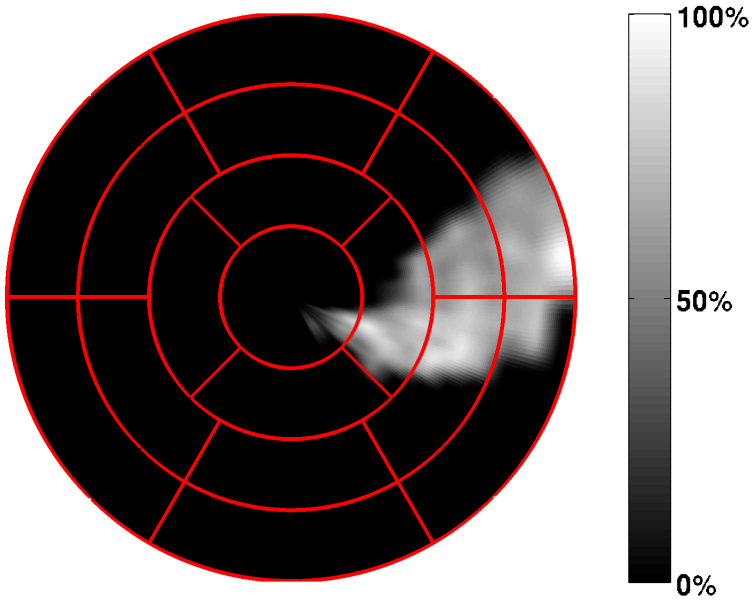

Figure 1.3 Sample bullseye showing scar transmurality. White represents fully transmural scar while black represents healthy myocardium.

scar can be characterized by segmenting the myocardium and defining all pixels above a patient-dependent threshold as scar. The amount and transmurality of scar can also be projected to the AHA bullseye for simplified viewing (Figure 1.3).

1.3.5 Limitations of Current Techniques

In order to use MRI as a pre-procedural planning tool for CRT, maps of regional dyssynchrony, maps of myocardial scar and the locations of the coronary veins must all be co-registered to each other. While the dyssynchrony images are acquired through the cardiac cycle, both angiography and LGE images are only acquired during the diastolic phases of the cardiac cycle. In addition, although both techniques use T1-weighting for image contrast, the differences in resolution, image orientation and respiratory positions make co-registration cumbersome. In addition, patient respiratory positions can change between breath-holds, further complicating co-registration. *A sequence that can be used for both angiography and LGE imaging would eliminate co-registration, simplifying the*

post-image processing necessary to make MRI a feasible pre-procedural planning tool for targeted LV lead implantation for CRT.

1.4 Atrial Fibrillation

Atrial fibrillation (AF) is the most common sustained cardiac arrhythmia, defined as a state in which the atrium quivers or "fibrillates" irregularly. AF affects approximately 1-2% of the population. It has been associated with a 5 fold increase in stroke, with direct costs in the US totaling to ~$6 billion per year (35,36).

AF is initiated with an electrical "trigger" or ectopic beat, with 90% of them originating in the pulmonary veins and 10% originating outside the pulmonary veins (37). These triggers travel down the pulmonary vein into the left atrium, inducing reentrant circuits causing the atria to quiver or fibrillate. If the reentrant circuits spontaneously terminate, the patient is considered as having paroxysmal AF. Each trigger and subsequent AF episode modifies the atrial substrate, causing electrical and structural remodeling, including atrial enlargement(38,39). The remodeling can progress to a point which reentrant circuits cannot spontaneously terminate. In these cases, patients are classified as having persistent AF.

1.5 Pulmonary Vein Antrum Isolation

Patients with paroxysmal AF who are resistant to at least one antiarrhythmic drug often undergo Pulmonary Vein Antrum Isolation (PVAI) to electrically isolate the pulmonary veins to prevent triggers from reaching the atrium. It is estimated that approximately 100,000 ablation procedures for AF occur annually in the US (40). Standard equipment involves a multipolar mapping catheter placed in the coronary sinus,

a pulmonary circular mapping catheter to record for pulmonary vein isolation and an ablation catheter used for pulmonary vein isolation. To check that the pulmonary veins have been fully isolated, a mapping catheter paces the coronary sinus while the circular mapping catheter records signals at the pulmonary veins to determine whether conduction into the vein has or has not been blocked. There are two different methods used for PVI: radiofrequency ablation and cryoballoon ablation.

1.5.1 Radiofrequency Ablation

Radiofrequency ablation uses an irrigated tip radiofrequency catheter for point-by-point ablation around the pulmonary veins (Figure 1.4, left) (41). RF energy is delivered approximately 5 mm away from the PV ostia with lesions aimed to continuously encircle each PV. Typically, energy is limited to 30W with temperature set to 50-60°C to prevent later PV stenosis. RF energy is applied for 30 seconds – 1 minute.

While uncommon, there are complications associated with RF ablation. The most lethal complication associated with RF ablation is atrio-esophageal fistula, which occurs in approximately 0.2% of patients but accounts for 15.6% of mortality cases (42). As the posterior left-atrial wall can be in close proximity to the esophagus, RF energy has the potential to damage the esophagus and create a fistula. Additionally, approximately 1.2% of patients who undergo RF ablation experience thromboembolic events, most commonly within the first two weeks following ablation (43). Another rare complication involve phrenic nerve injury, which affects 0.5% of patients and is more likely to occur in the inferoanterior portion of the RSPV due to its proximity to the right phrenic nerve (44). However, rapid recovery of function can likely be attained if the RF procedure is stopped immediately.

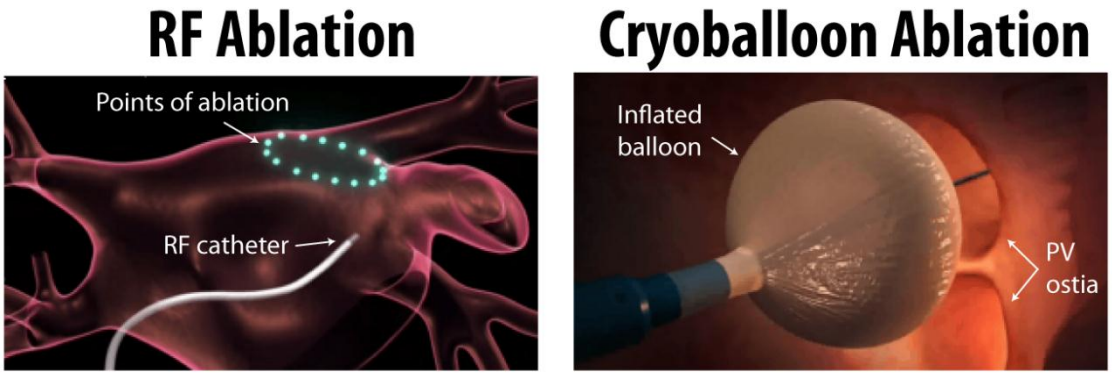

Figure 1.4 Methods for RF ablation (left) and cryoballoon ablation (right) are shown. The RF catheter performs point by point ablation around the pulmonary veins while the cryoballoon presses an inflated balloon against the PV ostia.

1.5.2 Cryoballoon Ablation

Cryoballoon ablation (Arctic Front, Medtronic, Minneapolis, MN, USA) has become increasingly popular due to its ease of use and reduction of complications as compared to RF ablation (Figure 1.4, right) (45). This method inflates a balloon at the base of the pulmonary veins, presses the balloon against the ostia, and injects nitrous oxide for cryoablation of the tissue in contact with the balloon. Different sized balloon diameters (23/28mm) can be used for individualized therapy for each pulmonary vein if pre-procedural imaging is available. Two balloons are used per vein with approximately 5 minutes of contact (46). Afterwards, additional touch-up with a cryocatheter, RF catheter, or even additional balloons may be applied to cover regions that are missed by the balloons.

Cryoballoon ablation eliminates the risk of atrio-esophageal fistula, little to no risk of PV stenosis, has decreased chance of thrombogenicity, but carries a slightly increased risk of phrenic nerve injury (47–49). Even though phrenic nerve injury rates vary from 8-11% across studies, the majority of these events are reversible (49,50). Using a larger sized balloon may further decrease risk of this complication (49).

1.5.3 Recurrence Post-PVI

While both ablation methods are widely used, both methods suffer approximately 30% recurrence rates (43,48,50). Although there are a limited number of studies regarding recurrence post-cryoballoon ablation, MRI has been used to investigate the scar patterns resulting from PVI by RF ablation using LGE imaging.

1.5.3.1 MRI Assessment for PVI

Scar assessment by MRI can be visualized with LGE imaging 1-3 months post RF ablation. This time period is chosen because the atrial wall undergoes inflammatory changes and scar development in the first month post ablation, and early after injury, LGE imaging cannot differentiate between inflammation and scar.

The majority of current MR protocols do not acquire angiography images, but acquire LGE images using a whole-heart, navigator- and ECG-gated, inversion-recovery gradient-echo sequence 15 minutes post-contrast injection. A TI scout is used to determine the optimal TI time (270 – 310 ms), and images are acquired in the transverse orientation with 1.25x1.25x2.5 resolution. The atrial wall is segmented by manually tracing the inner atrial wall, dilating the borders until the outer atrial wall, and manually refining the dilated outer border. Criteria to classify scar in the segmented atrial wall has varied across studies, with studies using 3-6 standard deviations above normal tissue (51).

1.5.3.2 LGE Factors Associated with Recurrence

Multiple studies have agreed that non-recurrence has been linked to increased volume of scar (52–54). Complete encirclement of the pulmonary veins by scar as determined qualitatively has also found to be associated with non-recurrence (53). There is currently no consensus as to whether fewer gaps on an individual or multiple pulmonary veins is

associated with recurrence. One study found that more gaps in the RIPV was associated with recurrence, but another study found that more gaps in the LIPV was associated with recurrence (54,55).

1.5.4 Limitations of Current Techniques

Current angiographic imaging techniques typically use contrast-enhanced, breath-held 3D SSFP or FLASH sequences (56,57). While these sequences have clear delineation of the inner atrial wall, these images are not used in the segmentation process (51). Reasons again can be attributed to differences in resolution and respiratory positions, complicating co-registration to LGE images. In addition, choosing the proper inversion time plays a large role in image quality, but the 10 minute acquisition time of the LGE sequence prevents the option to acquire images with multiple TIs in the case the first TI is not properly chosen.

Atrial wall segmentation on LGE images is challenging due to its thin nature (2-4 mm) thus spanning only 4-5 pixels on MRI images. In addition, contrast between the atrial wall and the blood pool is often poor, making manual segmentation of the atrial wall subjective. *A sequence that can acquire both angiographic and LGE images would eliminate the subjectivity associated with atrial wall segmentation and improve the accuracy of pulmonary vein encirclement post-ablation.*

1.6 Summary

We present two cases that would greatly benefit from an MR technique that uses the same sequence to acquire both angiography and LGE images. Using a sequence that would have inherently co-registered angiography and LGE images would eliminate co-

registration between myocardial scar and coronary vein images to provide maps to prospectively assess whether patients should undergo CRT. In addition, such a sequence would improve atrial wall segmentation to allow accurate evaluation of post-ablation scarring for PVI.

Chapter II

HYPOTHESIS AND SPECIFIC AIMS

2.1 Central Hypothesis

We hypothesize that we can develop a sequence that shares k-space from a single acquisition to create co-registered magnetic resonance angiography (MRA) and late gadolinium enhanced (LGE) images for: (1) pre-procedural left ventricular (LV) lead placement for biventricular pacemaker implantation and (2) cryoballoon ablation assessment in creating continuous scar encircling the pulmonary veins.

2.2 Approach

We modified a 3D, contrast-enhanced, navigator- and ECG-gated, inversion recovery pulse sequence using the IDEA pulse sequence development platform (Siemens Healthcare, Malvern, PA) to create a combined sequence by using Shared K-space (SharK) data. Combining acquisition of angiography and scar data results in inherently co-registered images, making it possible to directly overlay coronary vessel anatomy on top of scar to guide LV lead implantation. Co-registered angiography and scar images will also simplify endocardial segmentation to allow for more accurate atrial wall segmentation to quantify scar distribution from ablation to treat atrial fibrillation. To achieve these goals, the following specific aims were investigated:

2.3 Aim 1: Validation of a Respiratory-Gated FLASH sequence for Angiography and LGE Imaging

We propose to compare the images acquired by a respiratory-gated FLASH sequence against x-ray venography and breath-held PSIR images to validate that a respiratory-gated FLASH sequence can be used for both angiographic and LGE imaging.

In order to combine imaging of angiography and LGE imaging in a single sequence, we need to validate that the sequence can perform as well as its respective gold standards. We will compare the ability of the respiratory-gated FLASH sequence to visualize the coronary venous anatomy to x-ray venography for LV lead planning. We will also compare the ability of the respiratory-gated FLASH sequence to quantify scar against 2D PSIR as well as a high-resolution FLASH sequence without respiratory motion.

2.3.1 Aim 1a: Comparison of MR Angiography and X-Ray Venography for Coronary Vein Imaging

We propose to assess the capability of a respiratory-gated FLASH sequence to visualize the coronary venous anatomy against the current gold standard, x-ray venography.

In order to use the combined angiography and LGE sequence for pre-procedural planning in CRT patients to determine whether a patient has a coronary vein suitable for LV lead implantation, the ability of the angiography sequence for coronary vein visualization must compared against the current gold standard, x-ray venography. We hypothesized that MRI will be capable of visualizing the coronary venous anatomy as well as x-ray venography. Patients scheduled to undergo CRT will receive a cardiac MRI and x-ray venography during the CRT procedure. Veins will be graded on both

modalities to determine the extent of the coronary vein anatomy that can be visualized by MRI as compared to x-ray venography and to determine whether MRI can identify the vein used for LV lead implantation.

2.3.2 Aim 1b: Validation of Respiratory-Gated LGE Imaging in Ex-Vivo Hearts

We propose to image ex-vivo porcine hearts to determine the accuracy of the respiratory-gated FLASH sequence in imaging LGE compared to the clinical standard, breath-held PSIR image and a gold standard, a high-resolution LGE image with no respiratory motion.

In order to validate the respiratory-gated sequence used for LGE imaging, we need to compare this sequence against the clinical standard, breath-held PSIR images and a gold standard, a high-resolution inversion-recovery FLASH sequence without respiratory or cardiac motion. We hypothesized that the respiratory-gated LGE-FLASH sequence will be as accurate as or more accurate than the clinical standard, 2D breath-held phase-sensitive inversion recovery (PSIR) when compared against a high-resolution, fully sampled inversion-recovery LGE image with no respiratory motion. A cardiac MR exam will be performed on an *ex-vivo* porcine heart with a 3-month old infarct that has received an intravenous dose of gadolinium 15-20 minutes prior to sacrifice. A respirator will be used to simulate breathing motion on the *ex-vivo* heart while the LGE-FLASH images are acquired. The PSIR and gold standard sequences will be acquired without any motion. The endo/epicardial borders and scar tissue will be segmented and all images will be compared on scar volume and geometry.

2.4 Aim 2: Development of a Combined Angiography and LGE Sequence

We propose to develop an MR sequence for combined angiography and late gadolinium enhanced scar imaging.

We will develop a sequence to enable reconstruction of an angiography and LGE in a single sequence by Sharing K-space (SharK). The base sequence will be a 3D, navigator- and ECG-gated, inversion-recovery FLASH sequence. This sequence will use a centric-ordered k-space acquisition scheme and acquire central k-space when there is the highest concentration of gadolinium in the blood. After a full set of k-space is acquired, a portion of central k-space will be re-acquired. The angiographic images will be reconstructed with the initially acquired central k-space while the LGE images will be reconstructed with the later acquired central k-space. Both image sets will share the outer portions of k-space to create to full sets of k-space. We hypothesize that

2.5 Aim 3: Application of the SharK sequence in Patients

We propose to apply the SharK sequence on patients with myocardial scar and patients who have undergone pulmonary vein isolation

To demonstrate the utility of the SharK sequence, we propose to apply the sequence in two sets of patients: (1) Patients with known previous myocardial infarction and (2) Patients who have undergone cryoballoon ablation for pulmonary vein isolation. These patient populations were chosen due to the presence of myocardial scar in both clinical cases as well as the need to have co-registered angiography and scar images, either for clinical planning or for accurate segmentation.

2.5.1 Aim 3a: Application of SharK Sequence on Patients with Myocardial Scar

We propose to test our combined sequence on patients with myocardial scar to determine the amount of k-space that can be shared from angiographic to LGE images.

We propose to apply the combined sequence in patients with known previous myocardial infarct to determine the number of extra partitions that should be acquired for the LGE reconstruction in the SharK sequence. We hypothesize that acquiring an additional 25% of k-space is necessary for a sufficient LGE reconstruction. We will test this hypothesis by acquiring two separate, full sets of k-space and creating multiple LGE reconstructions by retrospectively sharing different amounts of outer k-space. Myocardial scar will be characterized on all reconstructions and the original LGE image will be used as a gold standard for comparison.

2.5.2 Aim 3b: Application of SharK Sequence on Patients Post-PVI Treatment

We propose to: (i) use our combined sequence on AF patients who have undergone cryoballoon ablation to assess scar encirclement from PVI and (ii) create image processing methods for enhanced visualization.

In order to further demonstrate the utility of the SharK sequence, we propose to apply the SharK sequence on AF patients who have undergone cryoballoon ablation to assess encirclement of the pulmonary veins post-ablation. We hypothesized that we could quantify the amount of scar encircling the pulmonary veins with images acquired from the SharK sequence. We will test this hypothesis by performing atrial wall segmentation

on the angiographic images and transferring the borders to LGE images to assess scar. In addition, we propose to develop new image processing algorithms to improve visualization of scar encircling the pulmonary veins. We will achieve this by creating pulmonary vein bullseyes about the pulmonary vein antrum to evaluate scar encirclement.

2.6 Significance and Innovation

Current methods for acquiring angiography and scar images use different sequences, making co-registration cumbersome due to differences in resolution, respiratory position, and image orientation. While sharing k-space has been used in other reconstruction algorithms(58–60), the methods proposed here would be first to share k-space between angiographic and LGE images. Benefits from sharing k-space between these two images include naturally co-registered images, more accurate myocardial segmentation, decreased MR imaging time, and higher spatial resolution images when compared to the current clinical standard for LGE imaging. Reduced LGE imaging time also allows for the capability to study the temporal behavior of contrast accumulation into scar.

The images produced from this sequence can be used for pre-procedural LV lead placement in patients undergoing CRT. Having co-registered angiographic and LGE images allows coronary vein maps to be easily combined with transmural scar maps to determine: (1) whether a patient has an ideal LV lead position and (2) whether this position has coronary vein access. This pre-procedural knowledge improves selection of patients to undergo CRT and the effectiveness of the therapy itself. Preventing patients who are not ideal candidates for CRT from undergoing the procedure can save the healthcare system ~$100,000/patient and may increase quality of life and lifespan (16).

The SharK sequence can also improve post-procedural PVI scar assessment. Using angiographic images for inner atrial wall segmentation eliminates the majority of subjectivity that comes from LGE image segmentation due to poor CNR between the blood and atrial wall. Accurate identification of the atrial wall leads to accurate characterization of scar encircling the pulmonary veins, which can be used toward pre-procedural planning for repeat ablations or reveal regions of the pulmonary veins that are consistently missed during ablation.

The goal of this thesis is to develop and test specialized sequence that acquires co-registered angiographic and LGE images to simultaneously simplify and improve image post-processing to provide knowledge toward improvements in CRT or PVI.

Chapter III

Comparison of MR Angiography and X-Ray Venography for Coronary Vein Imaging

Adapted from "Performance of 3D, navigator echo-gated, contrast-enhanced, magnetic resonance coronary vein imaging in patients undergoing CRT" by Adrian Lam, Luis F Mora-Vieira, Michael Lloyd, and John Oshinski. J Interv Card Electrophysiol (61)

3.1 Introduction

In order to validate that a respiratory-gated FLASH sequence can visualize the coronary venous anatomy for left ventricular lead planning in Cardiac Resynchronization Therapy to be able to use in a combined sequence, we need to compare this sequence against the current clinical standard for coronary vein imaging, x-ray venography. Cardiac Resynchronization Therapy (CRT) uses a biventricular pacemaker to create synchronous contraction of the ventricles of the heart. The left ventricular (LV) pacing lead is typically implanted through the coronary venous system at an epicardial site along the lateral LV wall. Studies have shown that the location of LV pacing lead affects CRT response and the optimal lead location is in the latest contracting segment of the heart that is not primarily myocardial scar tissue (19,21). Since the coronary veins are only imaged during LV lead implantation by retrograde venography and x-ray fluoroscopy, there is no way to know a priori if the lead can be implanted at an optimal location. Additionally, lead placement has a 12% implantation failure rate due to the inability to access the coronary sinus or the inability to find a stable pacing position due to unfavorable venous anatomy(62). Therefore, pre-procedural knowledge of the coronary

venous anatomy can help improve LV lead implantation success rates and determine whether the optimal lead implantation location has coronary vein access.

Studies using contrast-enhanced MRI for coronary vein imaging have shown that the technique is capable of visualizing the coronary venous vasculature(63,64). However, none of these studies have had corresponding x-ray venograms to validate the existence of the coronary veins visualized by MRI, and most studies have small sample sizes (65). The small size and tortuous nature of the coronary vein tributaries leads to subjectivity when determining the existence of a vein, and hence validation of the veins imaged by MRI with a reference standard such as x-ray venography is necessary. *The objective of this study is to determine the accuracy of contrast-enhanced coronary vein imaging for visualizing coronary venous anatomy as compared to x-ray venography, and to determine whether the vein that is ultimately used for lead implantation is identified by a pre-procedure MRI.*

3.2 Methods

3.2.1 Patient Population

Patients (n=19, 9 male, age 70 ± 10 years) scheduled to undergo CRT from 01/2011 – 05/2013 at Emory University Hospital were included in this study. Patients received a cardiac MRI 6 hours to 1 week before x-ray venography, which occurred during the CRT procedure. The patients met current clinical criteria for CRT (EF < 35%, QRS duration > 120 ms, New York Heart Association Class III+, heart failure despite stable medication for 1 month) (66) . This study was approved by the Institutional Review Board (IRB) and HIPAA compliant, and all patients gave written informed consent.

3.2.2 MRI Protocol

All cardiac magnetic resonance (CMR) exams were performed on a 1.5T MRI (Avanto or Espree, Siemens Medical Systems) system using a six-element phased-array cardiac coil. Short and long axis cine images of the left ventricle were acquired. The cine vertical long axis (VLA) was used to find the resting period of the coronary sinus (67). The coronary venous anatomy was imaged using a 3D whole-heart, navigator and EKG-gated, inversion-recovery FLASH sequence with a centric k-space trajectory. A gadolinium-based contrast agent (0.2 mmol/kg) was slowly infused at a rate of 0.3 mL/s, followed by an equal amount of saline. Acquisition started 15 - 30 seconds after the start of contrast injection to ensure contrast was present in the coronary veins (68). The sequence parameters were: TR = 3.3 ms, TE = 1.49 ms, flip angle = 15°, voxel size = 0.64 x 0.64 x 0.75 mm^3, inversion time = 200 ms, readout bandwidth = 610 Hz/pixel, and number of segments per heartbeat = 30.

3.2.3 X-Ray Venography

Catheter-based x-ray venography was performed during the CRT procedure, immediately before pacemaker lead implantation by an experienced cardiac electrophysiologist (M.L.) to visualize the coronary venous system. The coronary sinus (CS) was cannulated with an introducer sheath and a balloon catheter was inflated to occlude the coronary sinus. An iodinated contrast agent was injected retrograde through the coronary sinus to visualize the venous system. Cine images at 30° left anterior oblique (LAO) and right anterior oblique (RAO) were acquired during contrast injection and were used as a reference for LV lead positioning(69). LAO and RAO single frame

views were taken after LV lead implantation and were used along with the cine images to determine the vein segment in which the lead was implanted.

3.2.4 MR Coronary Vein Image Grading

MR coronary vein images were graded for visibility based on the following segments: coronary sinus (CS), posterior and anterior interventricular (PIV/AIV), posterior vein of the left ventricle (PVLV) and left marginal vein (LMV) (Figure 3.1). MRI images were graded on a scale of 0-3 (3 = sharp borders, high contrast between vessel lumen and myocardium, 2 = fair lumen/myocardium contrast, 1 = noisy lumen, poor contrast with myocardium, 0 = not visible/non-existent). Images were evaluated independently by an MRI scientist and a cardiac electrophysiologist.

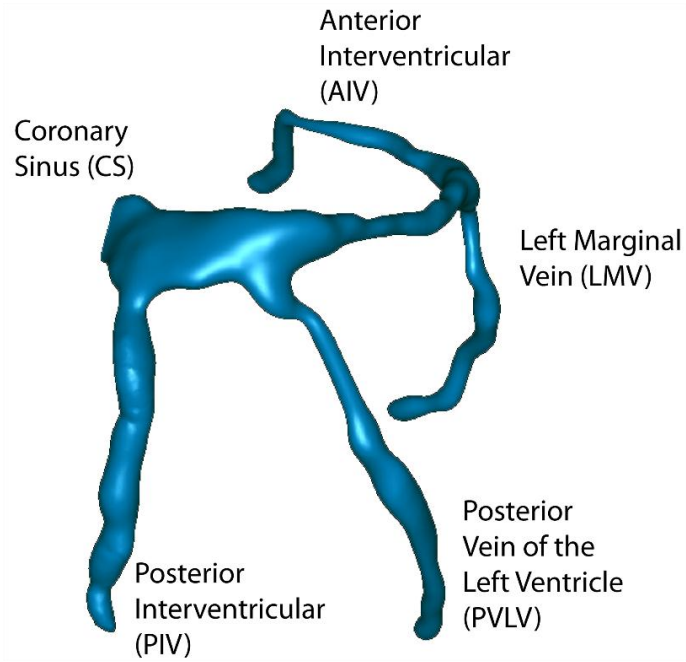

Figure 3.1 Coronary vein anatomy segmented from MRI coronary vein images using Segment (Medviso AB; Lund, Sweden (70)) and smoothed using Geomagic (Raleigh, NC).

3.2.5 MRI to X-Ray Venogram Visibility

Coronary veins were also given a binary classification on MRI of 'visible' or 'not visible'. A vein needed to have an average score of ≥ 1 between readers in order for the vein to be considered 'visible' by MRI. Vein segments on x-ray venograms were graded as visible or not visible by a cardiac electrophysiologist and used as a gold standard for visibility comparison. Only veins visible by x-ray venography were considered in the analysis.

3.3 Results

3.3.1 X-Ray Venography

X-ray venography was successfully performed in all 19 patients. Three x-ray venograms were of non-interpretable quality due to insufficient balloon occlusion of the coronary sinus as determined by the grading electrophysiologist and excluded in the x-ray venogram to MRI concordance comparisons. Therefore, final comparisons were done in 16 subjects.

3.3.2 MR Coronary Vein Image Grading

The coronary veins were successfully imaged by MR and x-ray venography in all 19 patients (Table 3.1). Acquisition time of the whole-heart MR sequence was 9.8 ± 2.5 min with navigator efficiency of 48 ± 15%. MR coronary vein image quality scores are shown in Table 1. The CS was observed in all patients (19/19) and had an average image quality score of 3.0. The PIV and AIV were observed in all but one patient (18/19) and had slightly lower image quality scores, 2.3 and 2.4 respectively. The PVLV was observed in

15/19 patients and the LMV was observed in 17/19 patients and had the lowest image quality scores, 1.6 and 1.9 respectively.

3.3.3 MRI to X-Ray Venogram Visibility

X-ray venography imaged the CS in 100% (16/16) of patients, the PIV in 70% (13/16) of patients, the PVLV in 60% (11/16) of patients, the LMV in 85% (15/16) of patients, and the AIV in 75% (15/16) of patients. Of these vein segments seen by x-ray venography, MRI was capable of resolving all of the CS segments, 12/13 of the PIV segments, 8/11 of the PVLV segments, 13/15 of the LMV segments, and 15/16 of the AIV segments. In total, MRI visualized 90% (64/71) vein segments (Table 3.2).

Table 3.1 MR visibility score and the average vein score among all patients are shown above. Values are averaged between two graders and veins were excluded and considered nonexistent if the average vein score was less than 1.

	CS	PIV	PVLV	LMV	AIV
MR Visibility Score	19 (100%)	18 (95%)	15 (79%)	17 (89%)	18 (95%)
Average Vein Score	3.0 ± 0.2	2.3 ± 0.7	1.6 ± 1.1	1.9 ± 0.8	2.4 ± 0.9

Table 3.2 X-ray venogram and MR visibility for the coronary veins are shown above. Coronary veins were excluded from the MR image quality score calculation if the vein was not visible by x-ray venography.

	CS	PIV	PVLV	LMV	AIV
Venogram Visibility (n = 16)	16	13	11	15	16
MR Visibility	16 (100%)	12 (92%)	8 (73%)	13 (87%)	15 (94%)
MR Image Quality Score	2.9 ± 0.3	2.0 ± 0.8	1.4 ± 1.1	1.7 ± 0.9	2.2 ± 1.1

3.3.4 Coronary Vein LV Lead Placement

The coronary vein branch used for LV lead placement was imaged by x-ray venography in 14/16 patients. Lead placement could not be determined by x-ray venogram images in one case because the final lead position was not imaged in one case and multiple LV lead implantation attempts in different branches in the other case. The most common vein used for LV lead placement was the LMV, which was used in 10 patients. The lead was placed in a PVLV in 3 patients and in the AIV in one patient. The vein used for LV lead placement was visible by MR images in all patients and had an average MR visibility score of 1.9.

3.4 Discussion

The major findings of this study were: 1) MRI was able to visualize 90% of the coronary venous anatomy when compared to the gold standard, retrograde x-ray venography and 2) MRI was able to visualize the vein used for LV lead implantation for all patients. These results show that MRI can be used as a tool for pre-procedural planning for patients undergoing CRT.

There were cases in which MR was not able to resolve particular coronary veins as seen by x-ray venography. These cases most commonly occurred in the lateral branches, such as the PVLV and LMV, and this is reflected by their slightly lower image quality scores. The lower scores are expected due to the vein's small size and in-plane orientation, which leads to decreased contrast between the vessel and myocardium and partial volume effects. Although MRI may not be able to resolve all of the smaller branches, these branches may not be clinically relevant. Smaller coronary vein branches are typically more difficult to cannulate and may have a greater risk of dissection of

perforation. A higher vein quality score of the vein used for LV lead implantation demonstrates that MRI is capable of sufficiently resolving all clinically relevant veins.

There were multiple cases in which a vein was visible on the MRI images but not on the venogram images. This occurred with 5 PIVs and 6 PVLVs. Since this study uses x-ray venography as the gold standard for coronary vein imaging, all veins identified by MRI but not by x-ray venography could be considered false positives by MRI. However, the balloon used in x-ray venography is inflated in the coronary sinus and can also block contrast from flowing down the PIV and occasionally the PVLV. Therefore, veins may be identified using MRI but not by x-ray venography. A method which eliminates potential issues with blocking the PVLV or PIV with the balloon is necessary to discern whether the veins that were solely visible by MRI are "false positives" or are veins that are present but not seen by x-ray venography.

There were multiple cases with low quality x-ray venograms, including three cases in which insufficient balloon occlusion of the coronary sinus resulted in limited opacification of the coronary vein anatomy and two cases in which the vein used for LV lead implantation was not visible by venography. However, based on prior experience, electrophysiologists are capable of estimating the general position and angle of a missing branch to guide the LV lead wire down a coronary vein not visible on the x-ray venograms. This is non-ideal, as the placement of the lead in an optimal location for these cases relies on physician experience and skill to move the guide wire into a branch that cannot be seen. Pre-procedural coronary vein imaging by MRI would eliminate these cases, allowing physiologists to more accurately estimate the location and angle of the desired implanting coronary vein branch before attempting lead implantation.

There were limitations to this study. This was a retrospective study and only enough contrast was injected retrograde into the coronary sinus for x-ray venography as deemed necessary by the performing electrophysiologist. This led to cases with low quality x-ray venograms and balloon occlusion at the PIV/PVLV. Since both x-ray venograms and MR coronary vein images were graded by users, there is subjectivity in determining the existence of a vein. A larger sample size would also help strengthen the capability of MRI to resolve the coronary venous anatomy. Lastly, these studies were done at 1.5T using a 6-channel coil. Studies have shown that image quality can be improved by performing studies on a 3T MRI with a 32 channel coil for maximum SNR (65). However, most CMR studies are still performed at 1.5T because of better consistency of SSFP imaging at 1.5T (71).

3.5 Conclusions

We were able to show that MRI is capable of visualizing 90% of the coronary veins seen by the current gold standard, x-ray venography. Additionally, all veins used for LV lead placement in CRT were seen in the MRI. These results validate the 3D, navigator and ECG-gated, inversion recovery FLASH sequence for use as the angiography portion of the Shared K-space sequence.

Chapter IV

Validation of Respiratory-Gated LGE Imaging in Ex-Vivo Hearts

4.1 Introduction

Late gadolinium enhancement (LGE) imaging is the gold standard for myocardial scar assessment has been extensively used clinically for viability studies (72). LGE works on the principle that gadolinium contrast distribution and washout kinetics are different between healthy myocardium and infarcted myocardium. Normal myocardium is primarily composed of densely packed myocytes with little extracellular space, which decreases gadolinium diffusion into myocardium. In contrast, infarcted myocardium has increased interstitial space from loss of myocytes and scar tissue formation resulting in increased contrast diffusion into regions of scar. The limited vasculature in regions of scar decrease washout kinetics. The increased concentration of gadolinium in regions of infarction leads to hyperintensity on T1-weighted images.

Validation of T1-weighted late-gadolinium enhancement has been achieved by comparing the hyperintense regions on LGE images of infarcted ex-vivo animal hearts to tetrazolium chloride (TTC) stained tissue slices. This stain reacts with dehydrogenase enzymes in healthy tissue to create a blue or red formazan pigment to differentiate alive or dead tissue. 2D, breath-held, phase-sensitive inversion-recovery has emerged as a popular sequence for LGE scar imaging due to its high contrast between healthy myocardium and infarcted myocardium (73,74). This sequence uses an inversion pulse and acquires phase-sensitive images that differentiate negative and positive longitudinal

magnetization, reducing the need for precise nulling of healthy myocardium with the inversion pulse (73).

The purpose of this chapter is to compare respiratory-gated, LGE-FLASH sequence used as the base sequence for Shared K-space, to the clinical standard, 2D, breath-held, PSIR images, and to a high-resolution gold standard. The comparison will be achieved by imaging an excised pig heart that had been given a dose of gadolinium immediately prior to sacrifice with the three different LGE sequences and comparing the resulting sca imagesr. *We hypothesize that the respiratory-gated sequence will be as accurate as the PSIR images at quantifying scar when compared against the high-resolution gold standard.*

4.2 Methods

4.2.1 Pig Heart Preparation

Three pigs were provided in collaboration with Dr. Murali Padala (Assistant Professor, CT Surgery, Emory University School of Medicine) and given an infarct by occluding the Left Anterior Descending (LAD) coronary artery one year prior to imaging. The pigs were given a dose of gadolinium (0.2 mmol/kg, ProHance; Bracco Imaging, Milan, Italy) 15-20 minutes prior to sacrifice. The hearts were subsequently removed and rinsed in saline. The heart was propped upright by inserting a bamboo skewer through the left atrium in a cross and balancing the heart on top of a beaker (Figure 4.1). To reduce tissue-air artifact, the heart was immersed in silicon oil. The beaker was placed inside a box that will be subject to simulated respiratory motion. A 6-channel body coil was placed on top of the heart and box for imaging.

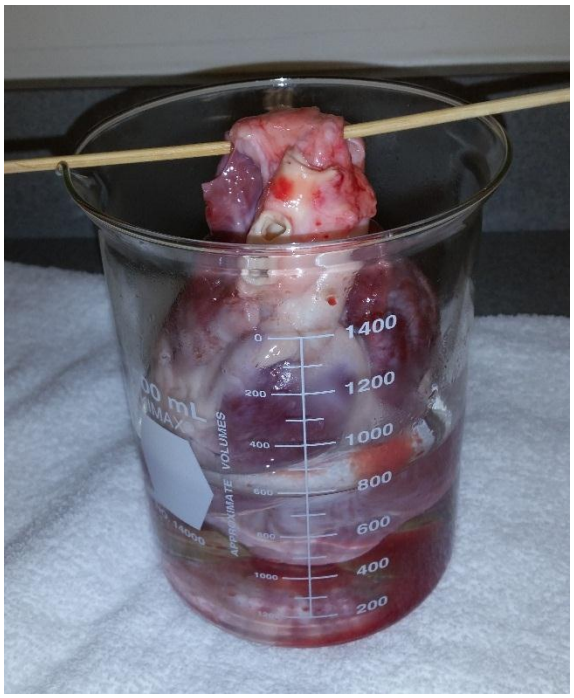

Figure 4.1 A bamboo skewer was inserted through the atrium to prop up the heart in a beaker. The heart was immersed in silicone oil to eliminate air-tissue interface artifact.

4.2.2 Respiratory Motion Simulation

To simulate respiratory motion, a sealed bag was placed at the base of the box with two pipes protruding from the bag (Figure 4.2). A platform was placed on top of the bag that would rise and fall as the bag inflated and deflated. The pipes were connected to a respirator (Large Animal Controlled Ventilator, Harvard Apparatus, Holliston, Massachusetts) that pumped air in and out of the bag at a rate of 30 bpm. The respirator was later replaced by manually breathing into the tubes at a normal breathing rate, as the heart was too heavy to move the heart consistently.

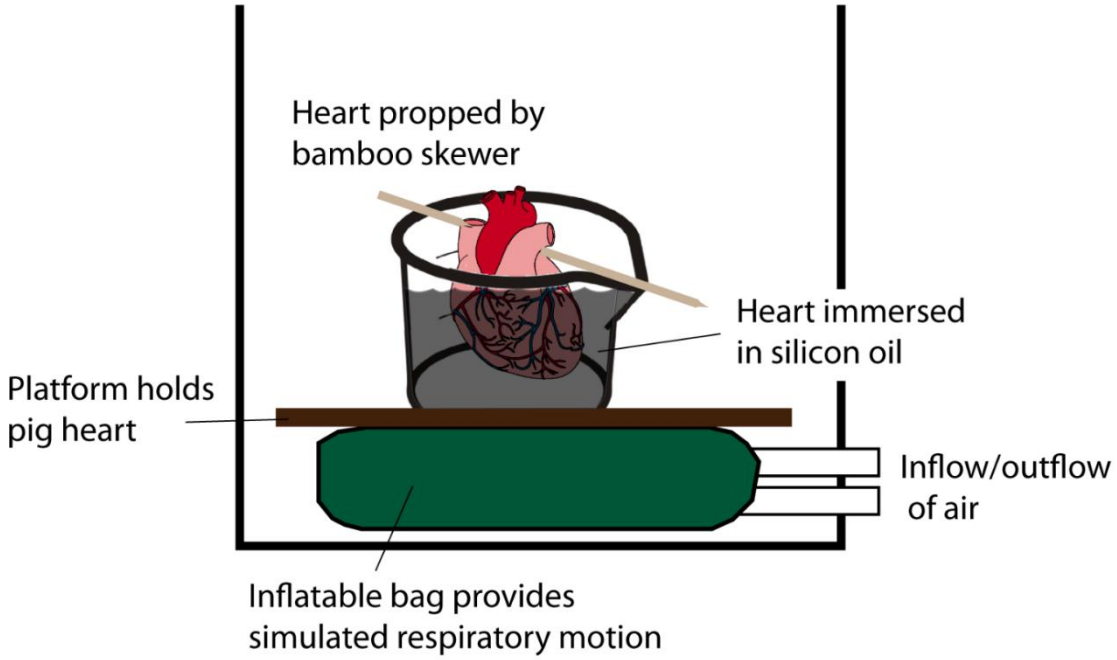

Figure 4.2 Box with inflatable bag to simulate respiratory motion. The two tubes allow inflow and outflow of air. The platform is placed atop the bag to provide a flat surface for the heart to rise and fall

4.2.3 MR Protocol

All pig hearts were imaged on a 3T MRI (TimTrio/Prisma Fit, Siemens Healthcare, Erlangen, Germany). A simulated ECG trigger (1 second/cardiac cycle) was set by using the Siemens IDEACMDTOOL in the physiology monitoring unit on the scanner. A Look-Locker inversion recovery sequence was acquired at a mid-short axis slice to determine the optimal inversion time for nulling of myocardial tissue. Three different sequences were used to evaluate late LGE (Table 4.1):

Table 4.1 Sequence parameters for the three sequences used for LGE imaging

	PSIR	RG-FLASH	HR-FLASH
Flip Angle	25°	15°	15°
TR (ms) / TE (ms)	2.93 /1.46	2.05 /1.25	2.05 /1.25
Respiratory Gated	No	Yes	No
Pixel Spacing (mm^2)	1.3-1.7 x 1.3-1.7	1.1-1.3 x 1.1-1.3	0.6 x 0.6
Slice Thickness	4-7 mm	0.75 mm	0.6 mm
Phase/Slice	80% / N/A	90%/50%	100% / 100%
Acceleration	None	GRAPPA x 2	None

1. PSIR: PSIR images using standard resolution and contrast parameters were acquired and used as the clinical standard.
2. RG-FLASH: Respiratory motion was simulated by using a respirator attached to sealed bag, and the navigator-gated, LGE-FLASH sequence was applied. This is the sequence used as the basis for shark sequence and the one used in the human studies. The navigator was placed at the top of the silicone oil–air interface.
3. HR-FLASH: A high-resolution, fully k-space sampled, ECG-gated, inversion-recovery, LGE-FLASH sequence was used as the gold standard for comparison

4.2.4 Image Processing

The myocardium was segmented by manually tracing the endocardial and epicardial borders for the PSIR, RG-FLASH, and HR-FLASH images. To determine the scar threshold for all images, an ROI was placed over a segment of healthy myocardium and all pixels greater than $\mu \pm 2\sigma$ of the ROI were considered scar (75).

4.2.5 Scar Comparison

Scar across images acquired with different scan techniques were evaluated by two different methods: total scar volume and total scar area. Results between all tests were compared using a two-tailed, paired t-test between the HR-FLASH and PSIR images as well as between the HR-FLASH and RG-FLASH images.

4.2.5.1 Total Scar Volume

The total scar volume was calculated by calculating the total number of myocardial pixels with intensity greater than the scar threshold over the entire imaging volume and multiplying by the voxel size. The difference in scar volume was determined by taking the absolute difference in scar volume calculated by HR-FLASH images and the PSIR or RG-FLASH images.

4.2.5.2 "Thickness Normalized" Scar Area Comparison

To normalize for differences in slice thickness, a combined average intensity image was created from RG-FLASH and HR-FLASH slices that corresponded to each PSIR slice. The volume enclosed by each PSIR slice was determined, and all RG-FLASH/HR-FLASH slices bounded by this volume were combined by averaging the images together. The combined average intensity images created from the RG-FLASH/HR-FLASH slices has an effective slice thickness that is the same as the PSIR slices. The total number of pixels above the scar threshold on each combined average intensity RG-FLASH/HR-FLASH image and corresponding PSIR slice was calculated and multiplied by the pixel size to determine the total area of scar coverage for each image.

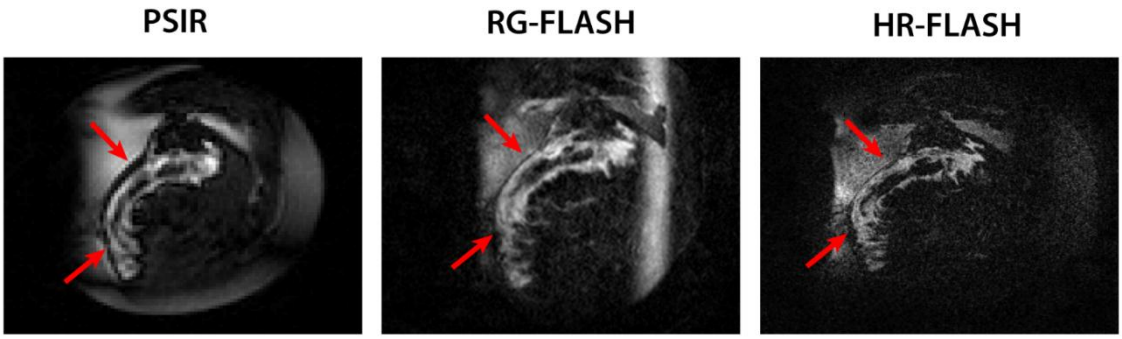

Figure 4.3 Corresponding slice from each LGE sequence. Red arrows notate regions of enhancement. Qualitative similarities can be seen across all three sequences

4.3 Results

Three hearts were successfully imaged *ex-vivo* with MRI (Figure 4.3). Qualitative similarities can be seen across all LGE images. The HR-FLASH images shows in detail the heterogeneity of scar due to its small voxel sizes. The PSIR images show significantly less detail when compared to the HR-FLASH images due to the higher slice thickness. The effect of respiratory motion can be seen on the RG-FLASH images, as edges are less defined when compared to both PSIR and HR-FLASH images.

4.3.1 Scar Volume Comparison

The average scar volume was 240.10 ± 31.8 cm^3, 261.1 ± 125.0 cm^3, 233.6 ± 103.2 cm^3 as imaged by the PSIR, RG-FLASH and HR-FLASH sequences respectively. The average absolute scar volume difference was 78.6 ± 99.7 cm^3 between the PSIR and HR-FLASH images and 31.1 ± 29.4 cm^3 between the RG-FLASH and HR-FLASH images. (Figure 4.4). Although scar volume on PSIR images was typically higher than scar volume on RG-FLASH or HR-FLASH images, there were no significant differences between all three scan types. These results suggest that the RG-FLASH can quantify scar

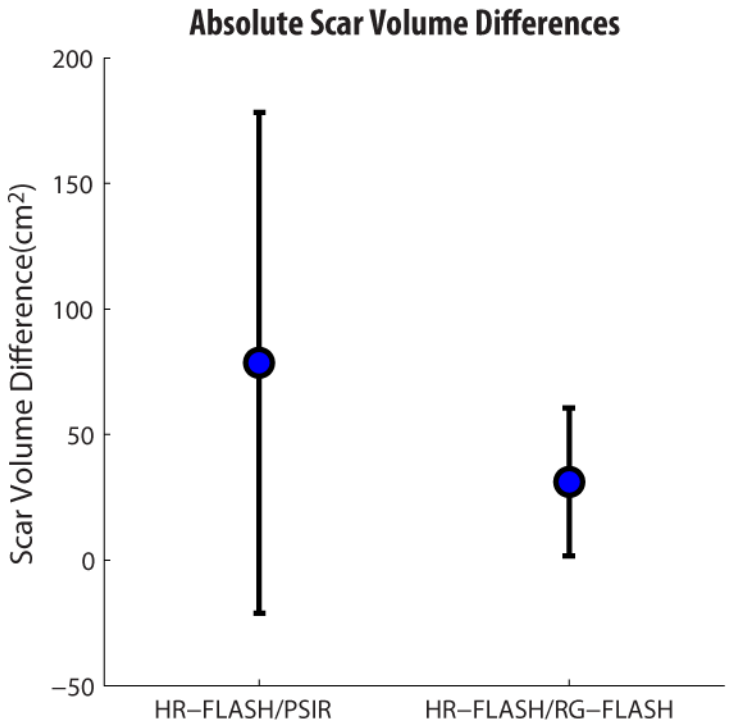

Figure 4.4 Differences in scar volume as quantified by the HR-FLASH images and the PSIR/RG-FLASH images. Error bars represent standard deviation in absolute scar volume differences between heart samples.

volume as accurately as PSIR images, and is not significantly different from the gold standard HR-images in quantifying scar volume.

4.3.2 Thickness Normalized Scar Area Comparison

The average scar area across the all pig hearts was 4.58 ± 2.93, 3.69 ± 2.60, and 3.6 ± 2.20 cm^2 for the PSIR, RG-FLASH, and HR-FLASH sequences respectively (Figure 4.5). A paired t-test showed significant differences between the two FLASH scar areas and the PSIR scar areas ($p < 0.05$) but no significant differences between the HR-FLASH and RG-FLASH scar areas ($p = 0.06$). This suggests that the RG-FLASH sequence is as good as the HR-FLASH sequence and is better than the PSIR sequence in quantifying scar area. A linear regression comparing the HR-FLASH scar areas against the PSIR and RG-

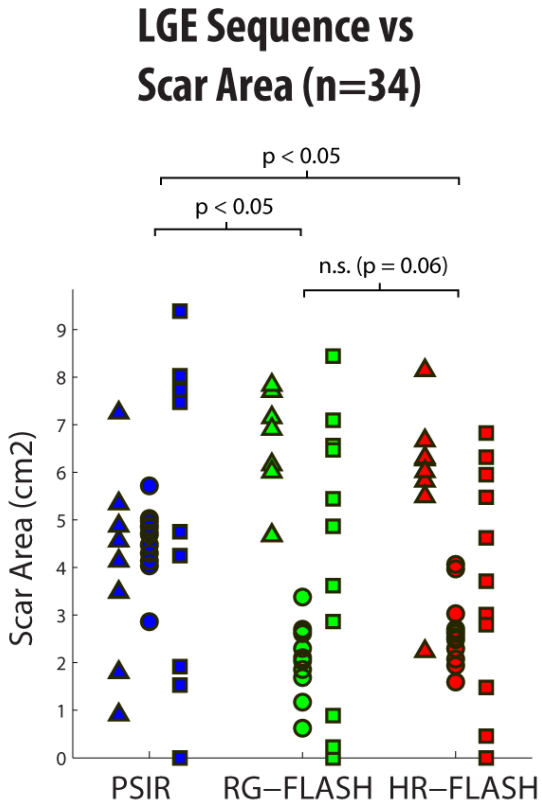

Figure 4.5 Scar area for corresponding slices on PSIR, HR-FLASH and RG-FLASH images are shown. Different shapes represent different heart samples.

FLASH scar areas showed that the scar area on PSIR images had a moderate relationship to scar area on HR-FLASH images while scar area on RG-FLASH images had a strong relationship to scar area on HR-FLASH images (Figure 4.6).

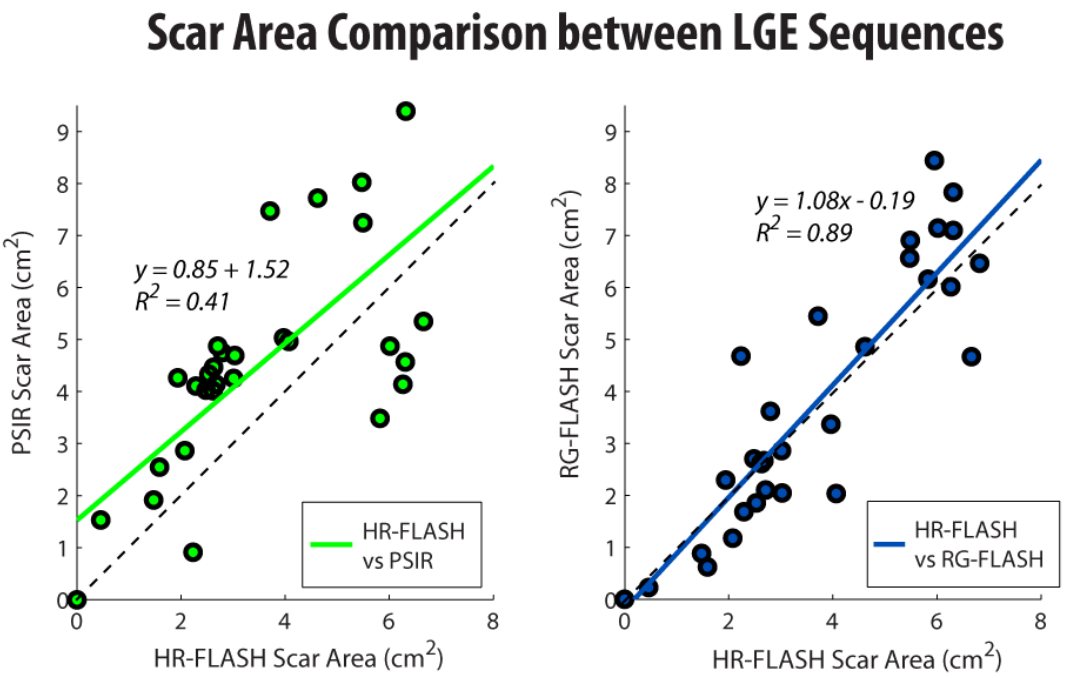

Figure 4.6 Linear regression to compare scar area for HR-FLASH images against PSIR and RG-FLASH images. Dotted lines represent y=x for comparison.

4.4 Discussion

We have validated the respiratory-gated FLASH sequence used in the SharK sequence by showing that: (1) the RG-FLASH sequence is equivalent to the current clinical standard, a PSIR sequence and a gold standard, a fully-sampled, high resolution FLASH sequence in quantifying scar volume, and (2) the RG-FLASH sequence is more accurate than a PSIR sequence and is not statistically different from fully-sampled, high resolution FLASH sequence in quantifying scar area when comparing across a "thickness normalized" scar area slice.

When comparing total scar volume on RG-FLASH images to the HR-FLASH and PSIR images, there were no significant differences, suggesting that a respiratory-gated FLASH sequence is as accurate as the current gold standard for volumetric scar imaging

over the entire myocardium. Although non-significant with only 3 hearts included, it is unlikely for image noise to fully account for the differences seen in scar volume between the PSIR and HR-FLASH images. While the PSIR images are undersampled by 20% when compared to the fully sampled HR-FLASH images, the ~40x larger voxel sizes of PSIR images result in much higher SNR. As such, differences in measured scar volume can more likely be associated to partial volume effects from measuring volume on PSIR slices that are 5-9 times thicker than the RG-FLASH or HR-FLASH images. While other studies comparing different LGE sequences and their ability to quantify scar volume found no difference between sequences, slice thicknesses were similar across sequences, limiting partial volume effects (76–78). The partial volume effect has been previously demonstrated qualitatively by summing multiple thinner MR slices to create an image with an effective thicker slice (35). This effect leads to intermediate-level hyperintensities that may still be above the scar threshold on the PSIR images depending on the scar geometry and scar heterogeneity, resulting in full voxels that can be considered scar or healthy myocardium when only a portion of the voxel is actually scar.

Creating a combined average intensity image with a higher slice thickness to normalize for partial volume effects does not eliminate the tendency for PSIR to overestimate scar when comparing scar areas across different slices. This may be due to the fact that through-plane partial volumes have been normalized between the sequences, but in-plane partial volumes play a larger role in the PSIR images due to the larger pixel sizes. However, it is important to note that averaging multiple thinner slices to create a thicker slice in the HR-FLASH and RG-FLASH sequences may not accurately represent the case when a thicker slice is acquired. Averaging slices together inherently blurs edges

of scar, leading to lower pixel intensities and less scar. As a result, the PSIR images may not be overestimating scar areas as significantly as calculated.

The correlation between the RG-FLASH/HR-FLASH images in "thickness-normalized" scar area shows a strong correlation due to the similarities in the sequence but has some variation due to blurred scar edges from respiratory motion on the RG-FLASH images. The correlation between the PSIR/HR-FLASH images only show a modest due to differences in voxel sizes. The HR-FLASH images show significant heterogeneity in scar throughout the heart and this heterogeneity cannot be captured by the PSIR images due to the much higher voxel sizes of the PSIR sequence. The differences in slice excitation between 2D and 3D sequences may also contribute to the variance seen. 2D sequences use RF pulses to excite individual slices and since it is not possible to excite a perfectly rectangular slice, the RF pulse leaks into neighboring slices. 3D sequences excite the entire volume and include an additional phase encoding gradient for the slice direction to allow acquired partitions to be contiguous. As a result, it is anticipated that this difference can be mitigated by using a higher resolution, 3D PSIR sequence.

It is important to note that the simulated respiratory motion is different from true respiratory motion as the simulated respiratory motion only moved the heart over a range of ~8 mm while true respiratory motion may vary over a range of ~20 mm. However, we found that the images from the simulated respiratory motion resulted in images with blur similar to that seen when acquiring navigated-gated images in patients, likely because the respiratory simulation creates more irregular motion when compared to physiologic

breathing. Regardless, differences between the respiratory-gated FLASH sequence and the high-resolution FLASH sequence were non-significant.

4.4.1 Limitations

The small sample size limits the reliability of the t-test, though the trends shown are in line with previous results. Segmentation and ROI selection for scar thresholding was also performed manually leading to potential for bias. As the silicon oil signal was higher on PSIR images than the RG-FLASH or HR-FLASH images, making some regions of enhancement adjacent to silicon oil difficult to differentiate, some voxels of silicon oil can potentially be mistakenly segmented. Immersion of the heart in deuterated water to may simplify segmentation to prevent errors in segmentation in future studies.

4.5 Conclusions

We were able to show that the respiratory-gated FLASH sequence is as accurate as the current clinical standard, a PSIR sequence as well as the gold standard, a high-resolution FLASH sequence in quantifying scar volume, and is better than the PSIR sequence in quantifying scar area. The results validate that a respiratory-gated FLASH sequence can be used for the LGE portion of the combined angiography and LGE sequence.

Chapter V

Development of a Combined Angiography and Late Gadolinium Enhancement (LGE) Pulse Sequence

5.1 Introduction

Contrast enhanced sequences have been extensively used for cardiac MR, most notably for angiography and late gadolinium enhanced (LGE) scar imaging. In order to image the coronary arteries or veins which span a large volume across the ventricles, navigator-gated sequences that image k-space gated to acquire during diastole have been used to diminish respiratory and cardiac motion (65). A gadolinium contrast agent is injected at a slow infusion rate (0.3 mL/s @ 0.2 mmol/kg) to prolong its presence during angiographic imaging. Contrast accumulates in regions of fibrosis 10-20 minutes post contrast due to increased extracellular myocardial space and decreased washout kinetics. LGE scar imaging is performed during this period of time, which allows characterization of location, size, and transmurality of myocardial scar. The gold standard for LGE imaging is by using a 2D, breath-held phase-sensitive inversion recovery (PSIR).

Knowledge of the location of vasculature surrounding the heart with respect to the location of myocardial scar is important for pre-procedural planning of electrophysiological therapies. This requires co-registration between angiography and LGE image stacks, which is complicated by the differences in respiratory positions, image resolution, and image orientation. Additionally, in order to assess myocardial scar, segmentation is required on the endocardial and epicardial borders. Although these features are well delineated on angiography images, there is often poor contrast of the

blood-myocardium border on LGE images, making segmentation a subjective process. As a result, having co-registered angiography and LGE images would greatly simplify - image processing and improve assessment of myocardial scar.

While angiography and scar images are currently acquired using different sequences, both sequences often nearly image the same field of view and are focused on enhancing T1 contrast. The major difference in the two sequences is the time at which these sequences are acquired – the angiography sequence is acquired immediately after contrast infusion while the LGE sequence is acquired 10-20 minutes post-contrast. This suggests that a whole-heart, T1-weighted sequence can be used to continuously image the heart to acquire both angiography and LGE images.

The purpose of this work was to develop a sequence which would combine acquisition of angiography and LGE by sharing k-space from the angiography images to the LGE images to decrease the amount of time needed to acquire a full LGE k-space set and provide inherently co-registered images.

5.2 Methods

The Siemens Integrated Development Environment for Application and Image Calculation Environment (IDEA/ICE) interface was used to develop the pulse sequence and image reconstruction programs that were later exported to the clinical scanners for debugging and application.

5.2.1 Sequence Theory

The combined sequence was based off a 3D, whole heart, ECG- and navigator-gated, inversion recovery fast low-angle shot (FLASH) sequence (65). The base sequence

parameters were: TR = 3.3 ms, TE = 1.49 ms, flip angle = 15°, inversion time = 200 ms, readout bandwidth = 610 Hz/pixel, and number of segments per heartbeat = 47. 70 – 100 partitions with voxel size 1.3 x 1.3 x 1.5 mm^3 were acquired and interpolated to 140 – 200 partitions with 0.64 x 0.64 x 0.75 mm^3 voxel size. The generalized autocalibrating partially parallel acquisitions (GRAPPA) technique was used for parallel imaging for a phase acceleration factor of 2. The total scan time was 4.19 minutes assuming 100% navigator efficiency with a heart rate of 71 beats per minute (bpm).

K-space is acquired using a centric reordering scheme to acquire the center frequencies during the initial slow infusion gadolinium for maximum blood SNR. After k-space acquisition is completed (~10 minutes after contrast infusion), contrast will have diffused into regions of myocardial scar and a portion of the center of k-space will be re-acquired with a reverse-centric reordering to create an LGE image (Figure 5.1). The angiography images (SharK1) will use the initially acquired center portion of k-space during contrast infusion while the LGE images (SharK2) will use the re-acquired center portion of k-space. The outer portion of k-space will be shared between both sets of images.

5.2.2 Pulse Sequence Development

The CV_nav sequence provided by Siemens Healthcare (Erlangen, Germany) was used as a starting point for sequence development. The k-space reordering was modified from a linear-ordered partition to a centric-ordered partition to acquire the majority of image contrast during maximal concentration of gadolinium in the blood. The sequence "`RunLoopLength`" was modified to allow re-acquisition of centric k-space after the

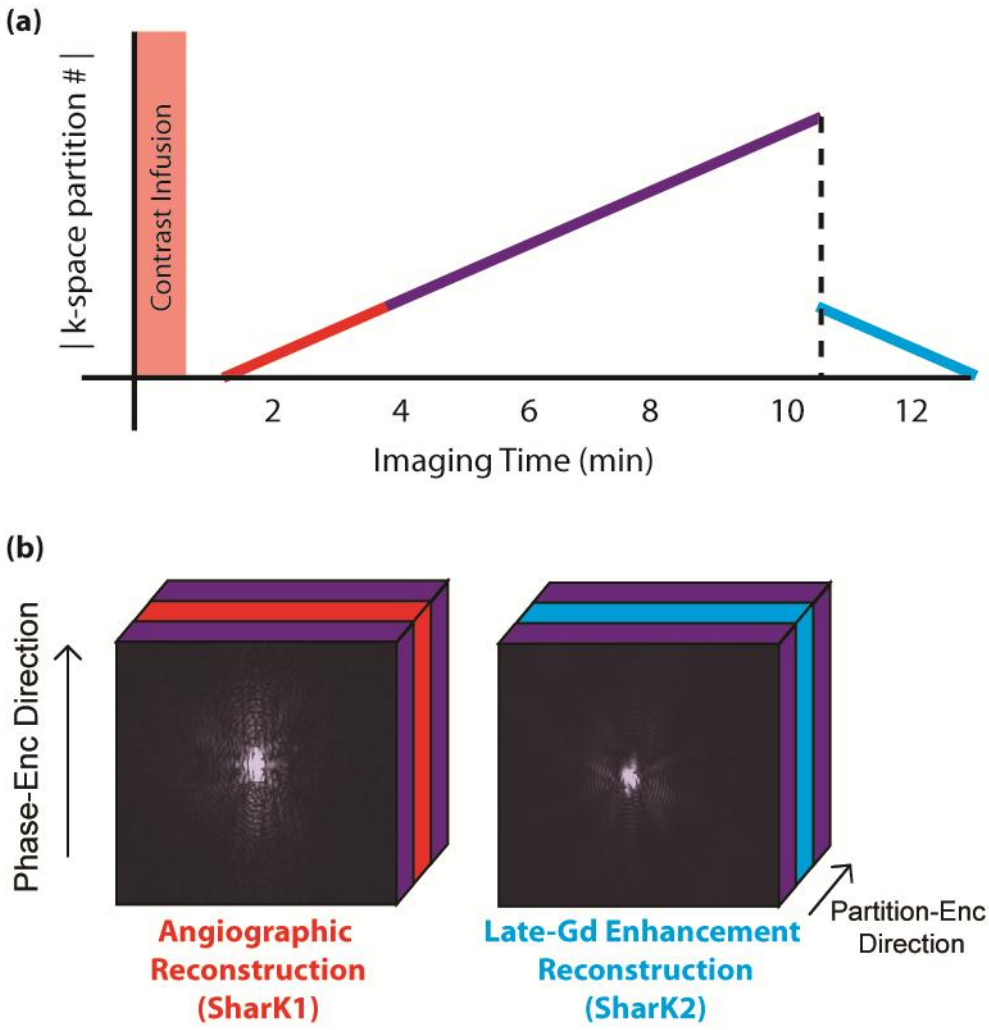

Figure 5.1 Shared K-space (SharK) sequence. Top: K-space partition acquisition is shown versus time. Centric k-space is acquired during slow infusion of contrast and again after full acquisition of k-space. Bottom: Reconstruction methodology used to create angiographic and LGE images. The initially acquired centric k-space (red) is used for the angiographic reconstruction while the later acquired centric k-space (blue) is used for the LGE reconstruction. Outer k-space (purple) is shared between the two images

initial full k-space coverage. Dummy pulses were added at the beginning of the sequence for T1-equilibration. Two options for shared k-space acquisitions were implemented. Users could determine the number of extra centric partitions to acquire as a partial acquisition or directly after the full k-space coverage. The "IDA" dimension from the measurement data header was used to differentiate the initial k-space coverage from the

extra k-space partitions. Initially, an IDA value of “0” was used for all lines acquired in the initial k-space coverage while an IDA value of “1” to combine acquisition of partial k-space in the same sequence. Future versions did not change the IDA value but instead required separate measurements to allow for different inversion times in between acquisitions.

5.2.3 Image Reconstruction

An ICE program was developed based on the original image reconstruction program for online k-space sharing. This image reconstruction program acts as a pipeline, sending k-space lines through a pipeline, in which each part of the pipeline has a specific function, (e.g., Partition Fourier Transform, Phase Encode Filters) called functors. A Parc Data Storage (PDS) functor was created to store k-space to memory during angiography imaging and pull k-space from memory during LGE imaging. A zero-padding functor was added to initialize the missing partitions in a partial acquisition and acted as a fail-safe in case no data was stored in the PDS.

5.2.4 Combined Angiography and LGE Validation

After development of the pulse sequence and the image reconstruction pipeline for the SharK sequence, it is necessary to validate that the changes that were made were executed by the program. Experiments were carried out to validate: (1) proper k-space trajectory, (2) proper sharing of k-space by the modified ICE program, (3) the necessity for to have “dummy” pre-pulses, and (4) accurate execution of the reordering scheme.

5.2.4.1 K-Space Trajectory Validation

The sequence simulator and protocol editor, POET, was used to validate sequence functionality to ensure that extra partitions were acquired appropriately. Each partition and line number was output during simulation to a text file and the results were plotted to validate the number of partitions acquired and the reordering scheme.

5.2.4.2 Shared K-space Validation

The image reconstruction pipeline was validated by imaging a static phantom with the SharK sequence: once for full "angiographic" k-space data and once for partial "LGE" k-space data that shared the initial "angiographic" k-space data. Another full set of k-space was acquired afterwards to determine the image variance between acquisitions. Images were compared by calculating the mean pixel-by-pixel absolute differences based on normalized images (Figure 5.2).

5.2.4.3 Dummy Pulse Validation

Dummy pulses force the T1 magnetization to reach a steady-state before data acquisition beings and they prevent sharp changes in k-space that can cause ghosting. To validate the necessity to use dummy pulses to reach T1-equilibration for centric-ordered partition encoded sequences, full k-space coverage was acquired using with and without dummy pulses. Additionally, full k-space coverage was acquired with a TR = 1 or 2 seconds and the resulting images were compared.

5.2.4.4 Reordering Validation

The k-space reordering scheme can play a large role in the CNR of the image for angiography sequences. The k-space trajectory was validated in order to confirm that acquiring centric-ordered partitions increased SNR when compared to linear-ordered

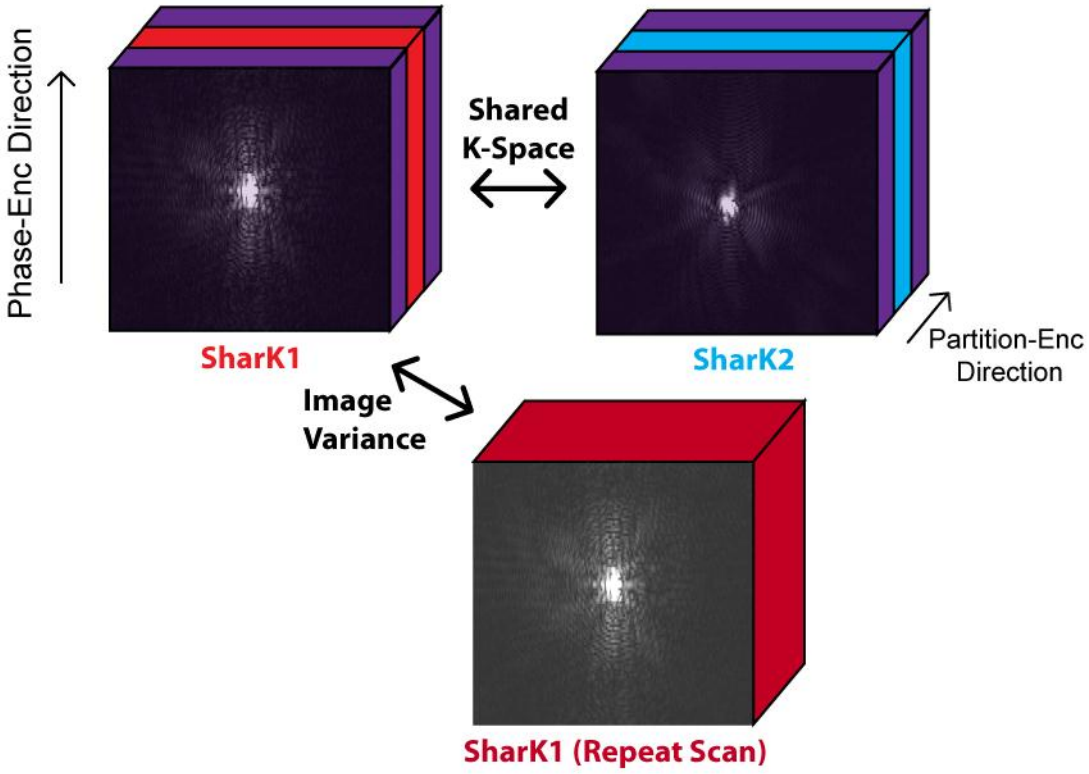

Figure 5.2 Shared K-Space validation. The SharK sequence will be acquired on a static phantom, and the two reconstructions (SharK1/SharK2) will be compared against each other. Image variance will be determined by repeating the first part of the SharK sequence for a new full set of k-space.

partitions. This was achieved by diluting a bottle containing an initial mixture of 1:500 ratio of water to gadolinium (MultiHance, Bracco Diagnostics, Princeton, NJ) with a flow pump running at 2 mL/s and imaging the intensity of the bottle at three time points: before flow, during flow, and after flow. The ECG-gated, inversion-recovery gradient echo sequence was used for imaging. Gating was performed with an artificial trigger using the IdeaCmdTool interface. Sequence parameters were: TR = 3.88 ms, TE = 1.9 ms, TI = 70 ms, FA = 12°, 11 segments per cardiac cycle. Four different reordering schemes were tested:

(1) linear-ordered phase encoding/linear-ordered partition encoding

(2) centric-ordered phase encoding/linear-ordered partition encoding

(3) linear-ordered phase encoding/centric-ordered partition encoding

(4) centric-ordered phase encoding/centric-ordered partition encoding

The pixel intensity of the initial mixture represents the maximum possible intensity due to contrast and was used to determine what percent of maximum intensity was achieved during flow with the respective reordering scheme. SNR was calculated by dividing the standard deviation from the mean from a sampled region-of-interest (ROI).

5.3 Results

5.3.1 Pulse Sequence and Image Reconstruction

The pulse sequence was successfully modified using the IDEA platform. The Sequence Special card was used to set all parameters related to the SharK sequence (Figure 5.3). The "SharK Reordering" checkbox activated the centric-ordered partition scheme. The "PartialSharK" modified the sequence to only acquire a partial set of k-space, as determined by the "# of Extra Pars". Since the pulse sequence cycles through each partition in full, the "# of Dummy Pulses" was limited to a multiple of *Base Resolution / Segments per Cardiac Cycle* to minimize sequence modification. The "IceSharKPDS Program" checkbox controlled whether the custom image reconstruction pipeline including the PDS would be used or whether the standard image reconstruction pipeline would be used.

The image reconstruction pipeline was successfully modified to use the PDS for k-space storage and retrieval (Figure 5.4). The custom functor, IceSharKPDSScanFunctor", was programmed to save the centric "# of Extra Pars" as set by the user to the PDS if

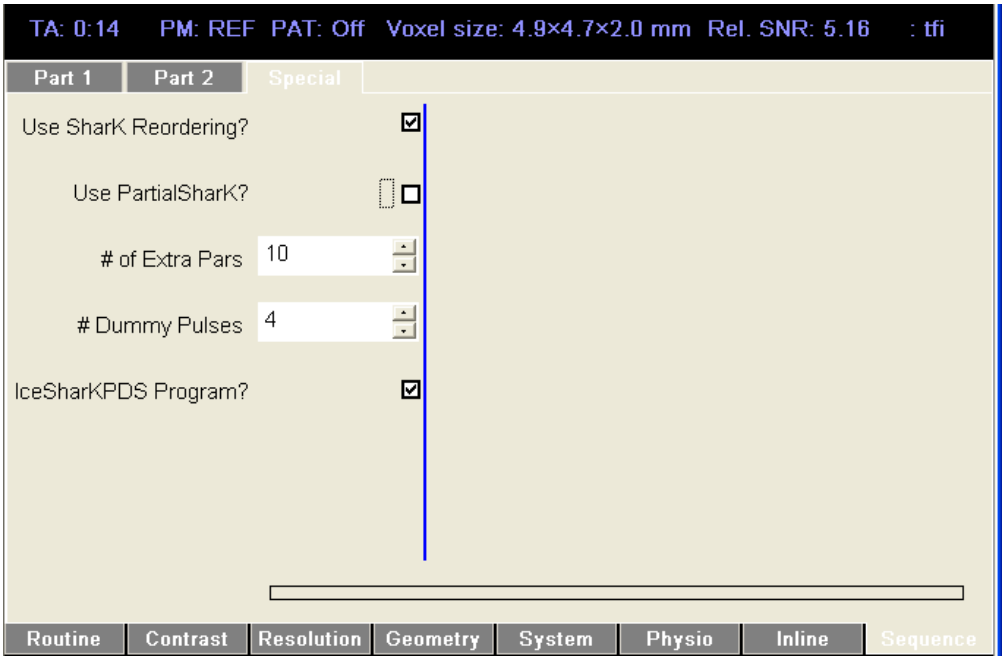

Figure 5.3 Sequence card showing UI parameters to control SharK sequence. Users can turn the reordering on/off, control whether a partial acquisition is performed, set the number of extra partitions to acquire for the partial acquisition, the number of dummy pulses, and whether to use the custom built IceProgram.

Figure 5.4 Ice Pipeline for image reconstruction. The added IceSharKPDSScanFunctor saves k-space from the angiographic data in the Parc Data Storage (PDS) and retrieves it when a partial SharK is acquired for the LGE reconstruction.

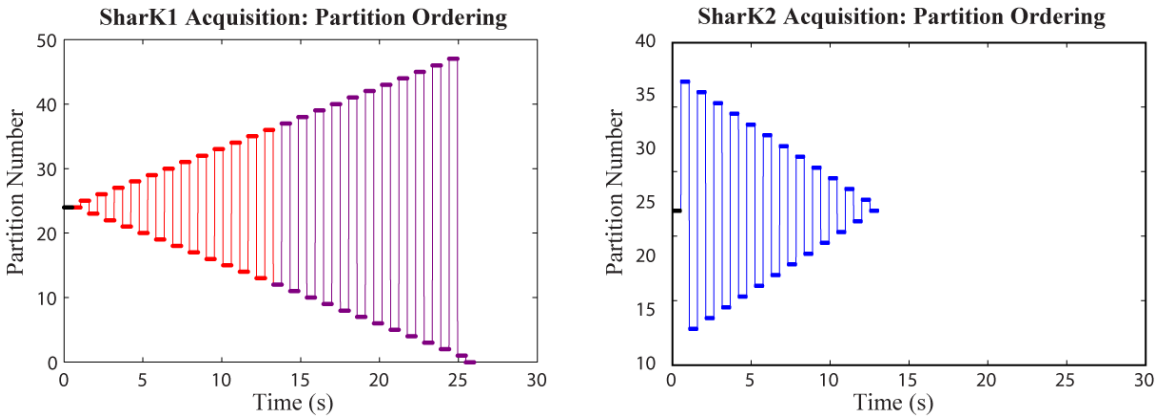

Figure 5.5 Validation of SharK sequence reordering using 48 partitions. (Left): The regular SharK (SharK1) acquisition acquires all partitions with a centric-ordering. Central partitions are acquired first (red) and then outer partitions are acquired (purple). (Right): A partial SharK (SharK2) acquisition only acquires a portion of central k-space in the reverse centric direction (blue). The outer partitions are shared from SharK1 to SharK2 to create a full set of k-space. Dummy pulses are acquired at the beginning of both sequences (black).

PartialSharK was not checked for angiography imaging and to retrieve the centric "# of Extra Pars" if PartialSharK was not checked for LGE imaging. Partial acquisitions were zero-padded in the case that no k-space was saved previously during a PartialSharK acquisition.

5.3.2 K-Space Trajectory Validation

The pulse sequence was validated using the POET sequence simulation feature (Figure 5.5). The original sequence was changed to have a centric-reordering for angiographic k-space acquisition and reverse-centric reordering for the partial LGE k-space acquisition. Dummy pulses are acquired at the beginning of the sequence but are not used in the image reconstruction.

5.3.3 Shared K-Space Validation

Imaging a static phantom with the SharK sequence and reconstruction revealed no qualitative differences between the angiography (SharK1) and LGE (SharK2) images

(Figure 5.6). The normalized absolute image difference between repeat scans showed a range of ± 10% difference, with an average absolute difference of 0.68% (Figure 5.7). The range of the normalized absolute image difference between the two reconstructed SharK images was ± 8% with an average absolute difference of 0.62%, within the range and absolute difference of the repeat scans, validating the image reconstruction pipeline.

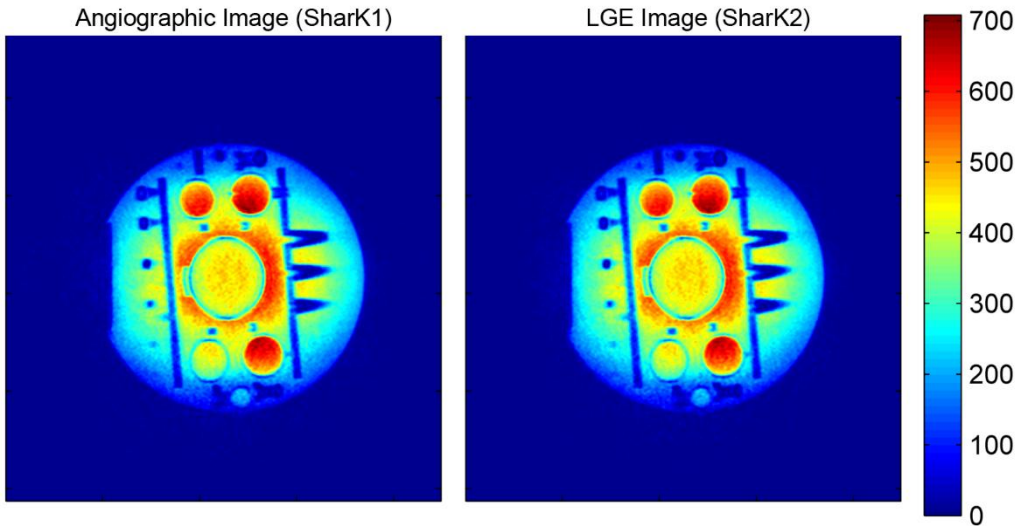

Figure 5.6 Angiographic (SharK1) and LGE (SharK2) images are shown above. Since the phantom does not change over time, both SharK1 and SharK2 are the same.

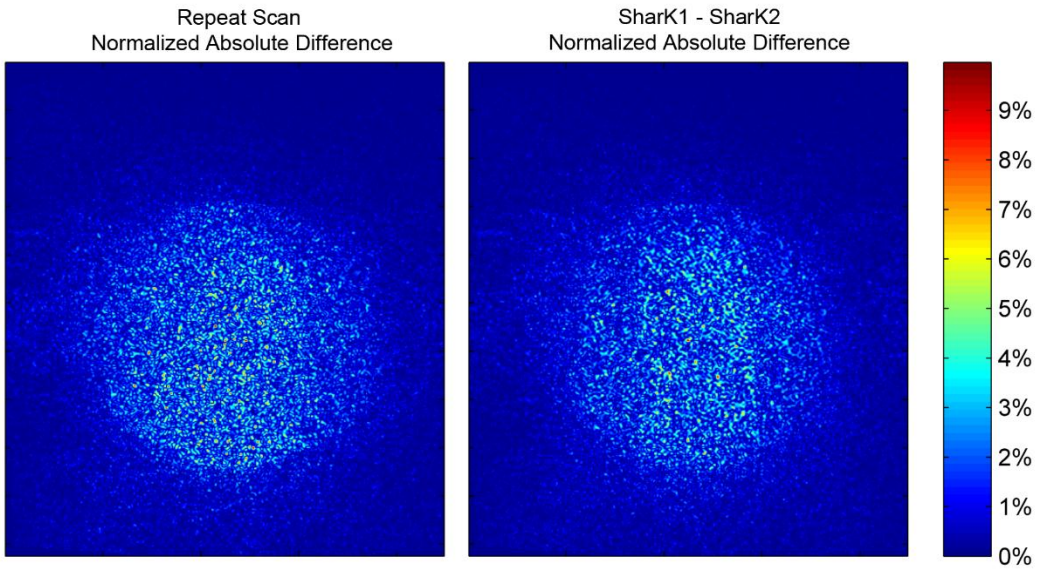

Figure 5.7 Normalized absolute differences between two repeat scans and SharK1 – SharK2 reconstructions. Image variance between two repeat scans falls in the range between the two SharK reconstructions, validating the image reconstruction pipeline.

5.3.4 Dummy Pulse Validation

Significant ghosts appeared only when using a centric-ordered partition encoding scheme. When compared to the original linear-ordered partition encoding scheme, the ghosting appeared when TR = 1 s but disappeared when TR = 2 s (Figure 5.8). This suggested that ghosting was a result of acquiring the center of k-space before the magnetization had reached a steady state. Extending the TR = 2 s allowed sufficient time for the magnetization to recover to its original state before continuing acquisition. This issue was resolved by using three dummy RF pulses and fake acquisitions to ensure T1 equilibration before starting to acquire k-space. Since the loop structure of the pulse sequence does not allow acquisition of a partial partition, a minimum of one partition must be acquired as a dummy partition before moving on to the actual acquisition.

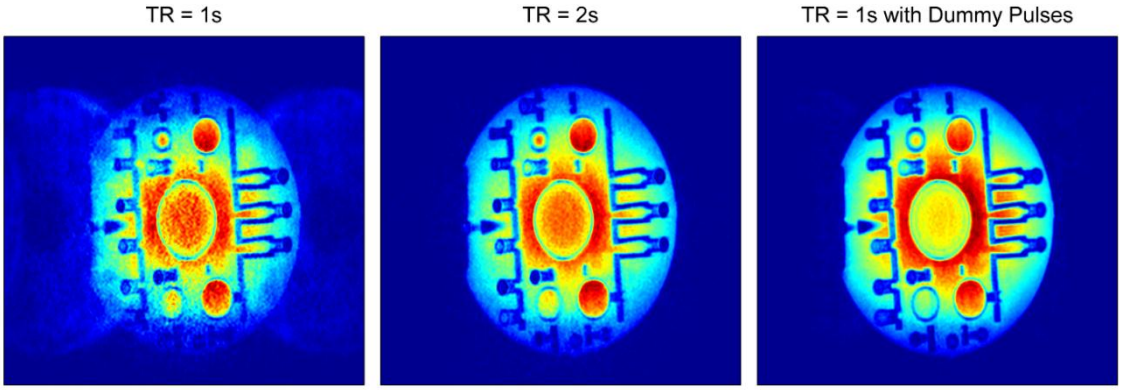

Figure 5.8 (Left-to-Right) 1 second TR, 2 second TR, and 1 second TR with dummy pulses. All images are acquired with centric-ordered partition encoding reordering scheme. Ghosts can be seen in 1 second TR due to lack of T1 equilibration before acquisition of k-space center.

5.3.5 Reordering Validation

The four combinations of reordering schemes:

(1) linear-ordered phase encoding/linear-ordered partition encoding

(2) centric-ordered phase encoding/linear-ordered partition encoding

(3) linear-ordered phase encoding/centric-ordered partition encoding

(4) centric-ordered phase encoding/centric-ordered partition encoding

were successfully imaged at all three time points: baseline, during flow, and post-flow (Figure 5.9). The centric-phase encoding linear partition-encoding case was repeated twice while all other cases were repeated three times. A region of interest was selected to determine the average intensity at each time point. All intensities were normalized to the average intensity from baseline. Results showed that regardless of phase-encoding scheme, using a centric-ordered partition reordering scheme resulted in an approximate 10% increase in SNR when compared to a linear-ordered partition reordering scheme. The centric phase-encoding, centric partition-encoding schema retained ~95% of the maximum SNR when compared to the initial intensity and was the best reordering choice for imaging.

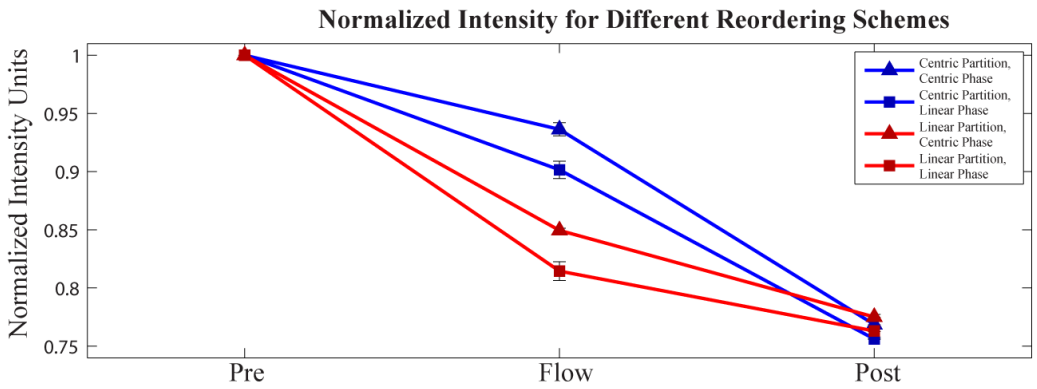

Figure 5.9 A bottle with doped gadolinium was diluted with a constant flow rate to determine the optimal reordering scheme for angiographic imaging. Imaging was performed before flow (pre), during flow (Flow), and after flow (post). Intensities are normalized against pre-flow pixel intensity values.

5.4 Discussion

We successfully modified the base pulse sequence to create the SharK sequence and successfully uploaded and executed the sequence on the clinical MRI. We validated the modified image reconstruction, centric-ordered partition encoding reordering as well as proving the necessity for additional dummy pulses when using a centric partition encoded reordering scheme. The images that result from applying this sequence on a static phantom result in images nearly identical to standard full k-space acquisitions, showing that the image reconstruction properly shares outer k-space between the two reconstructions. Flow experiments demonstrated ~10% increase in SNR when switching from a linear-ordered partition encoding scheme to a centric-ordered partition encoding scheme. Lastly, the presence of ghosts was reduced when adding dummy pulses to allow T1-eqilibration before acquiring data.

The increase in SNR gained from using a centric-ordered partition-encoded sequence is expected when compared to linear-ordered partition-encoded sequences as the center of k-space contains the DC component, and imaging this component at higher concentration

would naturally result in higher signal intensities. In addition, the small differences between centric-ordered phase encoding sequences and linear-ordered phase encoding sequences are expected due to the minor differences in the acquisition of the true center of k-space which is more dependent on the acquiring at the center partition location as opposed to the center phase location.

Most current MR angiography sequences use an elliptic centric reordering for k-space acquisition. This ordering starts acquisition at the center of 3D k-space and spirals outwards in the phase and partition directions equally. This reordering scheme has shown favorable results for angiography imaging of the renals and carotids (79,80). We opted to use a centric-ordered partition encoding, centric-ordered phase encoding for the SharK sequence for ease of modification in both the pulse sequence development and image reconstruction environments.

The use of dummy pulses for T1 equilibration before acquiring the center of k-space is expected as sharp changes in magnetization in the frequency domain near the center of k-space would result in ghosts in the image domain. As images are typically acquired using linear-ordered partitions, magnetization reaches a steady state by the time the sequence acquires the center of k-space, making T1-equilibration in linear-ordered partition encoded sequences unnecessary.

Dummy pulses have been used previously to drive the system to equilibrium before image acquisition. This is especially important in sequences that use variable flip angles throughout the sequence as this prevents the system from ever reaching the steady-state equilibrium (81). In this case, up to 16 dummy pulses may be used. In the case of the

SharK sequence, 3-4 dummy pulses are usually performed before image acquisition and is sufficient to reach steady-state due to the lower flip angle compared to other sequences.

5.4.1 Limitations

There were limitations in this work. It is important to note that the dilution experiments to compare the effect of different reordering schemes is a vast simplification of true dilution of gadolinium contrast in the body as the bottle used in the experiment represents only a single compartment that lacks any convective transport of gadolinium. In addition, the dilution rate in the flow experiment decreases in concentration at a rate 1/t (where t is the time from the start of dilution) as opposed to physiological dilution of gadolinium, which follows an exponential decrease in signal (82). However, similar or better gains can be expected when using a centric-ordered partition encoding direction in humans due from this sharper exponential decrease in gadolinium concentration after the initial infusion due to increased mass transport resulting from convective transport of gadolinium through the bloodstream. Improvements in SNR also increase blood-myocardial CNR, allowing more accurate myocardial or atrial wall segmentation.

5.5 Conclusion

We were able to develop a combined angiography and LGE SharK sequence by acquiring the center of k-space twice and sharing outer k-space between the two image sets. SNR were maximized by using a centric-ordered partition encoding, centric-ordered phase encoding reordering schemes. Dummy pulses were necessary at the beginning of the sequence for T1-equilbration before beginning k-space acquisition to minimize

ghosting. The LGE portion of the SharK sequence will subsequently be validated against a gold standard before use of the developed sequence in patients.

Chapter VI

Application of SharK Sequence on Patients with Myocardial Infarction

6.1 Introduction

MRI is capable of identifying myocardial scar by late gadolinium enhancement (LGE) imaging. In the standard clinical protocol, patients are given an intravenous dose of a gadolinium-based contrast agent that accumulates into regions of scar 10-15 minutes post-contrast injection due to increased extracellular space and decreased washout kinetics in scar tissue. The current gold standard for LGE imaging is a 2D, breath-held phase sensitive inversion recovery (PSIR) sequence. Multiple slices are acquired in the short- and long-axis orientation over the LV. While 2D PSIR images are currently the gold standard for LGE, there are multiple limitations to the sequence. The differences in respiratory position, image resolution, and image orientation make LGE images difficult to co-register to angiography images. In addition, slices are typically ~7 mm thick, limiting the ability to resolve scar.

The developed SharK sequence overcomes many of the limitations of the 2D, breath-held PSIR sequence by using the same sequence for both angiography and LGE imaging. This creates inherently co-registered angiography and LGE images such that coronary vein maps can be directly overlaid on top of transmurality scar maps to allow pre-procedural planning for CRT. As the angiography and LGE images acquire the same field

of view but are acquired at different times, it is possible to share k-space between the two acquisitions to reduce imaging time. However, as more of outer k-space is shared from the angiography images to the LGE images, LGE contrast and edge sharpness decrease due to the lack of higher frequencies related to LGE. This raises an important question: How much k-space can be shared between angiography and LGE images while still maintaining adequate scar characterization?

The purpose of this chapter is to determine the tradeoff between the amount of k-space that can be shared between angiography and LGE images and sequence acquisition time. This will be achieved by imaging patients with known previous myocardial infarction and acquiring two sets of k-space from the 3D inversion recovery navigator-echo gated sequence to create a range of retrospective Shared K-space LGE image stacks with various degrees of shared k-space data that can be used for analysis.

6.2 Methods

6.2.1 PreSERVE Study

Patients were obtained from an ongoing trial at Emory University Hospital aiming to provide an intravenous dose of mesenchymal bone marrow cells in patients with ST segment elevated myocardial infarction (STEMI). To be eligible for the study, patients must have been diagnosed with STEMI symptoms in the emergency room and have successful reperfusion by percutaneous coronary intervention within 12 hours. The patient's LVEF must be $\leq 45\%$ as measured at most 24 hours post-reperfusion for study eligibility. Eligible patients received a 1.5T MRI to evaluate cardiac function and infarct size.

6.2.2 MR Protocol

Four patients from the PreSERVE study received a contrast MRI exam (1.5T Avanto, Siemens Healthcare, Erlangen, Germany). Additional MR sequences inserted into the original protocol to acquire respiratory-gated angiography and LGE images. A slow infusion of contrast (0.2 mmol/kg @ 0.3 mL/s) was administered, and a 3D, contrast-enhanced, navigator- and ECG-gated, inversion recovery FLASH sequence was acquired twice – once 45 seconds to 1 minute after contrast injection, and again 20 – 25 minutes after contrast injection. 52 partitions were acquired in a transverse orientation over the region of scar with a centric-ordered phase encoding, linear-ordered partition encoding reordering and interpolated to 104 final partitions for partial coverage of the heart. A 2D breath-hold PSIR sequence was acquired in the short-axis orientation along the length of the LV 10 – 15 minutes after contrast injection.

6.2.3 Retrospective Reconstruction

Raw data was available for three out of four patients for retrospective SharK reconstruction; the fourth data set appeared corrupt from improper data transfer. 3D SharK LGE images were created by developing an ICE program that shared partitions during offline retrospective reconstruction. The `wipMemBlock.alFree[]` parameters could be changed before reconstruction to control the percentage of centric partitions that would be sent to the PDS when reconstructing the 3D LGE image stack. The angiography reconstruction would then obtain the saved partitions from the PDS and replace the corresponding central partitions from the PDS partitions to create the 3D SharK LGE image stack (Figure 6.1). Different percentages (1/8, 2/8s, 3/8s, etc…) of k-space were

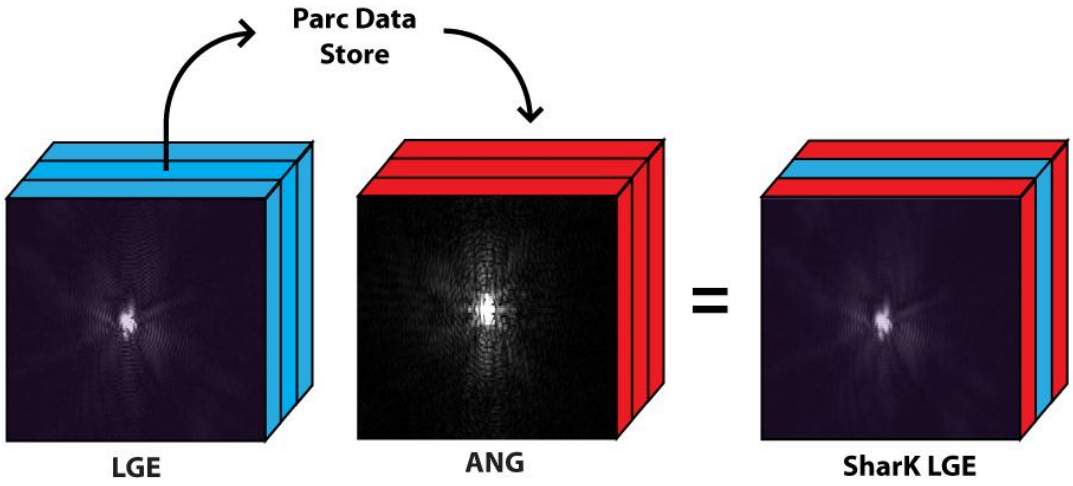

Figure 6.1 Ice pipeline showing retrospective reconstruction of SharK LGE image stacks. Different amounts of central k-space were saved in the Parc Data Store to create a range of SharK LGE reconstructions.

retrospectively shared between the first and second acquisitions to create the 3D SharK LGE image. A higher SharK percentage represents a greater percentage of shared k-space between angiography and LGE acquisitions, decreasing the number of LGE partitions that would need to be re-acquired after the angiography images.

6.2.4 Myocardial Segmentation

Software was developed to project the transverse angiography/LGE images and SharK LGE images onto the AHA 17-segment bullseye. All transverse images were reformatted to the short-axis orientation by using the image orientation information and a linear interpolation algorithm. Endo/epicardial borders were segmented on the reformatted angiography images. The endocardium was manually segmented. The epicardial border was segmented by dilating the endocardial border and then manually refining the edges. The myocardium was extracted by subtracting the endocardial border from the epicardial border. 3D LGE images were registered to the angiography images

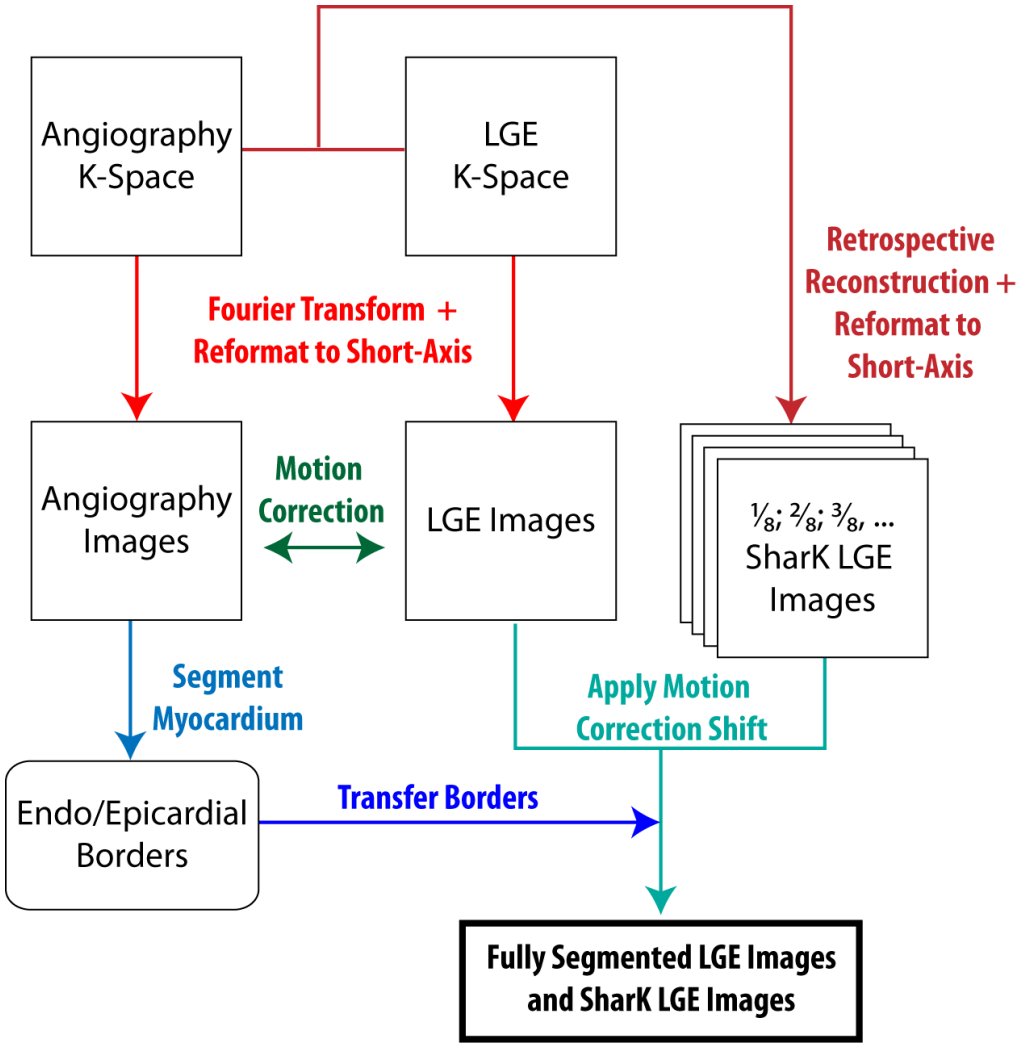

Figure 6.2 Flowchart showing steps for myocardial segmentation of LGE/SharK LGE images.

to correct for motion by finding the maximum 3D cross-correlation. Borders were then directly transferred from the angiography images to all LGE/SharK LGE image stacks (Figure 6.2). The endo/epicardial borders were segmented manually on the 2D, short-axis PSIR images.

6.2.5 Scar and Coronary Vein Projection to AHA Bullseye

Radial spokes separated by 1° were drawn outwards from the centroid of each LV epicardial slice. The myocardial pixels that the spokes passed over were determined using

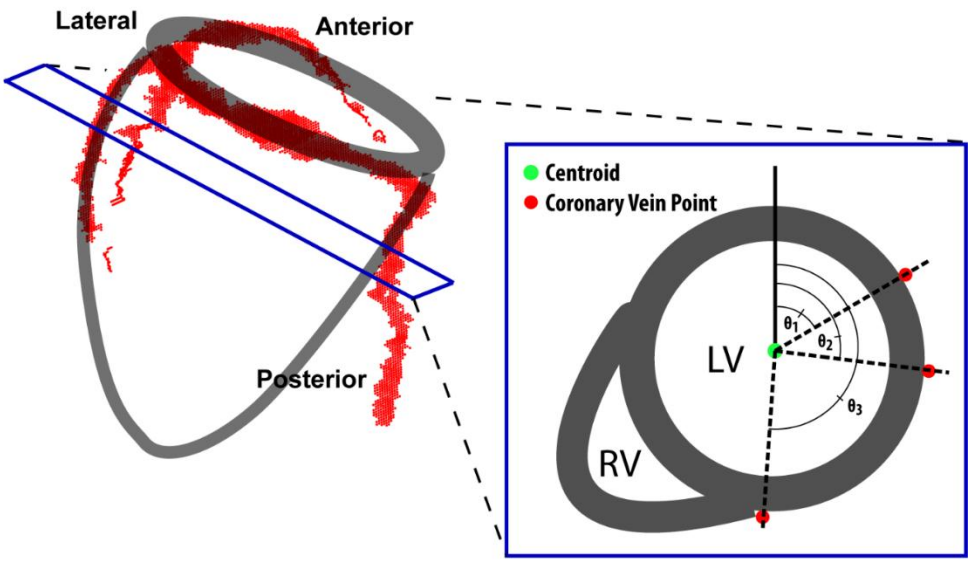

Figure 6.3 The closest short-axis slice to the coronary vein point determines the r-coordinate on the AHA bullseye. The angle of the coronary vein points as determined from the centroid of the LV determines the θ-coordinate on the AHA bullseye

a nearest-neighbor algorithm. A scar threshold was set by selecting a segment of healthy myocardium and calculating two standard deviations above the mean intensity value of the segment. Myocardial pixels above this intensity were considered scar. The same segment was selected across all LGE and LGE-SharK image stacks for thresholding. Transmurality was calculated by dividing the percentage of the radial spoke that was scar by the total length of the radial spoke. Transmurality values were then projected onto the 17-segment AHA bullseye. The coronary veins were manually selected on the transverse coronary vein images to produce a point cloud in 3D. The polar (r,θ) coordinates of each point in the coronary vein point cloud was calculated separately. The closest short-axis slice to each point determined the radial (r) distance on the bullseye. The point relative to the centroid of corresponding short-axis slice was used to determine the angular (θ) location of the coronary veins on bullseye (Figure 6.3). The coronary vein points were plotted on the AHA scar bullseye.

6.2.6 3D FLASH LGE vs 2D PSIR

Scar identified on reformatted 3D FLASH LGE images was compared to scar identified on 2D PSIR-LGE images. The resulting scar bullseyes for the 2D PSIR LGE images, 3D FLASH LGE images, and 3D FLASH LGE images without motion correction were also visually compared.

6.2.7 3D FLASH LGE VS 3D SharK LGE

The complete 3D FLASH LGE images were compared to all SharK LGE reconstructions, with the complete 3D FLASH LGE image stack as the standard. The following parameters were calculated for comparison:

i. The total scar volume for all SharK LGE reconstructions was calculated, and the absolute error was calculated against the original LGE image stack by Eq 6-1:

$$\frac{|ScarVol_{FLASH\ LGE} - ScarVol_{SharK\ LGE}|}{ScarVol_{FLASH\ LGE}} \times 100\% \qquad \text{(Eq 6-1)}$$

ii. A pixel-to-pixel comparison was performed on the myocardial pixels of LGE images compared against the corresponding myocardial pixels on SharK LGE images. All myocardial pixels were classified as scar or healthy based on whether the pixel intensity was greater than the scar threshold. This allowed the creation of a 2x2 contingency table to perform a sensitivity and specificity analysis on a per pixel basis.

iii. Scar bullseyes for the LGE image was compared against scar bullseyes for each SharK LGE reconstruction. Myocardial spokes on all bullseyes were classified as non-viable myocardium (< 50% transmural spoke) or viable myocardium (> 50% transmural spoke) to allow creation of a 2x2 contingency table. Sensitivity and

specificity were also calculated to assess scar bullseye spoke viability of the full LGE images compared against all the SharK LGE reconstructions.

Results were used to determine the amount of k-space that can be shared between angiography and LGE images while maintaining accuracy of scar detection.

6.2.8 Combined Myocardial Scar and Coronary Vein Maps

The motion correction performed during segmentation to co-register angiography and LGE FLASH images allows the coronary vein maps to be directly superimposed on top of and myocardial scar maps. This allowed a combined coronary vein and myocardial scar displays that could be used for LV lead planning prior to CRT implantation.

6.3 Results

All angiography and LGE image stacks were successfully reformatted to the short-axis orientation for myocardial segmentation (Figure 6.4). While there was excellent contrast between the myocardium and blood on the angiography images, early enhancement was also visible on the angiography images that later became LGE scar, though the region of early enhancement appears larger than the scar enhancement on the LGE images. The scar location was anteroseptal in three patients and posterolateral in one patient.

6.3.1 3D FLASH LGE vs 2D PSIR

Comparing the 3D LGE-FLASH to the 2D LGE-PSIR images shows marked similarities between regions of anteroseptal scar, but the higher resolution of the 3D LGE-FLASH images afford the ability to clearly demarcate the border of the scar zone

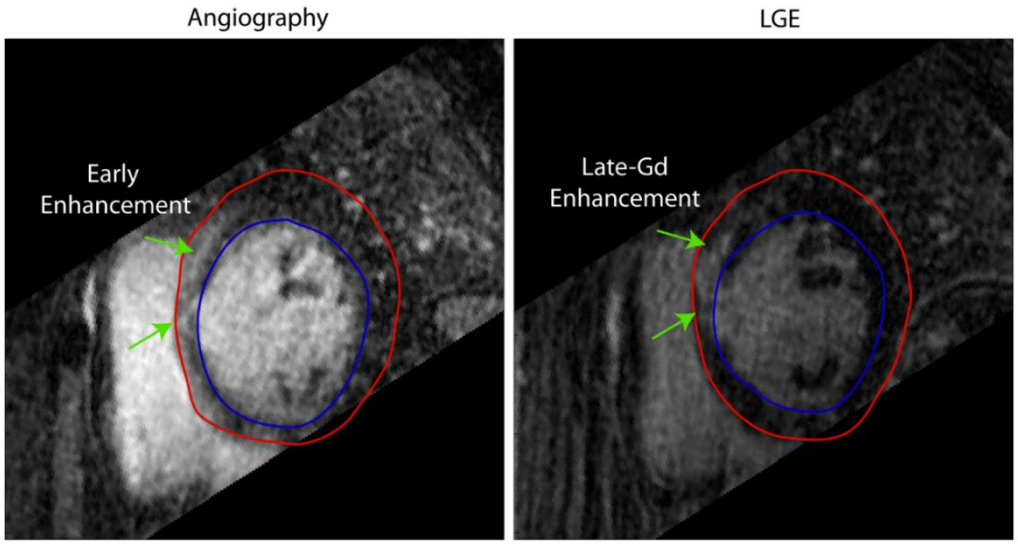

Figure 6.4 Angiography (left) and LGE (right) mid short-axis slice acquired during diastole in the PreSERVE patient study. Blue/red contours represent endo/epicardial borders Green arrows notate regions of early enhancement on the angiography images and late gadolinium enhancement or scar on the LGE images.

(Figure 6.5). The 3D LGE-FLASH bullseye without motion correction shows significant differences in regions of enhancement and healthy myocardium due to false inclusion of the blood pool and missed enhancement in the myocardium segmentation, verifying the need to correct for motion between angiography and LGE image stacks even though both images use the same sequence repeated at different times. This need for registration can be attributed to differences in the gated respiratory position or patient movement between acquisitions.

6.3.2 3D FLASH LGE vs 3D SharK LGE

Seven SharK LGE image stacks were retrospectively reconstructed for each patient and projected onto the AHA bullseye (Figure 6.6). The percentage of shared k-space was incremented by $1/8^{th}$ for each reconstruction from 12.5% to 88.5% SharK. While the SharK bullseyes look qualitatively similar, differences can be seen at the edges of the

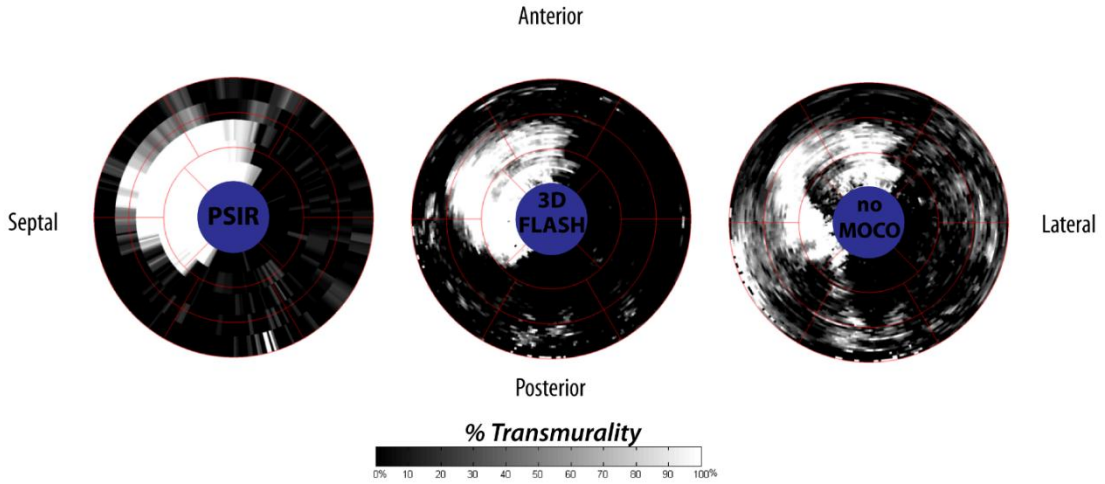

Figure 6.5 Bullseye comparison of 2D PSIR/clinical standard (left), 3D FLASH (middle), and 3D FLASH without motion correction (right). Distinct transmural similarities can be seen between the 2D PSIR and 3D FLASH bullseyes. The 3D FLASH without motion correction shows multiple regions of false scar transmurality, demonstrating the need to correct for movement between angiography and LGE scans before transferring endo/epicardial borders.

regions of scar (Figure 6.7). As more k-space is shared between acquisitions, the edges of scar become further blurred.

The absolute error in scar volume was calculated for all LGE and SharK reconstructions (Figure 6.8). The absolute error is approximately 2 ± 1% for all image stacks with less than 50% Shared K-space, but the absolute error and variation increases for image stacks sharing 50% of k-space and then increases sharply for image stacks sharing greater than 75% of k-space.

A pixel-by-pixel analysis between the original LGE image stack and all SharK LGE reconstructions was performed to assess the effect of Shared K-Space on LGE imaging (Figure 6.9). Sensitivity, or the percentage of correctly identified scar pixels, initially decreases linearly by approximately 3.5% for additional 12.5% of shared k-space. Specificity, or the percentage of correctly identified healthy myocardial pixels, decreased

linearly by approximately 0.5% for each additional 12.5% of shared k-space but was above 95% specificity for all SharK LGE image stacks.

Scar bullseyes were compared between the original LGE image stack and all SharK reconstructions. Sensitivity and specificity scores were calculated by spokes as nonviable or viable myocardium, where sensitivity and specificity define the percentage of myocardial spokes that are correctly labeled as non-viable and viable myocardium respectively as compared to the original LGE image stack (Figure 6.10). Sensitivity initially linearly decreases until 37.5 – 50% Shared K-space to 90% sensitivity, at which there is an inflection point. Sensitivity subsequently decreases more sharply when more than 75% k-space is shared between acquisitions. Specificity scores were near 100% across all SharK reconstructions as the majority of the left ventricle is viable myocardium, showing that there are very few "false negatives" or myocardial spokes that are falsely labeled as non-viable myocardium.

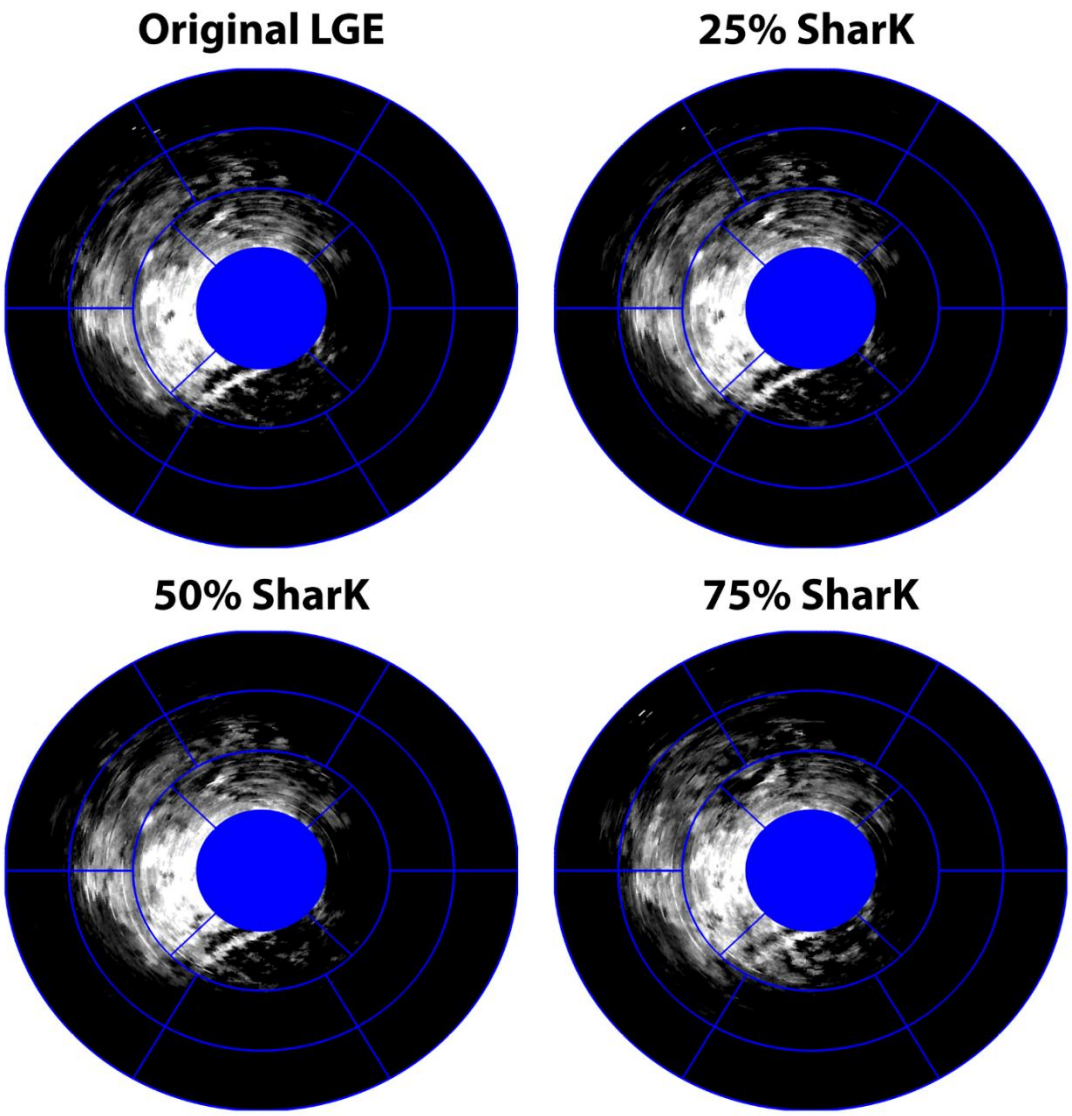

Figure 6.6 AHA bullseyes corresponding to the original LGE image stack and three SharK reconstructions. While bullseyes qualitatively look similar, the edges of scar appear more blurred as the percentage of shared k-space increases.

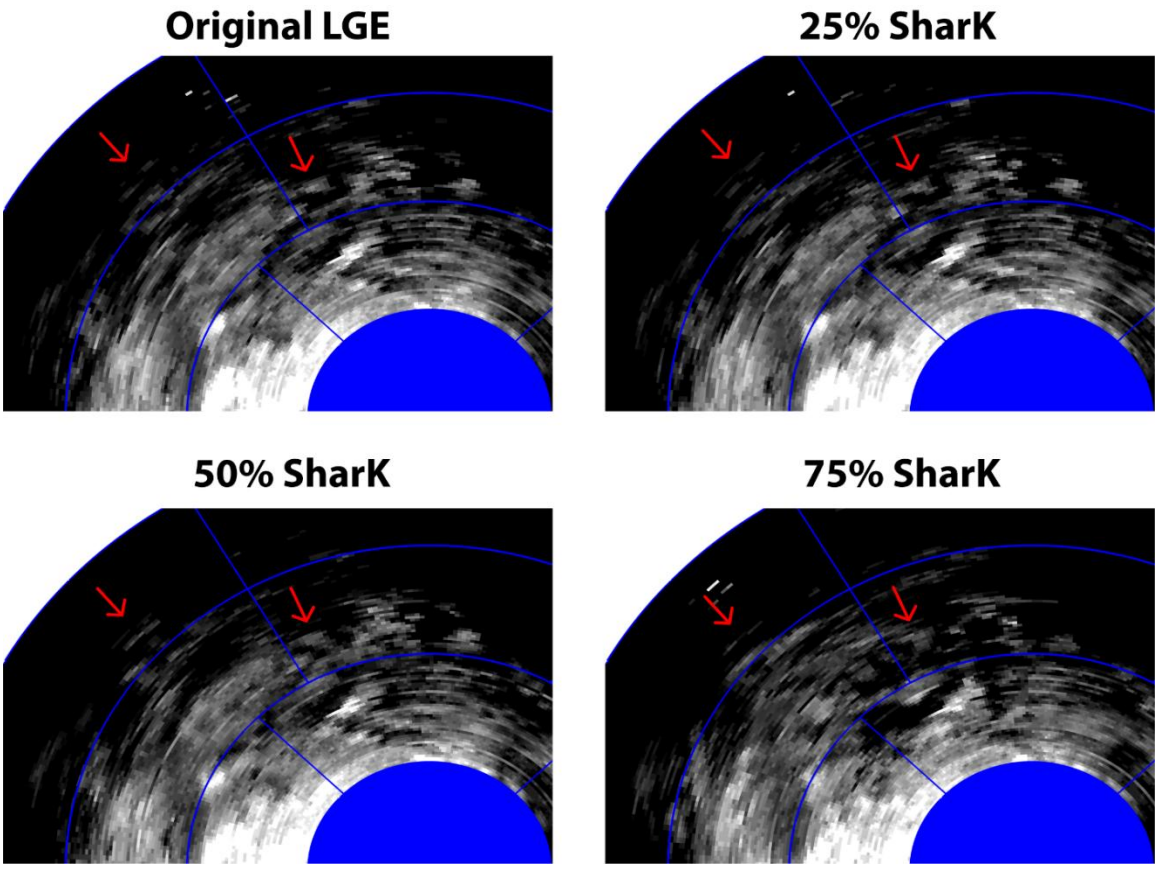

Figure 6.7 Magnified view of anteroseptal scar on the original and three different SharK reconstructions. As the percentage of Shared K-space increases, the edges of scar becomes increasingly distorted as compared to the original. Some of these areas are notated by red arrows

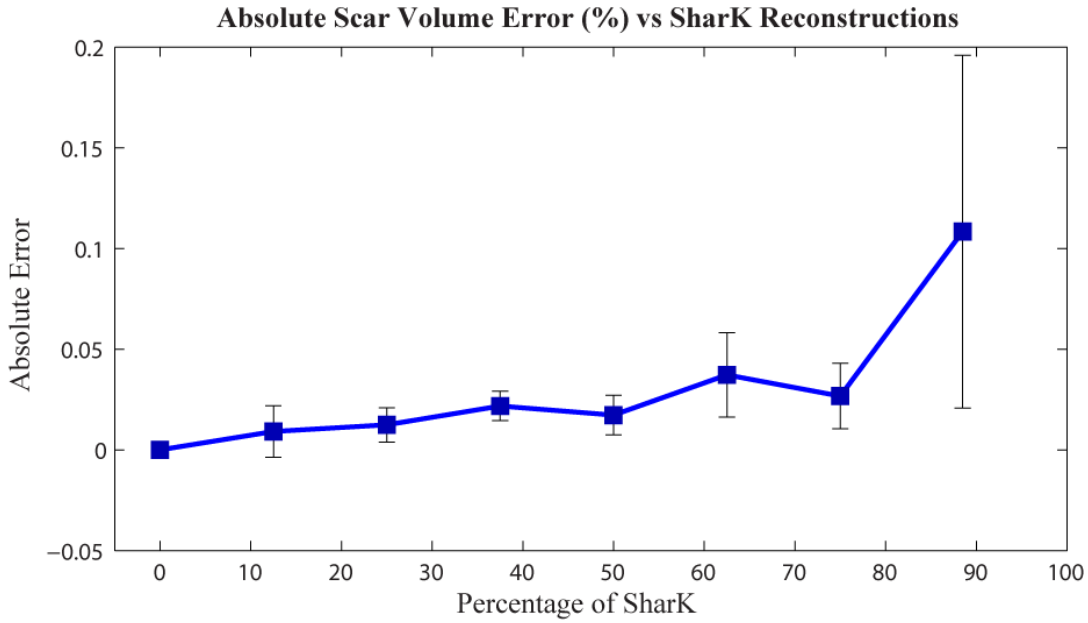

Figure 6.8 Absolute scar volume error for SharK Reconstructions as compared to the original LGE image stack

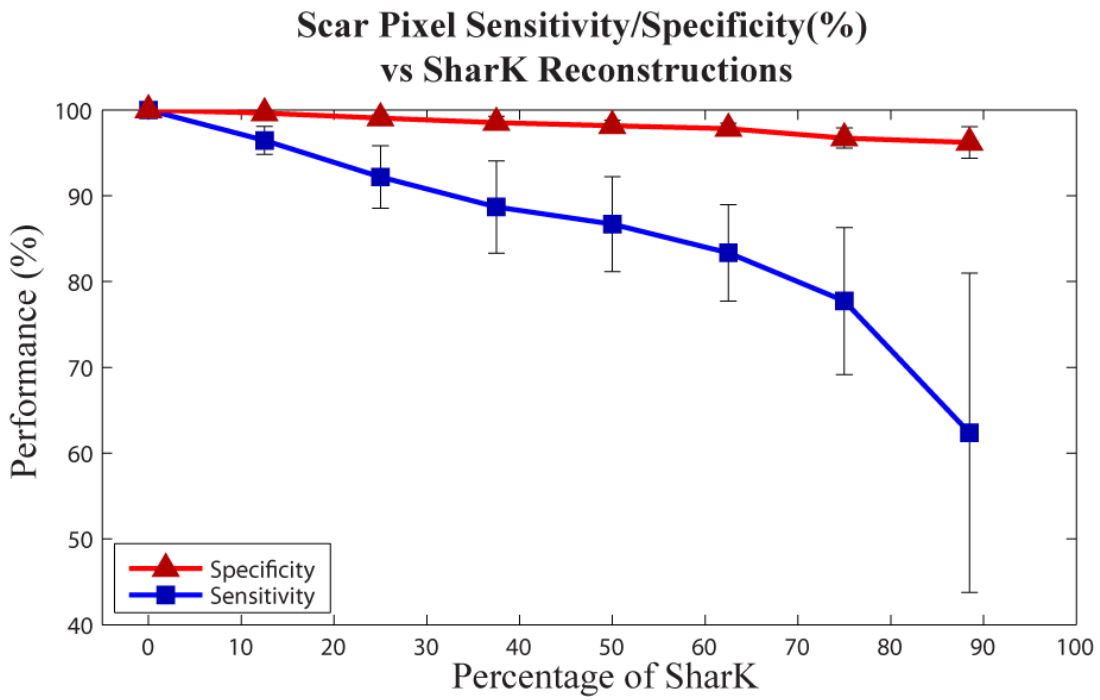

Figure 6.9 Sensitivity and specificity analysis of correctly identified scar pixels by performing a pixel-to-pixel comparison between the original LGE image and SharK reconstructions

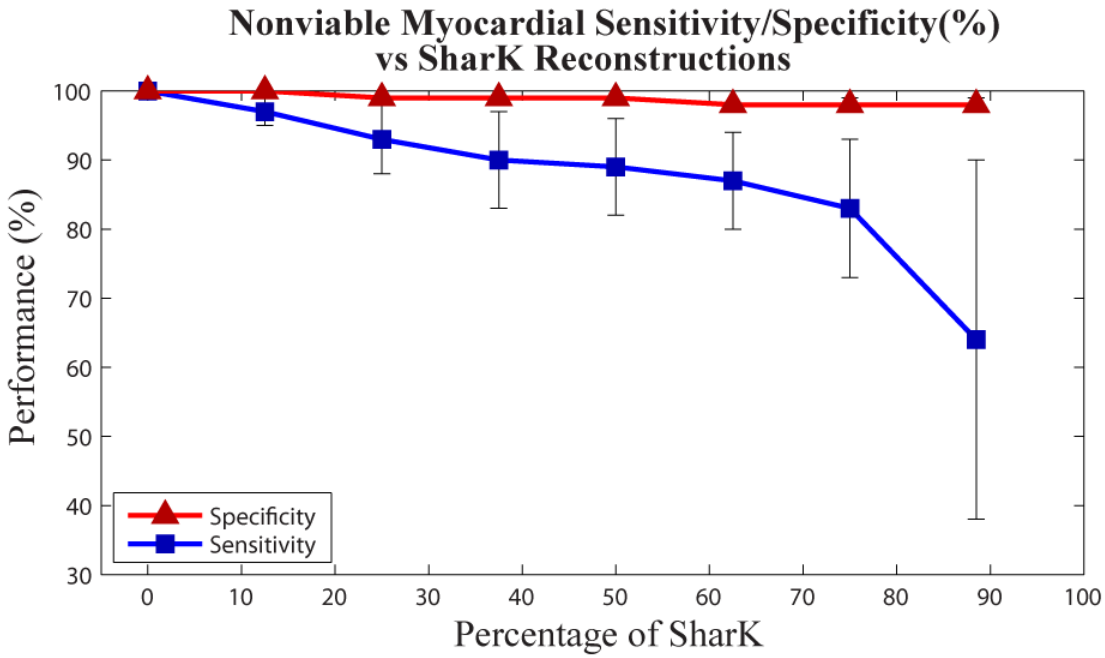

Figure 6.10 Sensitivity and specificity analysis of scar defining the percentage of correctly labeled viable myocardial spokes for different SharK reconstructions.

6.3.3 Combined Coronary Vein and Scar Maps

Since 3D angiography and 3D LGE-FLASH image stacks were co-registered during segmentation, identified coronary vein points could be directly overlaid onto the AHA scar bullseye (Figure 6.11). Due to the presence of anteroseptal scar, the anterior interventricular vein would be a poor candidate for LV lead implantation, while the left marginal vein would be a potential candidate for LV lead implantation depending on this patient's contraction pattern.

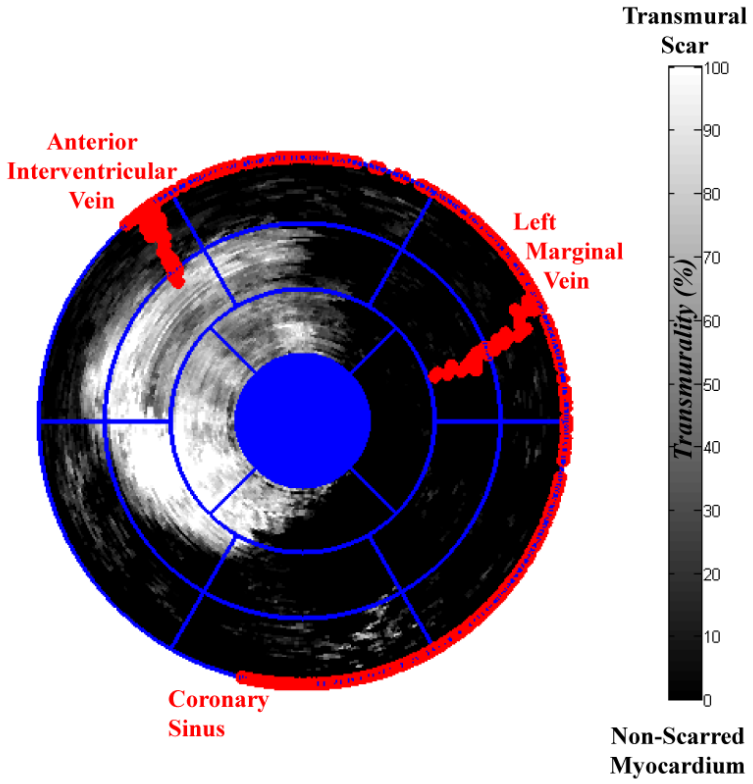

Figure 6.11 Sample bullseye showing scar transmurality in the left ventricle with coronary vein points (red) directly overlaid from co-registered angiography and LGE images. This map allow for simple pre-procedural planning for LV lead implantation

6.4 Discussion

By acquiring two full sets of k-space using the same 3D FLASH sequence, one immediately after contrast for angiography and another 20 minutes post-contrast for LGE, we were able to create re-formatted short-axis slices that could be used for retrospective comparison of multiple Shared K-space LGE reconstructions. Analyzing absolute scar volume error, sensitivity to detecting scar pixels, and sensitivity to nonviable myocardial spokes in a bullseye plot allowed quantitative comparison of reconstructions of various amounts of shared k-space. Acquiring both angiography and LGE images with the same sequence allows direct overlay of coronary vein maps and scar maps.

Multiple k-space sharing sequences have been previously developed, mainly to increase temporal resolution for applications such as bolus tracking or perfusion. Examples of sequences include the "keyhole" method, which acquires a reference image prior to contrast injection and repeats of central k-space are acquired to replace the central k-space lines in the reference image, or interleaved spirals which use higher sampling densities at the center of k-space (58,60). 3D time-resolved imaging of contrast-kinetics (3D-TRICKS) acquires alternating partitions between the central partitions and outer partitions over time multiple 3D angiographic image stacks. The SharK sequence is similar to the 3D-TRICKS sequence but does not acquire alternating central and outer partitions because the SharK sequence does not need high temporal resolution to track short-term contrast dynamics (59). However, the SharK sequence is the first sequence to share k-space over a long period of time (> 10 minutes).

The early scar enhancement seen in the angiography images is likely due to a combination of the physiologic effect of early accumulation of gadolinium in regions of inflammations and the physics effects of the reordering of the standard 3D free-breathing FLASH sequence used for LGE imaging. In a centric-ordered phase encoding, linear-ordered partition encoding sequence acquires the true center of k-space halfway through the sequence, or at least 4-5 minutes post contrast-injection. While the angiography images still show strong contrast between the blood and myocardium, it can potentially complicate automated algorithms for myocardial segmentation. However, it is anticipated that early enhancement would disappear when changing to a centric-ordered partition encoding sequence as the center of k-space would be acquired immediately after contrast-injection, limiting the amount of time for gadolinium to diffuse into regions of scar.

Early hyperenhancement post-contrast has been previously observed and can be associated to a number of factors including reduced regional blood flow or increased interstitial volume (83,84). However, studies suggest that these regions do not always represent regions of scar, but in fact, can partially consist of viable myocardium (85,86). This has been established by functional studies which show that regions of early enhancement exhibit significantly higher functional improvements when compared to other non-early enhancing regions (85).

The decrease in sensitivity as the percentage of shared k-space increases is expected as increasing the amount of shared k-space from the angiography images blurs the edges of the scar and decreases the intensity. This results in reduced amount of scar and decreased transmurality, as reflected by the decrease in sensitivity. The specificity does not change as much as the sensitivity between different SharK reconstructions because

blurring is less likely to increase the intensity of healthy myocardium to the extent that a viable myocardial spoke becomes non-viable. In addition, specificity remains above 95% for both measures as the majority of the left ventricle is composed of normal myocardium, making any falsely labeled scar pixels a minor contribution in the comparison.

From the parameters tested, an optimal amount of k-space sharing cannot be quantitatively determined. The decrease in sensitivity and specificity for scar assessment that result from shorter acquisition times demonstrate the trade-off as more k-space is shared between angiographic and LGE images. The small sample sizes and high standard deviations as the amount of shared k-space increases for scar volume make any differences between the original LGE image and the SharK LGE images non-significant. In addition, both sensitivity and specificity for proper identification of scar pixels or non-viable transmural spokes require that an arbitrary threshold be set for an optimal shared k-space value. Based on an average whole-heart, navigator-gated acquisition time of 9.8 ± 2.5 minutes, the tradeoff for each additional 10% of shared k-space is approximately 1 minute (61). While acquiring sharing less k-space leads to increased scar accuracy, the optimal myocardial nulling time changes over time due to gadolinium diffusion out of scar. As a result, sharing more k-space would allow acquisition of multiple LGE stacks changes with modified TI times to optimize myocardial nulling.

Saving scanner time in the clinic can be essential toward MR imaging protocols. CMR protocols can easily extend past the allotted one hour slot due to unforeseen setbacks such as patient movement during scans or patient inability toward breath holds. If there is sufficient time remaining, a full set of k-space should be acquired for LGE

images to maximize the accuracy of scar assessment on images. However, as MR scans often run behind schedule, the capability to shorten acquisition times by sharing k-space between angiography and LGE images can be crucial to still provide a sufficient high resolution scar image while staying within the assigned time slot.

Co-registration between 2D PSIR and 3D angiography images is challenging due to differences in the imaging sequence, such as respiratory positions, image orientation, and image resolution. Additionally, the variation in breath-holds between 2D PSIR slices makes each individual PSIR slice at a different position, and as a result, 2D PSIR images must be registered to angiography images slice-by-slice instead of as a stack, further complicating the process. Using the same 3D, respiratory-gated, inversion recovery FLASH sequence for both angiography and LGE images overcomes these issues. While some degree of co-registration is still necessary as the respiratory position can drift over time, it is appropriate to assume that a rigid co-registration algorithm can be used to properly align the two image stacks because both images share the same image positions and that respiratory motion creates motion primarily in the inferior-superior direction without significantly deforming the shape of the heart. In addition, the improvements in spatial resolution afforded by 3D imaging allow for significantly improved visualization of the scar borders.

In order to determine the sample size necessary to demonstrate the effectiveness of pre-procedural planning by using combined coronary vein/scar mapping along with contraction maps we assume that our patient groups will have similar response rates to previous retrospective studies. Assuming a CRT response rate of 80% in the patient group with an “optimal lead position” and a response rate of 55% in a control group, a

Fisher Exact Test with a power of 80% and significance of 0.05 requires 70 patients in each group (12,21).

It is important to note the difference is that the acquisition time of a full, whole-heart free-breathing FLASH sequence is 9.8 ± 2.5 min while the multiple 2D PSIR short-axis slices (10-15 slices) is 8.0 ± 0.7 minutes. The ease of co-registration, lack of breath-hold and ~20x increase in spatial resolution may be well-worth the slightly increased scan time in many applications. The acquisition time can be reduced to approximately the same or better than multiple 2D PSIR slices when applying the Shared K-space sequence to allow acquisition of fewer partitions.

6.4.1 Limitations

There are limitations in the retrospective SharK analysis to determine the optimal amount of k-space to share between acquisitions. Since the ordering of the proposed combined angiography and LGE sequence is not used in these patients, this study demonstrated proof-of-principle. The reordering of the sequence used in this study is a linear-ordered partition encoding ordering, and as a result, the outer partitions that are shared between the angiography and LGE images will be acquired at different times in the retrospective case when compared to the SharK sequence. In the case of retrospective reconstruction, the shared outer k-space partitions are acquired just after contrast injection and 8-9 minutes post contrast-injection, as opposed to the SharK sequence acquires all of the shared outer k-space partitions 6 minutes post contrast-injection due to the centric partition encoding. As there were no visible artifacts from retrospectively sharing k-space, we expect similar results from using a centric-ordered partition encoding

sequence due to the smaller time difference between acquisition of the shared outer k-space partitions and the additional centric partitions.

Since scans were added to a pre-existing MR research protocol, only a portion of the heart could be acquired using the 3D respiratory-gated FLASH sequence for angiography and LGE. of the lateral and anterior coronary venous anatomy while other patients only In addition, the acquisition time of the 3D respiratory-gated FLASH LGE sequence was always past the optimal LGE acquisition time as the study required the 2D PSIR images to be acquired at 15 minutes post-contrast. Lastly, the small sample size limits the assessment of Shared K-space on different scar sizes and shapes.

6.5 Conclusion

We performed retrospective Shared K-space reconstruction on patients with known previous myocardial infarction to generate a range of SharK LGE image stacks. By calculating the differences in absolute scar volume error, sensitivity to scarred pixels, and sensitivity nonviable myocardial spokes over the different SharK LGE image stacks, we were able to determine the effects of various k-space sharing on accuracy of scar detection. A SharK of 50% balances acquisition time and SharK LGE scar accuracy. Methodology to create combined coronary vein and scar maps that can be used to plan LV lead implantation in CRT patients was developed and applied in one patient.

Chapter VII

Application of SharK Sequence on Patients Post-PVI Treatment

7.1 Introduction

Atrial fibrillation (AF) is the most prevalent type of sustained cardiac arrhythmia, affecting approximately 1% of the global population (87). This arrhythmia is classified in two categories: paroxysmal if the fibrillation is intermittent and persistent if the fibrillation is continuous. Paroxysmal AF requires a trigger for arrhythmia initiation and 90% such triggers originate from the pulmonary veins. The trigger can induce multiple macro-reentrant circuits throughout the atria, causing the quivering known as fibrillation (37). If these re-entrant circuits terminate, either spontaneously or through drugs, the atria can return to normal sinus rhythm. Triggers can continue to arise to re-initiate the fibrillation. If the re-entrant circuits do not terminate, normal sinus rhythm cannot be established and the patient is in a continuous, or persistent, state of AF. In this state, PV triggers are unnecessary as the re-entrant circuits are self-sustaining.

Patients with AF who are resistant to at least one form of drug therapy often undergo pulmonary vein antrum isolation (PVAI), a procedure that electrically isolates the pulmonary veins from the left atrium. PVAI has been traditionally performed by radiofrequency (RF) ablation catheters, which use point-by-point RF energy to isolate the pulmonary veins (41). However, more than 30% of patients do not regain normal sinus rhythm and experience AF recurrence after ablation (88). This recurrence is associated with regions of myocardium which do not permanently scar after ablation. Cardiovascular Magnetic Resonance (CMR) imaging has shown that larger quantities of

scar as well as the formation of a continuous ring of permanent scar around the PVs post-RF ablation is correlated to procedural success(53,89).

Recently, cryoballoon therapy has gained increased interest due to its success in clinical trials and simplified ablation procedure. Cryoballoon ablation inflates a double-walled balloon catheter at the PV ostium, delivering cryo-energy to the pulmonary venous ostia via nitrous oxide within the balloon. Currently, the distribution of scar post cryoballoon ablation is not well defined, and encirclement parameters are qualitative (90). In comparison to RF ablation, the majority of studies report that cryoballoon ablation has similar or longer procedure and fluoroscopy times, though no studies have reported significant differences in AF recurrence between the two methods (47,48,50,91,92). However, one study compared the region of pulmonary vein reconnection between cryoballoon and RF ablation from patients who underwent repeat ablations by determining the site of the earliest PV potential as measured by a multipolar circular mapping catheter. This study reported that the number of reconnected pulmonary veins was similar, but the location of reconnection differed between the two ablation procedures (91). 74% of cryoballoon ablation reconnection sites were in the inferior portion of the pulmonary vein as compared to 17% of RF ablation reconnection sites.

The purpose of this work is to: (1) apply the SharK sequence to assess scar distribution in patients post PVI treatment and (2) create an algorithm to quantify the amount of scar encircling the pulmonary vein. This will allow a quantitative comparison of the of point-by-point RF ablation against cryoballoon ablation in their ability to create continuous encircled scar about the pulmonary veins. We will achieve this by imaging

patients 1-3 months post-PVI and developing the concept of a 2D “pulmonary vein bullseye” projection to quantify scar encirclement.

7.2 Methods

7.2.1 Patient Population

Patients (n = 7) who had undergone PVI cryoballoon ablation were recruited 1 - 3 months for a cardiac MRI after the ablation procedure. This study was approved by the Institutional Review Board (IRB). All patients gave written informed consent.

7.2.2 MR Protocol

All cardiac magnetic resonance (CMR) exams were performed on a 3.0 T MRI (Tim Trio, Siemens Healthcare, Erlangen, Germany) system using a six-element phased-array cardiac coil. Black-blood images were acquired to position the whole heart SharK sequence. The SharK sequence was acquired in the sagittal orientation rather than the standard transverse orientation to minimize partial volume effects of scar by acquiring images perpendicular to the pulmonary veins. A double dose of gadobenate dimeglumine at 0.2 mmol/kg (MultiHance, Bracco Diagnostics Inc, NJ, USA) was slowly infused at a rate of 0.3 mL/s, followed by an equal amount of saline. Acquisition of the angiography portion of the SharK sequence started ~90 seconds after the start of contrast injection. Late gadolinium enhancement was acquired 15 minutes post-contrast. A look-locker sequence at a mid-short axis slice was used to determine the optimal TI inversion time to null healthy myocardium. Sagittal phase-sensitive inversion recovery images in the sagittal orientation were acquired for full atrial coverage. Afterwards, either a full set of k-space was acquired, and 50% of central k-space was retrospectively shared or a 50%

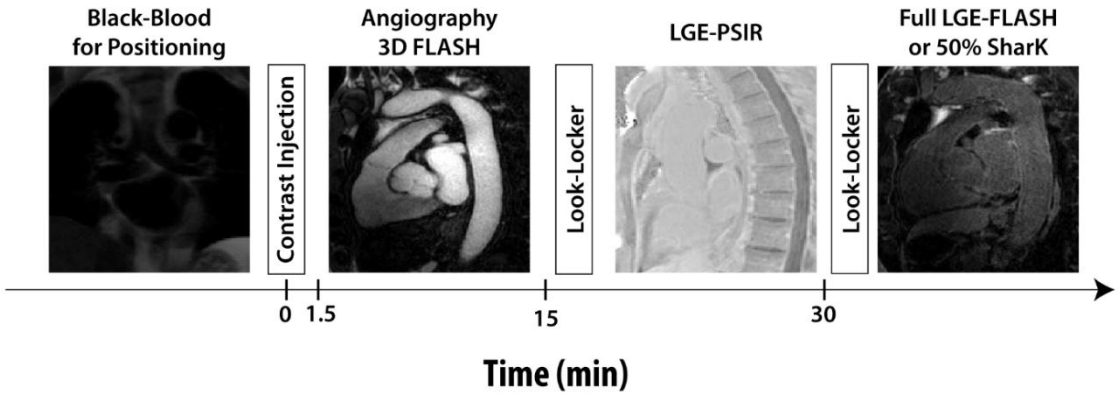

Figure 7.1 MR protocol used for atrial wall imaging

SharK was acquired for high-resolution LGE imaging (Figure 7.1).

7.2.3 Atrial Segmentation

The inner atrial wall was segmented on the angiography images by using an intensity threshold and then manually refining the borders. The angiography images were co-registered to the LGE SharK images by using a gradient-ascent algorithm to find the maximum correlation between the two image sets and borders were directly transferred from the angiography images to the LGE images. Since the average atrial wall thickness is approximately 2 mm, borders were dilated 3 pixels (~2.1 mm) to cover the majority of the atrial wall (93). This 3 pixel distance was defined as the epicardial dilation distance. A MATLAB graphical user interface was developed to allow users to easily change intensity thresholds to segment the left atrium (Figure 7.2).

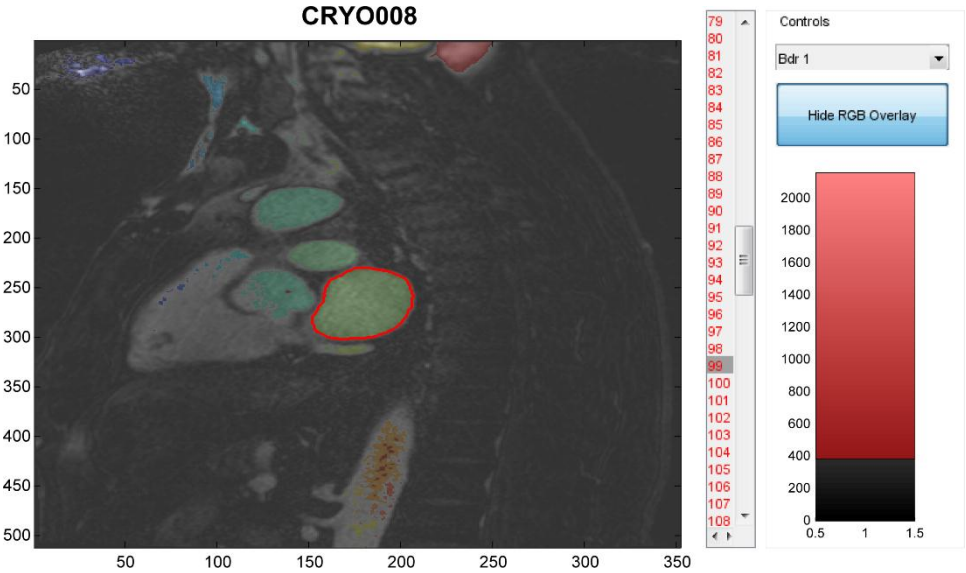

Figure 7.2 Intensity segmentation GUI allows users to select an intensity range (bottom right) to automatically find "blobs" (multi-colored overlay on MR image) within that range

7.2.4 3D Atrial Reconstruction

All pixels that comprised the inner atrial wall were exported as a point cloud and wrapped in Geomagic (Rock Hill, SC, USA) to create a 3D shell of the atrium (Figure 7.3). A plane perpendicular to each PV ostia and the left atrial appendix (LAA) was manually defined as the opening at the atrial body leading to the PV or LAA. The reconstruction was cut at these five planes to create six independent 3D structures (atrial body, LIPV, LSPV, RIPV, RSPV, and left atrial appendage). Files were exported as STL files into MATLAB. Intensities were projected to the 3D reconstruction using a k-nearest neighbors algorithm that found the eight closest atrial wall points and averaging the respective image intensities to create a 3D shell colored by pixel intensity.

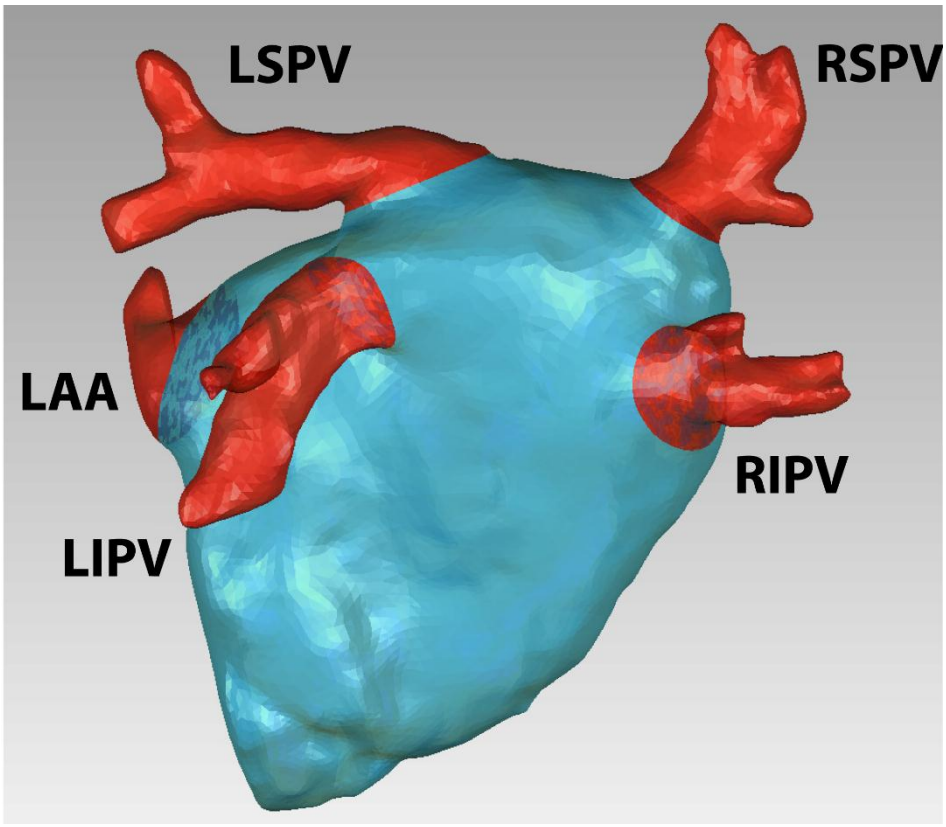

Figure 7.3 Geomagic was used for 3D reconstruction of the left atrium using an imported point cloud from MATLAB. L/R/S/I PV = Left/Right/Superior/Inferior pulmonary vein; LAA = Left atrial appendage. The borders of the red PVs at the blue atrial body represent the cutplanes for the PV ostia

7.2.5 Projection to Pulmonary Vein Bullseye

All atrial wall points were categorized to belong to one of the six structures based on the nearest distance to one of the six 3D structures (Figure 7.4). This prevented a point of enhancement that was categorized as part of one pulmonary vein to be associated with another pulmonary vein. For each pulmonary vein, the perpendicular plane previously defined was translated ±7 mm along its normal direction to create a boundary (Figure 7.5). Only atrial wall points between this boundary that belonged to either the corresponding pulmonary vein or the atrial body were included. Points were projected

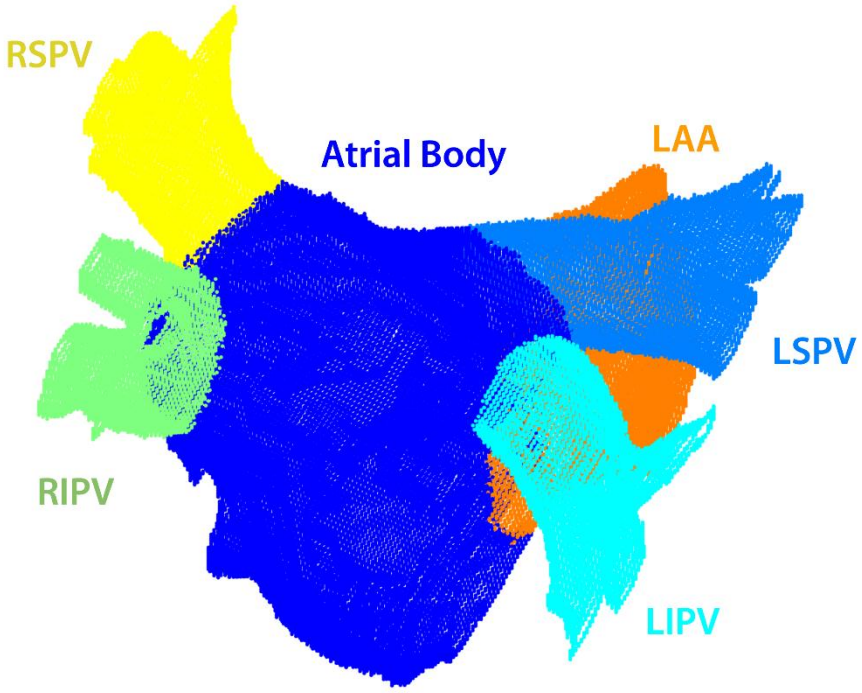

Figure 7.4 All atrial wall points have been categorized to belong to either a pulmonary vein, the atrial appendage, or the atrial body. Each of the six structures is represented with a different color.

onto a circular grid named a "pulmonary vein bullseye" using a polar projection algorithm. This algorithm projected the anatomical superior direction onto the PV plane, which was then defined as 90° on the bullseye. The plane was defined to have a radius of 10 (arbitrary units) on the bullseye, and points on the side of the plane closer to the atrial body had a radius 10 + $D_{DistanceFromPlane}$ while points on the side of the plane away from the atrial body had a radius 10 - $D_{DistanceFromPlane}$. After projection of all points onto the bullseye, a final bullseye grid was linearly interpolated, with one radial unit corresponding to 0.2 mm along the axis of the pulmonary vein. A portion of the left ventricle was sampled and pixels with intensity > $\mu \pm 6\sigma$ above the threshold was considered as scar (94).

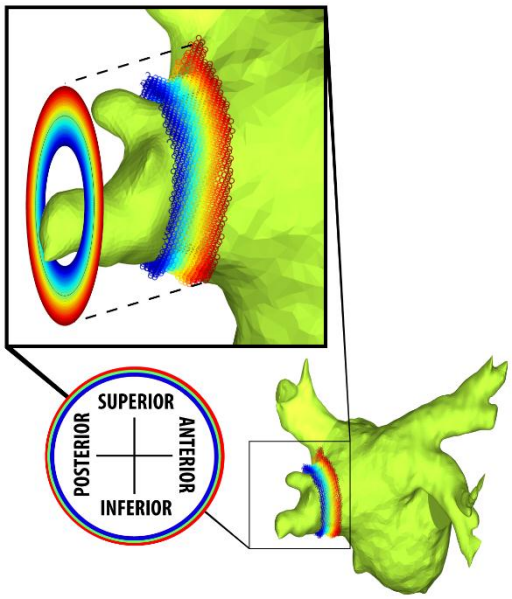

Figure 7.5 Polar projection algorithm to project atrial wall points onto the bullseye. Points that are situated closer to the atrial wall are projected onto outer rings of the bullseye while points further up the pulmonary vein are projected onto inner walls of the bullseye. The y-axis on the bullseye corresponds to the projected anatomically superior direction onto the PV plan

7.2.6 Encirclement Assessment

A separate GUI was developed for PVI assessment that automatically calculated bullseyes after LV sampling to determine the scar threshold (Figure 7.6). Bullseyes were combined over all patients to determine which regions of the pulmonary veins were ablated consistently over all subjects. Encirclement was quantified by assessing the continuity of scar around the PV ostia that would be necessary for continuous PV encirclement. A radial encirclement threshold was used to determine the number of degrees of ablation and was defined as the minimum number of continuous radial units on the bullseye mesh that was above the scar intensity threshold for a degree of encirclement. The radial encirclement threshold was 10 continuous radial units on the bullseye mesh, corresponding to approximately two MR image pixels (2.0 mm). This threshold was determined based on the certainty that two connected MR pixels

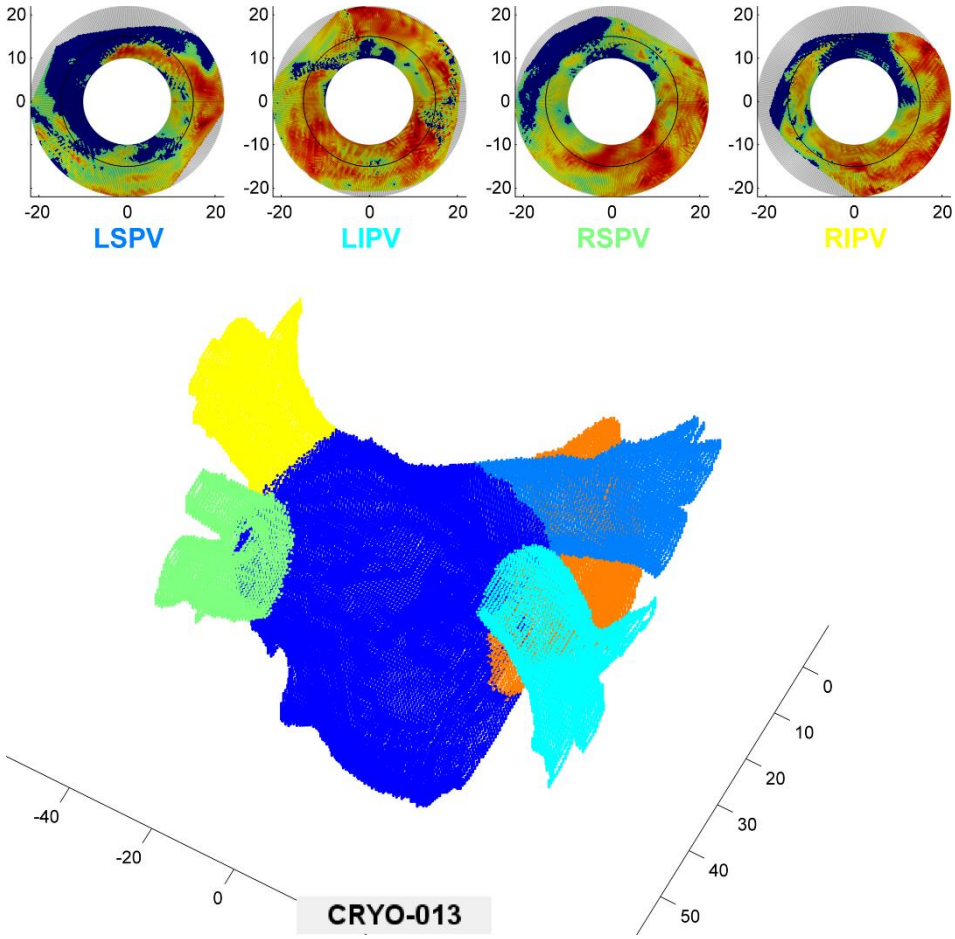

Figure 7.6 Pulmonary vein bullseye GUI developed in MATLAB. Pulmonary vein bullseyes are shown at top. Blue color indicates non-scarred atrial wall while all other colors indicate the interpolated pixel intensity of the scar. The point cloud represents all points from the atrial wall. The pulmonary vein label colors under the bullseye plots correlate to the colors on the atrial point cloud.

above the scar threshold represented a region of LGE. This allowed classification of all pixels in the 360° around the bullseye into ‘scarred’ or ‘non-scarred’ groups. The percent encirclement (out of 360°) was quantified by determining the total number of degrees that were scarred. Bullseyes from corresponding pulmonary veins across patients were directly compared to each other.

7.2.7 Sensitivity Analysis

A sensitivity analysis was performed by varying: (1) the epicardial dilation distance, (2) number of standard deviation for the scar intensity threshold, or (3) the radial encirclement threshold to evaluate their sensitivity to encirclement (Table 7.1). Only one parameter was changed while the other two parameters held constant. The epicardial dilation was evaluated between 1 – 5 mm, the scar threshold was evaluated between 1-10 standard deviations, and the radial encirclement threshold criteria was changed between 5-20 continuous pixels. Constant parameters used were: 3 pixel epicardial dilation, 6 standard deviations, and 10 radial unit encirclement threshold. A two-tailed paired t-test was used when appropriate for comparison of different parameters.

Table 7.1 Default values used for the epicardial dilation, scar intensity threshold, and radial encirclement threshold as well as the ranges tested to evaluate sensitivity to encirclement

	Default Value	Sensitivity Range
Epicardial Dilation	3 pixels	1 – 5 pixels
Scar intensity threshold	7 standard deviations	1 – 10 standard deviations
Radial encirclement threshold	10 units	5 – 20 units (5 unit increments)

7.3 Results

The left atrium was successfully imaged by MR in all 7 patients. Acquisition time for the angiography portion of the SharK sequence (full k-space) was 9.3 ± 2.0 minutes. 5 patients had PSIR images available, and full atrial coverage took 10.2 ± 4.8 minutes for PSIR acquisition. 5 patients had 50% SharK LGE images available and imaging time was 3.9 ± 0.5 minutes. Intensities were successfully projected to the atrium to 3D representation of encirclement (Figure 7.7).

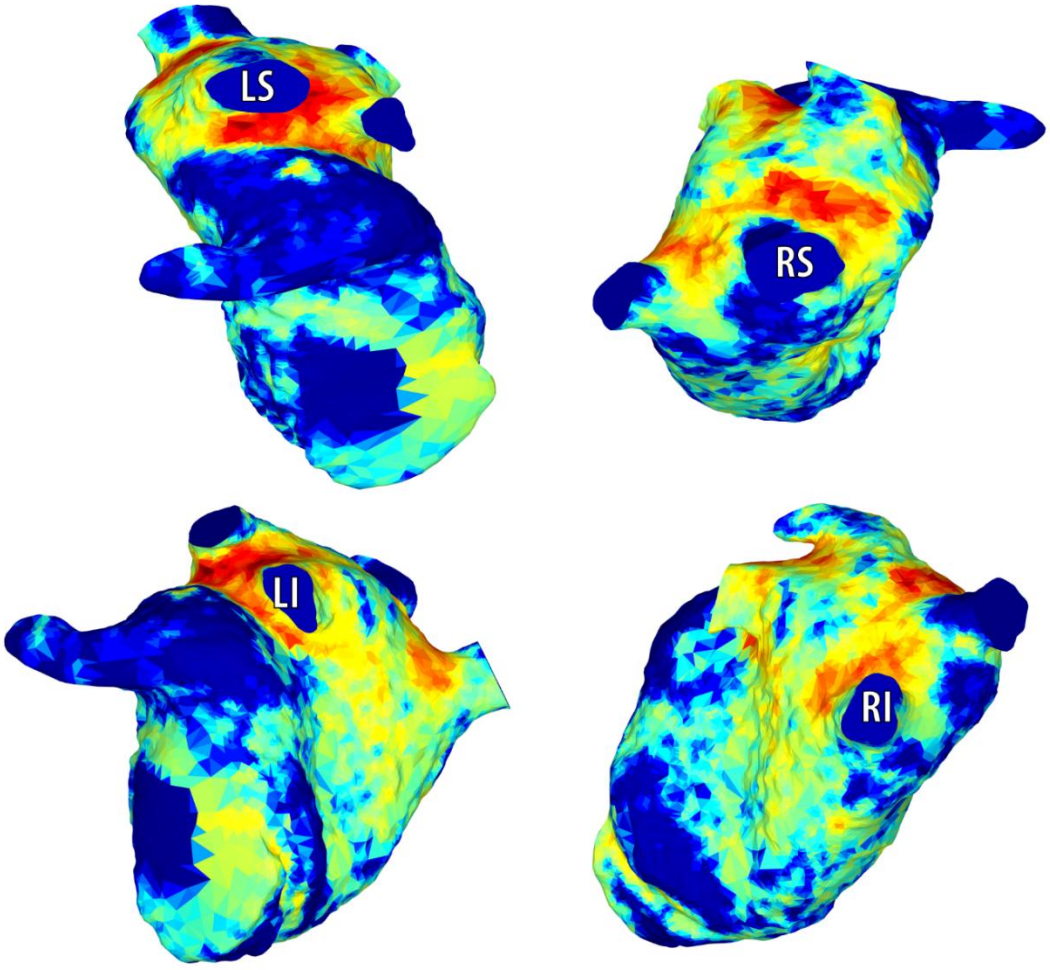

Figure 7.7 Sample cryoballoon patient with MR image intensities projected onto the atrium. Red indicates higher intensities. The ends of the pulmonary veins have been cut and are not colored in.

7.3.2 Encirclement Assessment

Pulmonary vein bullseyes were created for 7 cryoballoon ablation patients (Figure 7.8). The average encirclement for the four pulmonary veins was 88% ± 9%, 94% ± 8%, 83% ± 15%, and 81% ± 22% for the LSPV, LIPV, RSPV, and RIPV respectively. There

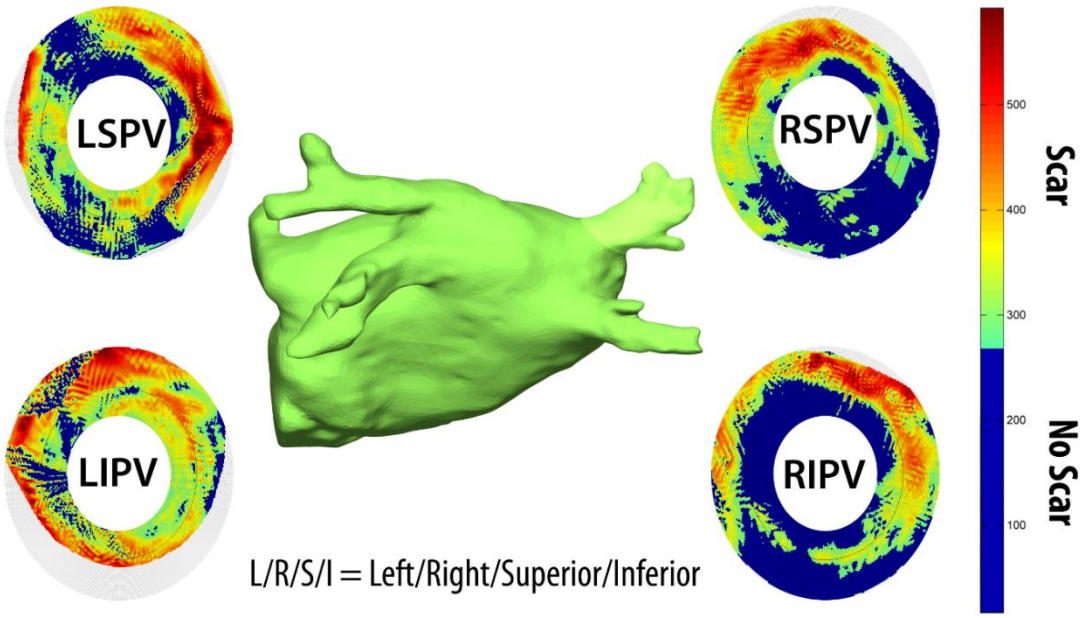

Figure 7.8 Sample pulmonary vein bullseye for a patient 1-3 months post cryoballoon ablation. Blue represents regions with no scar while all other colors represent the pixel intensity.

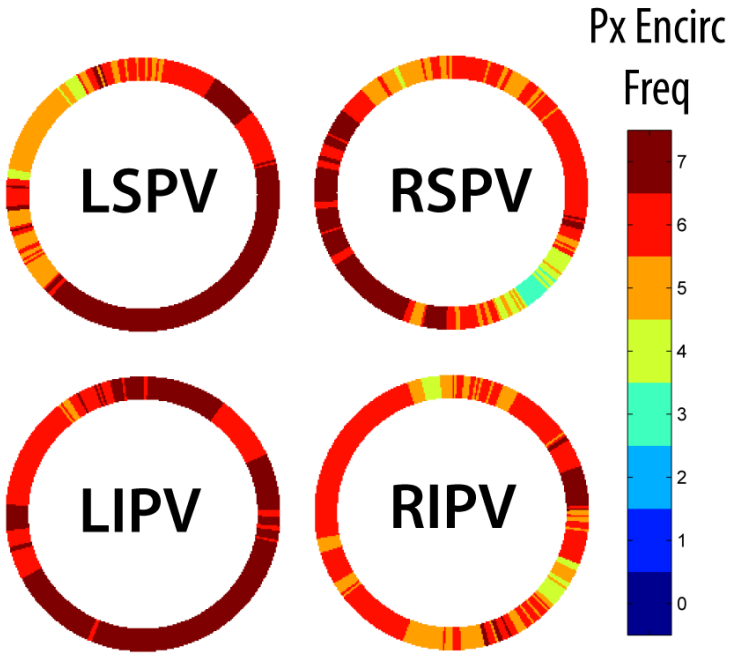

Figure 7.9 Total encirclement for all four pulmonary veins across 7 patients. Colors notate the number of patients that had a particular degree encircled.

was a 100° segment of the anteroinferior portion of the LIPV and 145° segment of the anteroinferior portion of the LSPV that was ablated in all patients. There was a 30° segment in the anteroinferior portion of the RSPV that was only ablated in 3/7 patients (Figure 7.9).

7.3.3 Sensitivity Analysis to Scar Parameters

The pixel dilation amount, number of standard deviations, and radial encirclement threshold used to determine scar were varied to determine their sensitivity in determining percent encirclement.

7.3.3.1 Epicardial Dilation

Encirclement decreased as the number of pixels dilated outwards from the endocardial border to the epicardial border increased (Figure 7.10). The difference in encirclement between dilating the epicardial border 1 pixel to 5 pixels was 9%. There

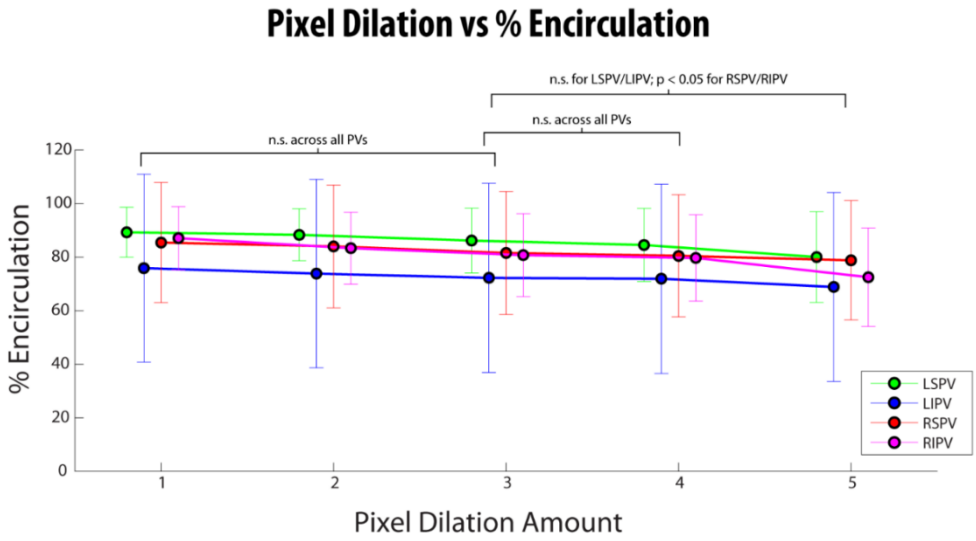

Figure 7.10 Percent encirclement decreases linearly for all pulmonary veins as epicardial pixel dilation increases from 1 pixel to 5 pixels.

was no significant differences when comparing a 3 pixel epicardial dilation to 1-4 pixel epicardial dilation distances across all pulmonary veins. The LSPV and LIPV had no significant differences while the RSPV and RIPV had significant differences when comparing a 3 pixel epicardial dilation to a 5 pixel epicardial dilation.

7.3.3.2 Scar Intensity Threshold

Percent encirclement appears to exponentially decay as the number of standard deviation increases when determining the scar threshold (Figure 7.11). Near complete encirclement is seen between 1-3 standard deviations, and begins decaying exponentially for standard deviations > 3. Average percent encirclement across all veins at 10 standard deviations is 45%.

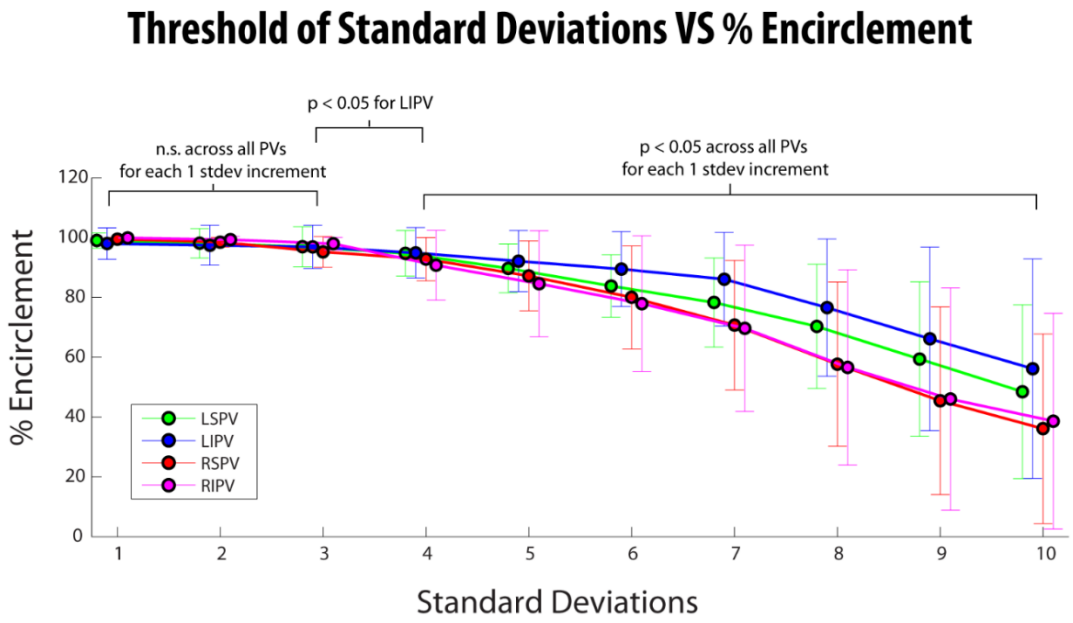

Figure 7.11 Percent encirclement decays exponentially for all pulmonary veins as the number of standard deviations in the scar threshold increases.

7.3.3.3 Radial Encirclement Threshold

Percent encirclement decays as the number of standard deviations from the mean wall signal intensity increases when determining the scar threshold (Figure 7.12). Near complete encirclement is seen between 1-3 standard deviations, and begins decaying exponentially for standard deviations > 3. Average percent encirclement across all veins at 10 standard deviations is 45%. There are no significant difference in encirclement between all PVs when comparing 1 standard deviation increments between 1-3 standard deviations. All PVs have significant differences in encirclement when comparing 1 standard deviation increments between 4 – 10 standard deviations.

The sensitivity analysis revealed that from all parameters used in the development of the pulmonary vein bullseye, scar encirclement is fairly insensitive to changes in the radial encirclement threshold that determines a degree of scar encirclement or the dilation

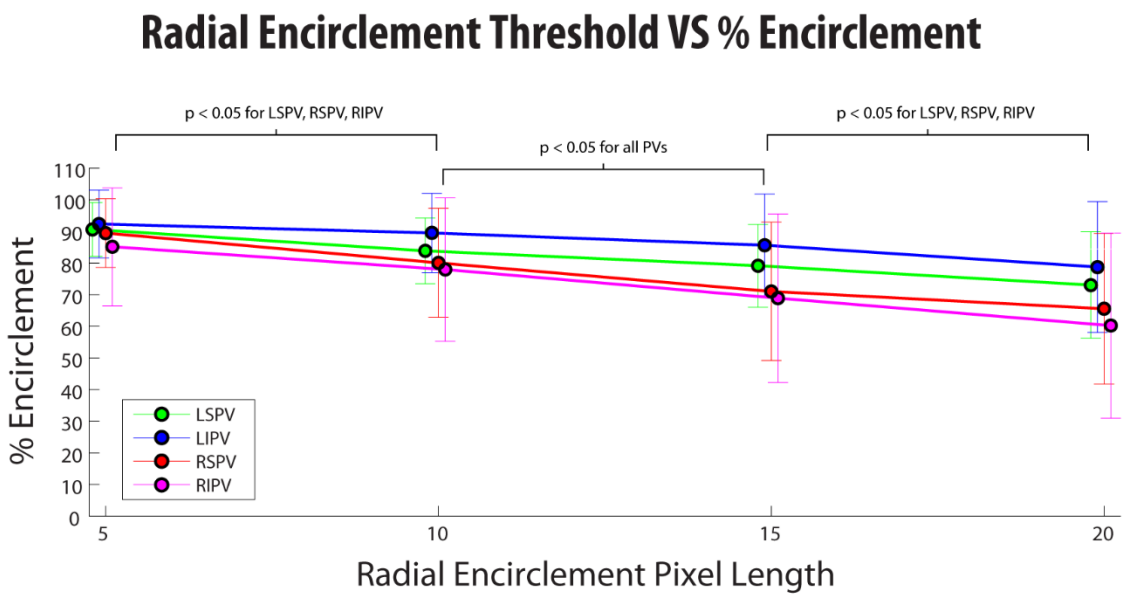

Figure 7.12 Percent encirclement linearly decreases as the radial threshold used to determine degrees of encirclement increases

threshold for atrial wall coverage. The methodology is most sensitive toward the number of standard deviations used for the scar threshold, and encirclement exponentially decays as the number of standard deviations increases.

7.4 Discussion

In this work, we have applied the SharK sequence on patients who have undergone PVI for treatment of AF. Acquisition of the SharK sequence allowed segmentation of the inner atrial wall borders on angiography images and transferring borders to SharK LGE images for accurate atrial wall segmentation. By applying a signal intensity threshold in the segmented wall section, we could visualize atrial wall scar in 3D. A pulmonary vein bullseye was then developed to enable simplified 2D viewing of scar for scar encirclement quantification. A sensitivity analysis revealed that the pulmonary vein bullseyes are resistant to changes in the radial encirclement threshold and epicardial pixel dilation amount but is very sensitive to the number of standard deviations used in determining the scar intensity threshold.

Application of the SharK sequence to evaluate scar encirclement for pulmonary vein isolation has multiple benefits over traditional methods of imaging, which rarely acquire or use angiography images in post-processing. When angiography images are acquired, a lower resolution (2 x 2 x 4 mm^3) breath-held sequence is often used, complicating the co-registration process for segmentation (54). Sharing k-space with the angiography sequence reduces imaging time proportional to the amount of k-space shared for LGE imaging. This opens up the option for acquisition of multiple LGE image stacks in the case the first is insufficient. This is especially important as there are currently no studies to determine the gadolinium accumulation in atrial scar for the optimal post-contrast LGE

imaging time. In addition, repetition of the sequence greatly simplifies co-registration. Since the respiratory position and resolutions have not changed, a rigid co-registration approach employing translating one image to the other is sufficient. We can segment the angiography images, which have clear delineation of the blood-atrial wall border, and then directly transfer the borders to LGE images to extract the atrial wall. Lastly, imaging in the sagittal orientation minimizes partial volume effects as the slice is oriented closer to the plane perpendicular to the pulmonary vein. Segmentation is also simpler in the sagittal orientation as this splits the left atrium into ellipsoids as opposed to the transverse orientation, which splits the left atrium in irregular shapes.

To our knowledge, this is the first work which has quantified encirclement of the pulmonary veins. Previous studies either used a binary "encircled/not-encircled" classification of pulmonary veins by visual assessment or divided each PV into six sectors, with graders rating the presence of gaps in LGE around the sectors (53,54). Our method of quantification eliminates the subjectivity that comes with qualitative grading and has is simpler than the traditional 3D representation of atrial wall scar as evaluation of encirclement can be performed in a single glance with the pulmonary vein bullseyes. This quantification becomes more important when trying to correlate recurrence with lack of encirclement, as simply classifying a vein as encircled or non-encircled may not be enough to explain the differences between those whose symptoms are recurrent compared to those who are not.

Some of our results for encirclement are similar to what has been shown previously, though these studies focus on LGE imaging post-RF ablation. The LIPV has been shown to have the fewest gaps in LGE and the most scar volume as compared to the other PVs,

consistent with our results which showed that the LIPV is the most completely encircled pulmonary vein (54,55). In addition, quantification of total scar volume about each pulmonary vein showed that the only vein with significantly less scar volume between non-recurrent and recurrent AF patients was the RIPV (55). While our study does not currently have enough patients to predict AF recurrence based on scar encirclement percentage, we expect similar results as we found the RIPV as the PV with the most variance in scar encirclement and expect this to be an important predictor for AF recurrence.

The sensitivity analysis revealed that percent encirclement decreased slightly as epicardial pixel dilation increased though this difference was nonsignificant. This is likely the case because increased dilation outside of the atrial wall border is more likely to include pixels that fall below the scar intensity threshold due to lack of enhancement. As the bullseye projection algorithm linearly interpolates the mesh used for the bullseye, the additional non-scarred wall points may slightly decrease the pixel intensities, but overall has little effect on encirclement. While differences became significant when comparing a 3 pixel epicardial dilation to 5 pixel epicardial dilation, the 5 pixel epicardial dilation includes regions that are outside the atrial wall. The number of standard deviations used for the scar threshold was most sensitive to change, as it exponentially decays as the number of standard deviations increases. This can be explained if we assume that the distribution of all scarred pixels to have a normal distribution, which is described with an exponential function. As the threshold increases, the number of pixels excluded increases exponentially due to the shape of the left side of the normal distribution causing the exponential decay in encirclement. Although the number of

standard deviations used in the scar threshold is the most sensitive to changes in encirclement, it is not possible to determine what threshold is the physiologically correct threshold without performing an animal study to allow for a histological analysis after imaging. Performing both *in-vivo* imaging of the heart and comparing the images to TTC-stained histology of the left atrium would allow a validated threshold to be set that would properly separate scar from healthy tissue. Encirclement decreases linearly as the radial encirclement threshold increases, which is expected due to the nature of the atrial scar. While differences in PV encirclement were significant as the radial encirclement threshold was incrementally increased 5 units, the differences were minor and on average only decreased by 5% encirclement between increments.

A power analysis revealed based on the current mean encirclement and variations calculated between the pulmonary veins that a minimum of 15 patients would be necessary to determine whether pulmonary veins have significantly different amounts of scar encircling the pulmonary veins. Based on previous work that patients with near complete encirclement of the pulmonary veins had 10% recurrence rates with the average 30% recurrence rates, a Fisher's Exact Test with a significance of 0.05 and power of 80% requires at least 50 patients in each group to show that full encirclement significantly reduces recurrence rates post-PVI (94,95).

7.4.1 Limitations

There are limitations to this study. There was insufficient number of patients to draw any conclusions regarding recurrence. The scar intensity threshold used ($\mu \pm 6\sigma$), while based off a previous study, does not have validation by *ex-vivo* imaging or histology (94). In addition, the threshold used is different from the majority of other studies, which uses

three standard deviations above the mean (53,89). Differences in the LGE sequence such as inversion time may attribute to different standard deviations used for the scar threshold. Our inversion times were typically in the range of 300-370 ms while others studies have used TI times of ranging from 230-280ms (52,96). Regardless, in order to determine the proper intensity threshold to differentiate scarred atrial wall from healthy atrial wall, a direct comparison of LGE images must be performed against histology.

It is important to note that the bullseye mesh resolution is higher than the MR image resolution. The interpolation performed to achieve the bullseye resolution smooths the MR image data and as a result may not represent the true intensity at a particular point.

7.5 Conclusion

We applied the previously developed SharK sequence on patients who underwent PVI for the treatment of atrial fibrillation. By creating algorithms for a pulmonary vein bullseye projection, scar encirclement could be objectively quantified, and we found the RIPV to have on average the least amount of scar encirclement. Quantitative encirclement values may be used to predict recurrence in future studies and to compare RF ablation to cryoballoon ablation.

Chapter VIII

Conclusions and Future Work

8.1 Summary

The overall goal of this project was to develop a MR sequence to combine acquisition of angiography and LGE images to eliminate co-registration issues between the two image stacks and to provide a more robust method for segmentation. The sequence was developed by modifying a 3D, navigator- and ECG-gated inversion recovery FLASH sequence to acquire centric k-space twice and share outer k-space between the two reconstructions. The angiography portion of the SharK sequence was validated by comparing it against x-ray venography while the LGE portion of the SharK sequence was validated by comparing it against the clinical standard, a PSIR sequence, and a gold standard, a fully sample high-resolution FLASH sequence. The tradeoff in sharing k-space to myocardial scar accuracy was determined by using a retrospective reconstruction to create multiple SharK LGE reconstructions and comparing them to the original LGE reconstruction. The sequence was then applied in cryoballoon ablation patients to quantify atrial wall scar encirclement by developing pulmonary vein bullseyes.

8.1.1 Aim 1a: Comparison of MR Angiography and X-Ray Venography for Coronary Vein Imaging

The 3D, navigator- and ECG-gated inversion-recovery FLASH sequence used was capable of resolving the coronary venous anatomy as compared to the current gold standard, x-ray venography, in order to be able to properly plan LV lead implantation. This was achieved by imaging patients with MRI and comparing the resulting

angiography images to x-ray venogram images acquired during CRT implantation. Results showed that MRI visualized 90% of the coronary venous anatomy and was capable of visualizing all of the veins used for LV lead implantation when compared to veins visualized by x-ray venograms, suggesting that MRI is suitable for imaging the coronary veins for LV lead placement for CRT. This validates the respiratory-gated FLASH sequence for angiography use in the combined sequence.

8.1.2 Aim 1b: Validation of Respiratory-Gated LGE Imaging in Ex-Vivo Hearts

The respiratory-gated LGE sequence used in the combined sequence was validated by *ex-vivo* imaging of infarcted pig-hearts that had been delivered a dose of gadolinium prior to sacrifice with MRI. A fully sampled, high-resolution FLASH sequence was used as the gold standard while the standard PSIR sequence was used as a comparison to a clinical standard. Respiratory motion was simulated by placing the heart on top of a bag that was inflated and deflated, and the heart was imaged using the navigator-gated FLASH sequence used in the developed SharK sequence. Scar was quantified by segmenting the myocardium and applying a threshold to extract scar. There were no significant differences in scar volume across all three sequences and that there was no significant difference between the respiratory-gated FLASH sequence and the high-resolution FLASH sequences in scar area across slices despite the additional motion artifact in the respiratory-gated FLASH sequence. However, scar area quantified by PSIR images was significantly higher than both the respiratory-gated and high-resolution FLASH sequences. Therefore, the respiratory-gated FLASH used in the combined sequence is at least as good as than the clinical standard, PSIR images at quantifying scar.

8.1.3 Aim 2: Development of a Combined Angiography and Late Gadolinium Enhancement Pulse Sequence

The Shared K-space (SharK) sequence was developed for combined angiography and LGE imaging by modifying the base navigator-gated cardiovascular pulse sequence in the Siemens IDEA interface to acquire using a centric-ordered partition scheme and to be able to share outer k-space between angiographic and LGE acquisitions. The changes in the reordering scheme were validated by simulating a dilution experiment testing a centric-ordered partition encoding, linear-ordered partition encoding sequence against other reordering schemes. Results showed that a centric-ordered partition encoding scheme had the highest SNR out of all reordering schemes tested. Additional dummy pulses were added in order to remove ghosting from images. The k-space sharing image reconstruction program was validated by imaging a static phantom and determining that the resulting images were similar.

8.1.4 Aim 3a: Application of SharK Sequence on Patients with Myocardial Infarction

The SharK sequence was applied toward patients with known previous myocardial infarction to determine the tradeoff in scar accuracy as more k-space is shared between angiography and LGE images, and methodology was developed to create combined coronary vein and scar maps. This was achieved by acquiring two full sets of k-space for angiography and LGE images and retrospectively sharing different amounts and determining the differences in scar. Three parameters were compared across different SharK reconstructions: scar volume, proper pixel classification of scar, and proper

classification of transmurality spokes in the AHA bullseye. Additionally, the combined coronary vein and scar maps demonstrated its ability to be used as a pre-procedural planning tool for LV lead implantation.

8.1.5 Aim 3b: Application of SharK Sequence on Patients Post-PVI Treatment

The SharK sequence was applied in patients who had undergone cryoballoon ablation to visualize the continuity of scar encircling the pulmonary veins and to develop a method to quantify this encirclement. By using a rigid co-registration, accurate segmentation could be performed on the high contrast angiography images and directly transferred to the LGE images to extract the atrial wall. A pulmonary vein bullseye projection algorithm was developed to simplify visualization of and to quantify the continuity of scar encirclement. We found that the LIPV consistently had the highest degree of scar encirclement with a 98° anteroinferior segment that was always ablated in all patients, but that the right pulmonary veins had 1.5-2x more variation in the degree of encirclement when compared to the left pulmonary veins.

8.2 Potential Future Work

8.2.1 Alternate K-Space Acquisition Schemes

The SharK sequence may benefit by using alternate k-space trajectories to enhance SNR or reduce image acquisition time. The simplest change would be to move from a centric-ordered partition and phase encoding reordering to an elliptical centric reordering to maximize acquisition of central k-space immediately post-contrast injection.

A centric-ordered compressed sensing reordering scheme may also be applied toward this sequence, due to the sparseness of angiography images (97). Compressed sensing uses random k-space subsampling or variable density k-space sampling to reconstruct images with noise-like artifacts. The noise-like artifacts can be subsequently removed with a discrete wavelet transform that enforces sparsity. The variable density k-space sampling can be modified to initially acquire central k-space then move outwards, similar to the elliptical centric reordering scheme. The acquisition of central k-space is similarly re-acquired after k-space sampling has completed, and outer k-space can also be shared to create the two angiography and LGE reconstructions.

3D radial acquisition patterns may also be of interest for this sequence. Radial acquisitions naturally sample k-space more densely at the center of k-space, making radial trajectories ideal for angiography imaging. Self-navigation has also been developed from 3D radial acquisition schemes by tracking a 1D projection from a single radial spoke at each cardiac cycle to calculate cardiac motion occurring from respiratory motion (98). K-space can then be motion corrected to produce a 100% acceptance navigator-gated sequence to reduce image acquisition time by 2-4x.

8.2.2 Time-Resolved LGE Imaging

Previously, LGE imaging by multiple, 2D short-axis PSIR images would take approximately 10 minutes, preventing any time-resolved imaging. By using the SharK sequence, a whole-heart image stack can be acquired every 3-5 minutes. Multiple LGE image stacks can be acquired over time to allow for time-resolved scar imaging, which may help in myocardial scar identification or help separating inflammation from scar.

After applying a rigid co-registration across all LGE image stacks through time, pixel-by-pixel intensity curves of each voxel of the 3D volume can be plotted versus time. Regions of blood, healthy myocardium, and scarred myocardium can be extracted from these curves. One would expect the intensity curve of healthy LV myocardium to be initially dark and stay mostly dark through all image stacks due to nulling of healthy myocardium. Regions of blood would start out bright due to gadolinium contrast, but decrease sharply after the initial angiography image. Only scarred myocardium would be initially dark but increase in signal intensity. The intensity curves can be clustered by using PCA or k-means clustering to automatically identify the different groups. The separated curves have multiple potential applications, including segmentation and tissue characterization.

8.2.2.1 Automated Segmentation

Fully automated cardiac segmentation has posed a challenge due to poor delineation between healthy myocardium, infarcted myocardium, and the blood pool. However, classifying regions of myocardial scar based on intensity curves over time instead of pixel intensities from a single instance would assist the segmentation process immensely, as the intensity curves of all three groups would have distinctly different intensity curves. Users would only need to draw a box around the heart to specify the region of interest, and the clustering algorithm would automatically separate out the tissue groups. This would make scar segmentation more robust than using an intensity threshold.

8.2.2.2 Continuous Radial Sampling

While LGE imaging is performed 15 minutes post-contrast as contrast has accumulated into regions of scar for the majority of patients, the rate of accumulation

may be different across patients. Continuously acquiring radial spokes after angiography would provide two options for reconstruction – one for higher temporal resolution and one for higher SNR by averaging k-space data. One option would use fewer radial spokes during reconstruction to allow higher temporal visualization of contrast diffusion into scar over time. Since the radial images are self-navigated, all images are naturally co-registered. By sampling a region of enhancement over time, it is then possible to determine the time at which contrast has sufficiently accumulated into regions of scar. The center of k-space can then be filled from radial spokes around this time point, while the outer portions of k-space can filled by averaging all of outer k-space that has been previously acquired centered about the time point. Using the center of k-space at the point of maximum contrast accumulation from a highly densely sampled radial acquisition and averaging outer k-space reconstruction from the continuous acquisition would provide a LGE reconstruction with high SNR and CNR.

8.2.2.3 Atrial Fibrosis

Previous studies have suggested that the amount of atrial fibrosis is correlated to success of PVI (38,99,100). Assessment of atrial fibrosis is performed using LGE imaging, but identification of atrial fibrosis is difficult due to low CNR between fibrotic atrial wall and healthy atrial wall. This is due to the low amount of gadolinium contrast diffusing into regions of atrial fibrosis, leading to low CNR between healthy and fibrotic atrial wall. By combining Shared K-Space and time-resolved LGE imaging, differentiation between normal atrial wall and fibrotic atrial wall is possible. Performing the SharK sequence on normal patients that would have little to no fibrosis would provide reference temporal curves of healthy atrial wall intensity over time, which can then be

used toward differentiating healthy from fibrotic atrial wall curves in patients with atrial fibrillation. This method would not rely on arbitrary thresholds leading to more robustness.

8.2.2.4 Complete Mapping for CRT

CRT success has been associated with LV lead implantation in a coronary vein that is situated in the latest contracting segment that is not myocardial scar. As this work has developed a sequence that combines acquisition of angiography and scar to eliminate co-registration issues, the final piece is to combine these maps with dyssynchrony maps. A potential way to achieve this without the need to co-register the 2D SSFP images with the angiography and LGE images would be to also acquire 2D SSFP images with a radial self-navigating acquisition scheme. As a result, dyssynchrony, angiography and LGE images will be naturally co-registered due to the motion correction performed during the self-navigation to allow direction projection of dyssynchrony maps, coronary venous anatomy and scar onto the same AHA bullseye.

8.2.3 Cryoballoon Ablation vs RF Ablation

That we have developed the concept of pulmonary vein bullseye and applied the SharK sequence to quantify encirclement in patients post cryoballoon ablation, there is a clinical need to determine the performance of cryoballoon ablation in creating continuous encirclement against point-by-point RF ablation. Despite the two different methods of ablation, studies have shown similar levels of recurrence. This raises important clinical questions regarding the PVI process. Is one method better than the other at isolating the pulmonary vein with fully encircled scar? Are there portions of the pulmonary veins that are naturally more difficult to isolate? And most importantly, is encirclement indicative

of procedural success? These questions can be answered by continuing to apply the SharK sequence toward both sets of patients and creating pulmonary vein bullseyes to allow one to quantitatively determine whether there are any differences between the two methods of ablation.

8.3 Conclusions and Clinical Implications

Overall, this dissertation research demonstrates that the SharK sequence can be used to create angiography and LGE images by sharing k-space between the two acquisitions. We have validated both the angiography and the LGE portion of the sequences by comparing them to their respective gold standards. These resulting images from the SharK sequence are easily co-registered for development of combined coronary vein and myocardial scar maps. These maps can be used for LV lead planning in patients undergoing CRT to determine whether an optimal implantation site exists and if it has coronary venous access. In addition, the images allow accurate atrial wall segmentation to PVI assessment. The concept of a pulmonary vein bullseyes was established and was shown to be robust in quantifying atrial wall scar encirclement. These bullseyes may be used in the future to determine how continuous scar encirclement plays a role in ablation therapy.

REFERENCES

1. Dickstein K, Authors/Task Force Members, Cohen-Solal A, et al. ESC Guidelines for the diagnosis and treatment of acute and chronic heart failure 2008‡: The Task Force for the Diagnosis and Treatment of Acute and Chronic Heart Failure 2008 of the European Society of Cardiology. Developed in collaborati. Eur J Heart Fail. 2008;10:933–989.

2. Hunt SA. ACC/AHA 2005 Guideline Update for the Diagnosis and Management of Chronic Heart Failure in the Adult: A Report of the American College of Cardiology/American Heart Association Task Force on Practice Guidelines (Writing Committee to Update the 2001 Guidelines for the Evaluation and Management of Heart Failure): Developed in Collaboration With the American College of Chest Physicians and the International Society for Heart and Lung Transplantation: Endorsed by the Heart Rhythm Society. Circulation. 2005;112:e154–e235.

3. Ho KK, Pinsky JL, Kannel WB, Levy D, Pitt B. The epidemiology of heart failure: the Framingham Study. J Am Coll Cardiol. 1993;22:A6–A13.

4. Sutton MGSJ, Sharpe N. Left ventricular remodeling after myocardial infarction pathophysiology and therapy. Circulation. 2000;101:2981–2988.

5. Burchfield JS, Xie M, Hill JA. Pathological Ventricular Remodeling: Mechanisms: Part 1 of 2. Circulation. 2013;128:388–400.

6. Anversa P, Beghi C, Kikkawa Y, Olivetti G. Myocardial response to infarction in the rat. Morphometric measurement of infarct size and myocyte cellular hypertrophy. Am J Pathol. 1985;118:484.

7. Berk BC, Fujiwara K, Lehoux S. ECM remodeling in hypertensive heart disease. J Clin Invest. 2007;117:568–575.

8. van den Borne SWM, Diez J, Blankesteijn WM, Verjans J, Hofstra L, Narula J. Myocardial remodeling after infarction: the role of myofibroblasts. Nat Rev Cardiol. 2010;7:30–37.

9. Cheng A, Helm RH, Abraham TP. Pathophysiological mechanisms underlying ventricular dyssynchrony. Europace. 2009;11:v10–v14.

10. Yu CM, Lin H, Zhang Q, Sanderson JE. High prevalence of left ventricular systolic and diastolic asynchrony in patients with congestive heart failure and normal QRS duration. Heart. 2003;89:54–60.

11. Bleeker GB. Cardiac resynchronization therapy: advances in optimal patient selection. S.l.: s.n.]; 2007.

12. Chung ES, Leon AR, Tavazzi L, et al. Results of the Predictors of Response to CRT (PROSPECT) Trial. Circulation. 2008;117:2608–2616.

13. Sandhu R, Bahler RC. Prevalence of QRS prolongation in a community hospital cohort of patients with heart failure and its relation to left ventricular systolic dysfunction. Am J Cardiol. 2004;93:244–246.

14. Zhan C, Baine WB, Sedrakyan A, Steiner C. Cardiac Device Implantation in the United States from 1997 through 2004: A Population-based Analysis. J Gen Intern Med. 2008;23:13–19.

15. Tracy CM, Epstein AE, Darbar D, et al. 2012 ACCF/AHA/HRS Focused Update of the 2008 Guidelines for Device-Based Therapy of Cardiac Rhythm Abnormalities. J Am Coll Cardiol. 2012;60:1297–1313.

16. Bristow MR, Feldman AM, Saxon LA. Heart failure management using implantable devices for ventricular resynchronization: Comparison of Medical Therapy, Pacing, and Defibrillation in Chronic Heart Failure (COMPANION) trial. J Card Fail. 2000;6:276–285.

17. Abraham WT, Fisher WG, Smith AL, et al. Cardiac resynchronization in chronic heart failure. N Engl J Med. 2002;346:1845–1853.

18. Kristiansen HM, Vollan G, Hovstad T, Keilegavlen H, Faerestrand S. The impact of left ventricular lead position on left ventricular reverse remodelling and improvement in mechanical dyssynchrony in cardiac resynchronization therapy. Eur Heart J - Cardiovasc Imaging. 2012;13:991–1000.

19. Becker M, Franke A, Breithardt OA, et al. Impact of left ventricular lead position on the efficacy of cardiac resynchronisation therapy: a two-dimensional strain echocardiography study. Heart. 2007;93:1197–1203.

20. Khan FZ, Virdee MS, Palmer CR, et al. Targeted Left Ventricular Lead Placement to Guide Cardiac Resynchronization Therapy. J Am Coll Cardiol. 2012;59:1509–1518.

21. Delgado V, van Bommel RJ, Bertini M, et al. Relative Merits of Left Ventricular Dyssynchrony, Left Ventricular Lead Position, and Myocardial Scar to Predict Long-Term Survival of Ischemic Heart Failure Patients Undergoing Cardiac Resynchronization TherapyClinical Perspective. Circulation. 2011;123:70–78.

22. Chalil S, Foley PWX, Muyhaldeen SA, et al. Late gadolinium enhancement-cardiovascular magnetic resonance as a predictor of response to cardiac resynchronization therapy in patients with ischaemic cardiomyopathy. Europace. 2007;9:1031.

23. Bleeker GB. Effect of Posterolateral Scar Tissue on Clinical and Echocardiographic Improvement After Cardiac Resynchronization Therapy. Circulation. 2006;113:969–976.

24. Bi X, Deshpande V, Carr J, Li D. Coronary Artery Magnetic Resonance Angiography (MRA): A Comparison between the Whole-Heart and Volume-Targeted Methods Using a T 2 -Prepared SSFP Sequence. J Cardiovasc Magn Reson. 2006;8:703–707.

25. Suever JD, Fornwalt BK, Neuman LR, Delfino JG, Lloyd MS, Oshinski JN. Method to create regional mechanical dyssynchrony maps from short-axis cine steady-state free-precession images: Mechanical Dyssynchrony Maps From SSFP Images. J Magn Reson Imaging. 2014;39:958–965.

26. Marsan NA, Westenberg JJM, Ypenburg C, et al. Magnetic resonance imaging and response to cardiac resynchronization therapy: relative merits of left ventricular dyssynchrony and scar tissue. Eur Heart J. 2009;30:2360–2367.

27. Rasche V, Binner L, Cavagna F, et al. Whole-heart coronary vein imaging: A comparison between non-contrast-agent- and contrast-agent-enhanced visualization of the coronary venous system. Magn Reson Med. 2007;57:1019–1026.

28. Stoeck CT, Hu P, Peters DC, et al. Optimization of on-resonant magnetization transfer contrast in coronary vein MRI. Magn Reson Med. 2010;64:1849–1854.

29. Ma H, Tang Q, Yang Q, et al. Contrast-enhanced whole-heart coronary MRA at 3.0T for the evaluation of cardiac venous anatomy. Int J Cardiovasc Imaging. 2010;27:1003–1009.

30. Arheden H, Saeed M, Higgins CB, et al. Measurement of the Distribution Volume of Gadopentetate Dimeglumine at Echo-planar MR Imaging to Quantify Myocardial Infarction: Comparison with 99mTc-DTPA Autoradiography in Rats1. Radiology. 1999;211:698–708.

31. Saeed M, Weber O, Lee R, et al. Discrimination of Myocardial Acute and Chronic (Scar) Infarctions on Delayed Contrast Enhanced Magnetic Resonance Imaging With Intravascular Magnetic Resonance Contrast Media. J Am Coll Cardiol. 2006;48:1961–1968.

32. Kim RJ, Chen EL, Lima JAC, Judd RM. Myocardial Gd-DTPA kinetics determine MRI contrast enhancement and reflect the extent and severity of myocardial injury after acute reperfused infarction. Circulation. 1996;94:3318–3326.

33. Nielsen G, Fritz-Hansen T, Dirks CG, Jensen GB, Larsson HBW. Evaluation of heart perfusion in patients with acute myocardial infarction using dynamic contrast-enhanced magnetic resonance imaging. J Magn Reson Imaging. 2004;20:403–410.

34. Messroghli DR, Radjenovic A, Kozerke S, Higgins DM, Sivananthan MU, Ridgway JP. Modified Look-Locker inversion recovery (MOLLI) for high-resolution T1 mapping of the heart. Magn Reson Med. 2004;52:141–146.

35. Kim MH, Johnston SS, Chu B-C, Dalal MR, Schulman KL. Estimation of Total Incremental Health Care Costs in Patients With Atrial Fibrillation in the United States. Circ Cardiovasc Qual Outcomes. 2011;4:313–320.

36. Camm AJ, Kirchhof P, Lip GYH, et al. Guidelines for the management of atrial fibrillation. Europace. 2010;12:1360–1420.

37. Haissaguerre M, Jais P, Shah DC, et al. Spontaneous initiation of atrial fibrillation by ectopic beats originating in the pulmonary veins. N Engl J Med. 1998;339:659–666.

38. Verma A, Wazni OM, Marrouche NF, et al. Pre-existent left atrial scarring in patients undergoing pulmonary vein antrum isolation: an independent predictor of procedural failure. J Am Coll Cardiol. 2005;45:285–292.

39. Benjamin EJ, Wolf PA, D'Agostino RB, Silbershatz H, Kannel WB, Levy D. Impact of atrial fibrillation on the risk of death the Framingham Heart Study. Circulation. 1998;98:946–952.

40. Driver K, Mangrum JM. Hybrid approaches in atrial fibrillation ablation: why, where and who? J Thorac Dis. 2015;7:159.

41. Cleveland Clinic. Catheter Ablation For Atrial Fibrillation (AFIB). 2011.https://www.youtube.com/watch?v=SZ_uIfj-hIQ. Accessed October 29, 2015.

42. Dagres N, Anastasiou-Nana M. Prevention of atrial–esophageal fistula after catheter ablation of atrial fibrillation: Curr Opin Cardiol. 2011;26:1–5.

43. Oral H. Risk of Thromboembolic Events After Percutaneous Left Atrial Radiofrequency Ablation of Atrial Fibrillation. Circulation. 2006;114:759–765.

44. Sacher F, Monahan KH, Thomas SP, et al. Phrenic Nerve Injury After Atrial Fibrillation Catheter Ablation. J Am Coll Cardiol. 2006;47:2498–2503.

45. MedtronicEurope. How Cryoballoon ablation works. 2014.https://www.youtube.com/watch?v=vMyVOrbfAFQ. Accessed October 29, 2015.

46. Klein G, Oswald H, Gardiwal A, et al. Efficacy of pulmonary vein isolation by cryoballoon ablation in patients with paroxysmal atrial fibrillation. Heart Rhythm. 2008;5:802–806.

47. Linhart M, Bellmann B, Mittmann-Braun E, et al. Comparison of Cryoballoon and Radiofrequency Ablation of Pulmonary Veins in 40 Patients with Paroxysmal Atrial Fibrillation: A Case-Control Study. J Cardiovasc Electrophysiol. 2009;20:1343–1348.

48. Schmidt M, Dorwarth U, Andresen D, et al. Cryoballoon versus RF Ablation in Paroxysmal Atrial Fibrillation: Results from the German Ablation Registry: German Ablation Registry-Different Energy Sources in AF Ablation. J Cardiovasc Electrophysiol. 2014;25:1–7.

49. Chun K-RJ, Schmidt B, Metzner A, et al. The "single big cryoballoon" technique for acute pulmonary vein isolation in patients with paroxysmal atrial fibrillation: a prospective observational single centre study. Eur Heart J. 2008;30:699–709.

50. Packer DL, Kowal RC, Wheelan KR, et al. Cryoballoon Ablation of Pulmonary Veins for Paroxysmal Atrial Fibrillation. J Am Coll Cardiol. 2013;61:1713–1723.

51. Harrison JL, Whitaker J, Chubb H, et al. Advances in CMR of Post-ablation Atrial Injury. Curr Cardiovasc Imaging Rep. 2015;8http://link.springer.com/10.1007/s12410-015-9336-y. Accessed September 22, 2015.

52. McGann CJ, Kholmovski EG, Oakes RS, et al. New magnetic resonance imaging-based method for defining the extent of left atrial wall injury after the ablation of atrial fibrillation. J Am Coll Cardiol. 2008;52:1263–1271.

53. Badger TJ, Daccarett M, Akoum NW, et al. Evaluation of Left Atrial Lesions After Initial and Repeat Atrial Fibrillation Ablation: Lessons Learned From Delayed-Enhancement MRI in Repeat Ablation Procedures. Circ Arrhythm Electrophysiol. 2010;3:249–259.

54. Taclas JE, Nezafat R, Wylie JV, et al. Relationship between intended sites of RF ablation and post-procedural scar in AF patients, using late gadolinium enhancement cardiovascular magnetic resonance. Heart Rhythm. 2010;7:489–496.

55. Peters DC, Wylie JV, Hauser TH, et al. Recurrence of Atrial Fibrillation Correlates With the Extent of Post-Procedural Late Gadolinium Enhancement:: A Pilot Study. JACC Cardiovasc Imaging. 2009;2:308–316.

56. TSAO HM, YU WEN., CHENG HUI., et al. Pulmonary vein dilation in patients with atrial fibrillation: detection by magnetic resonance imaging. J Cardiovasc Electrophysiol. 2001;12:809–813.

57. Dill T. Pulmonary Vein Diameter Reduction After Radiofrequency Catheter Ablation for Paroxysmal Atrial Fibrillation Evaluated by Contrast-Enhanced Three-Dimensional Magnetic Resonance Imaging. Circulation. 2003;107:845–850.

58. Van Vaals JJ, Brummer ME, Thomas Dixon W, et al. "Keyhole" method for accelerating imaging of contrast agent uptake. J Magn Reson Imaging. 1993;3:671–675.

59. Fink C, Ley S, Kroeker R, Requardt M, Kauczor H-U, Bock M. Time-resolved contrast-enhanced three-dimensional magnetic resonance angiography of the chest:

combination of parallel imaging with view sharing (TREAT). Invest Radiol. 2005;40:40–48.

60. Spielman DM, Pauly JM, Meyer CH. Magnetic resonance fluoroscopy using spirals with variable sampling densities. Magn Reson Med. 1995;34:388–394.

61. Lam A, Mora-Vieira LF, Hoskins M, Lloyd M, Oshinski JN. Performance of 3D, navigator echo-gated, contrast-enhanced, magnetic resonance coronary vein imaging in patients undergoing CRT. J Interv Card Electrophysiol. 2014;41:155–160.

62. van Rees JB, de Bie MK, Thijssen J, Borleffs CJW, Schalij MJ, van Erven L. Implantation-Related Complications of Implantable Cardioverter-Defibrillators and Cardiac Resynchronization Therapy Devices. J Am Coll Cardiol. 2011;58:995–1000.

63. Beshai JF, Grimm RA, Nagueh SF, et al. Cardiac-resynchronization therapy in heart failure with narrow QRS complexes. N Engl J Med. 2007;357:2461–2471.

64. Younger JF, Plein S, Crean A, Ball SG, Greenwood JP. Visualization of coronary venous anatomy by cardiovascular magnetic resonance. J Cardiovasc Magn Reson. 2009;11:1–8.

65. Ma H, Tang Q, Yang Q, et al. Contrast-enhanced whole-heart coronary MRA at 3.0T for the evaluation of cardiac venous anatomy. Int J Cardiovasc Imaging. 2010;27:1003–1009.

66. Duckett SG, Chiribiri A, Ginks MR, et al. Cardiac MRI to investigate myocardial scar and coronary venous anatomy using a slow infusion of dimeglumine gadobenate in patients undergoing assessment for cardiac resynchronization therapy. J Magn Reson Imaging. 2011;33:87–95.

67. Suever JD, Watson PJ, Eisner RL, Lerakis S, O'Donnell RE, Oshinski JN. Time-resolved analysis of coronary vein motion and cross-sectional area. J Magn Reson Imaging. 2011;34:811–815.

68. White JA, Fine N, Gula LJ, et al. Fused Whole-Heart Coronary and Myocardial Scar Imaging Using 3-T CMR: Implications for Planning of Cardiac Resynchronization Therapy and Coronary Revascularization. JACC Cardiovasc Imaging. 2010;3:921.

69. Scheffer M, van Gelder BM. Implantation Techniques of Leads for Left Ventricular Pacing in Cardiac Resynchronization Therapy and Electrocardiographic Consequences of the Stimulation Site. Adv Electrocardiograms - Methods Anal. 2012;53–80.

70. Heiberg E, Sjögren J, Ugander M, Carlsson M, Engblom H, Arheden H. Design and validation of Segment-freely available software for cardiovascular image analysis. BMC Med Imaging. 2010;10:1.

71. Bi X, Deshpande V, Simonetti O, Laub G, Li D. Three-dimensional breathhold SSFP coronary MRA: A comparison between 1.5T and 3.0T. J Magn Reson Imaging. 2005;22:206–212.

72. Dellegrottaglie S, Guarini P, Savarese G, et al. Cardiac magnetic resonance for the assessment of myocardial viability: from pathophysiology to clinical practice. J Cardiovasc Med. 2013;14:862–869.

73. Kellman P, Arai AE, McVeigh ER, Aletras AH. Phase-sensitive inversion recovery for detecting myocardial infarction using gadolinium-delayed hyperenhancement. Magn Reson Med. 2002;47:372–383.

74. Setser RM, Chung YC, Weaver JA, Stillman AE, Simonetti OP, White RD. Effect of inversion time on delayed-enhancement magnetic resonance imaging with and without phase-sensitive reconstruction. J Magn Reson Imaging. 2005;21:650–655.

75. Peters DC, Appelbaum EA, Nezafat R, et al. Left ventricular infarct size, peri-infarct zone, and papillary scar measurements: A comparison of high-resolution 3D and conventional 2D late gadolinium enhancement cardiac MR. J Magn Reson Imaging. 2009;30:794–800.

76. Viallon M, Jacquier A, Rotaru C, et al. Head-to-head comparison of eight late gadolinium-enhanced cardiac MR (LGE CMR) sequences at 1.5 tesla: From bench to bedside. J Magn Reson Imaging. 2011;34:1374–1387.

77. Kino A, Zuehlsdorff S, Sheehan JJ, et al. Three-Dimensional Phase-Sensitive Inversion-Recovery Turbo FLASH Sequence for the Evaluation of Left Ventricular Myocardial Scar. Am J Roentgenol. 2009;193:W381–W388.

78. Jablonowski R, Nordlund D, Kanski M, et al. Infarct quantification using 3D inversion recovery and 2D phase sensitive inversion recovery; validation in patients and ex vivo. BMC Cardiovasc Disord. 2013;13:110.

79. De Marco JK, Schonfeld S, Keller I, Bernstein MA. Contrast-enhanced carotid MR angiography with commercially available triggering mechanisms and elliptic centric phase encoding. Am J Roentgenol. 2001;176:221–227.

80. Wilman AH, Riederer SJ, King BF, Debbins JP, Rossman PJ, Ehman RL. Fluoroscopically triggered contrast-enhanced three-dimensional MR angiography with elliptical centric view order: application to the renal arteries. Radiology. 1997;205:137–146.

81. Li D, Dolan RP, Walovitch RC, Lauffer RB. Three-dimensional MRI of coronary arteries using an intravascular contrast agent. Magn Reson Med. 1998;39:1014–1018.

82. Walker-Samuel S, Leach MO, Collins DJ. Evaluation of response to treatment using DCE-MRI: the relationship between initial area under the gadolinium curve (IAUGC) and quantitative pharmacokinetic analysis. Phys Med Biol. 2006;51:3593–3602.

83. Wilke N, Simm C, Zhang J, et al. Contrast-enhanced first pass myocardial perfusion imaging: correlation between myocardial blood flow in dogs at rest and during hyperemia. Magn Reson Med. 1993;29:485–497.

84. Saeed M, Wendland MF, Masui T, Higgins CB. Reperfused myocardial infarctions on T1-and susceptibility-enhanced MRI: Evidence for loss of compartmentalization of contrast media. Magn Reson Med. 1994;31:31–39.

85. Rogers WJ, Kramer CM, Geskin G, et al. Early contrast-enhanced MRI predicts late functional recovery after reperfused myocardial infarction. Circulation. 1999;99:744–750.

86. Dendale P, Franken PR, Block P, Pratikakisc Y, De Roos A. Contrast enhanced and functional magnetic resonance imaging for the detection of viable myocardium after infarction. Am Heart J. 1998;135:875–880.

87. Fuster V, Rydén LE, Cannom DS, et al. 2011 ACCF/AHA/HRS Focused Updates Incorporated Into the ACC/AHA/ESC 2006 Guidelines for the Management of Patients With Atrial Fibrillation. J Am Coll Cardiol. 2011;57:e101–e198.

88. Cappato R. Worldwide Survey on the Methods, Efficacy, and Safety of Catheter Ablation for Human Atrial Fibrillation. Circulation. 2005;111:1100–1105.

89. McGann C, Kholmovski E, Blauer J, et al. Dark Regions of No-Reflow on Late Gadolinium Enhancement Magnetic Resonance Imaging Result in Scar Formation After Atrial Fibrillation Ablation. J Am Coll Cardiol. 2011;58:177–185.

90. Hunter RJ, Jones DA, Boubertakh R, et al. Diagnostic Accuracy of Cardiac Magnetic Resonance Imaging in the Detection and Characterization of Left Atrial Catheter Ablation Lesions: A Multicenter Experience. J Cardiovasc Electrophysiol. 2013;24:396–403.

91. Kühne M, Suter Y, Altmann D, et al. Cryoballoon versus radiofrequency catheter ablation of paroxysmal atrial fibrillation: Biomarkers of myocardial injury, recurrence rates, and pulmonary vein reconnection patterns. Heart Rhythm. 2010;7:1770–1776.

92. Gaita F, Leclercq JF, Schumacher B, et al. Incidence of Silent Cerebral Thromboembolic Lesions After Atrial Fibrillation Ablation May Change According

to Technology Used: Comparison of Irrigated Radiofrequency, Multipolar Nonirrigated Catheter and Cryoballoon. J Cardiovasc Electrophysiol. 2011;22:961–968.

93. Beinart R, Abbara S, Blum A, et al. Left Atrial Wall Thickness Variability Measured by CT Scans in Patients Undergoing Pulmonary Vein Isolation. J Cardiovasc Electrophysiol. 2011;22:1232–1236.

94. Knowles BR, Caulfield D, Cooklin M, et al. 3-D Visualization of Acute RF Ablation Lesions Using MRI for the Simultaneous Determination of the Patterns of Necrosis and Edema. IEEE Trans Biomed Eng. 2010;57:1467–1475.

95. Oral H. Pulmonary Vein Isolation for Paroxysmal and Persistent Atrial Fibrillation. Circulation. 2002;105:1077–1081.

96. Peters DC, Wylie JV, Hauser TH, et al. Detection of Pulmonary Vein and Left Atrial Scar after Catheter Ablation with Three-dimensional Navigator-gated Delayed Enhancement MR Imaging: Initial Experience1. Radiology. 2007;243:690–695.

97. Lustig M, Donoho D, Pauly JM. Sparse MRI: The application of compressed sensing for rapid MR imaging. Magn Reson Med. 2007;58:1182–1195.

98. Stehning C, Börnert P, Nehrke K, Eggers H, Stuber M. Free-breathing whole-heart coronary MRA with 3D radial SSFP and self-navigated image reconstruction. Magn Reson Med. 2005;54:476–480.

99. Akoum N, Daccarett M, Mcgann C, et al. Atrial Fibrosis Helps Select the Appropriate Patient and Strategy in Catheter Ablation of Atrial Fibrillation: A DE-MRI Guided Approach. J Cardiovasc Electrophysiol. 2011;22:16–22.

100. Boldt A. Fibrosis in left atrial tissue of patients with atrial fibrillation with and without underlying mitral valve disease. Heart. 2004;90:400–405.